Ministry of Higher Education and Scientific Research

Hassiba Benbouali University of Chlef

Faculty of Technology

Electrical Engineering Department

THESIS

submitted in partial fulfillment of the requirements for the degree of

DOCTORATE

In

Field: Electrical Engineering

Specialty: Electrical Control

By

Alla Eddine TOUBAL MAAMAR

Title of the thesis:

Contribution to the modeling and advanced control of a multilevel resonant inverter

Defended on: 20/01/2022, in front of the committee composed of:

Abdallah ZEGAOUI	Professor	Hassiba Benbouali University of Chlef	President
M'hamed HELAIMI	Professor	Hassiba Benbouali University of Chlef	Supervisor
Rachid TALEB	Professor	Hassiba Benbouali University of Chlef	Co-supervisor
Kadda ZEMALACHE MEGUENNI	Professor	Science and Technology University of Oran Mohamed-Boudiaf	Examiner
Tayeb ALLAOUI	Professor	Ibn Khaldoun University of Tiaret	Examiner
Abdelkader DJAHBAR	Professor	Hassiba Benbouali University of Chlef	Examiner
Saad MEKHILEF	Professor	Malaya University of Malaysia	Invited

Academic year: 2021/2022

Ministère de l'Enseignement Supérieur et de la Recherche Scientifique

Université Hassiba Benbouali de Chlef

Faculté de Technologie

Département Electrotechnique

THÈSE

Présentée pour l'obtention du diplôme de

DOCTORAT

Filière: Electrotechnique
Spécialité: Commande électrique

Par

TOUBAL MAAMAR Alla Eddine

Thème:

Contribution à la modélisation et la commande avancée d'un onduleur multiniveaux à résonance

Soutenue le: 20/01/2022, devant le jury composé de :

ZEGAOUI Abdallah	Professeur	Université Hassiba Benbouali de Chlef	Président
HELAIMI M'hamed	Professeur	Université Hassiba Benbouali de Chlef	Rapporteur
TALEB Rachid	Professeur	Université Hassiba Benbouali de Chlef	Co-rapporteur
ZEMALACHE MEGUENNI Kadda	Professeur	Université des Sciences et de la Technologie d'Oran Mohamed-Boudiaf	Examinateur
ALLAOUI Tayeb	Professeur	Université Ibn Khaldoun de Tiaret	Examinateur
DJAHBAR Abdelkader	Professeur	Université Hassiba Benbouali de Chlef	Examinateur
MEKHILEF Saad	Professeur	Université Malaya de Malaysia	Invité

Année académique: 2021/2022


بسم الله الرحمن الرحيم

First and foremost, I would like to express our deepest sense of gratitude to God, who gave us the strength and the patience to get this work done.

I want to express my most sincere gratitude and thank my Supervisor, **M'hamed HELAIMI**, Professor at the Hassiba Benbouali University of Chlef, for guiding and supporting me throughout the course of doctoral formation. I would also like to thank my Co-Supervisor, **Rachid TALEB**, Professor at the Hassiba Benbouali University of Chlef, for his encouragement, help, and advice. I want to thank the doctoral formation committee CFD and the main responsible for the habilitation project, **Mohamed BOUNADJA**, Professor at the Hassiba Benbouali University of Chlef; thank you for all your helpful advice and information.

I warmly thank Professor. **Saad MEKHILEF** and the staff of PEARL Laboratory, Electrical Engineering Department, Faculty of Engineering, University Of Malaya, Kuala-Lumpur-Malaysia for offering me the possibility and giving me the facilities to carry out part of this research work. Also, I want to thank Professor. **Mostefa KERMADI** for the valuable helpful and information that he shared with me.

I am very grateful for the scholarship awarded by the faculty of Technology (UHBC) that has partially supported my travel and research at Malaya University. I am also thankful for the grants provided by the Malaya University and the UAE University which supported the publication of some of my researches.

I want to thank my thesis committee members; Prof. **Abdallah ZEGAOUI**, and Prof. **Abdelkader DJAHBAR**, Hassiba Benbouali University of Chlef; Prof. **Kadda ZEMALACHE MEGUENNI**, Science and Technology University of Oran Mohamed-Boudiaf; Prof. **Tayeb ALLAOUI**, Ibn Khaldoun University of Tiaret; who agreed to evaluate this thesis work and for all of their guidance, constructive comments and suggestions through the discussion process. The discussion, ideas, and feedback are invaluable, thank you so much for your time and effort to review the thesis.

I want to thank my colleagues in UHBC University, all members of LGEER, and all Electrotechnics Department-Faculty of Technology members; professors, students, and employees, for the wonderful moments. Thanks to their kindness and friendliness. Also, I want to thank especially a laboratory staff and department employees for all the facilities they provided me to advance my researches.

I owe my deepest gratitude to my beloved **Mother**, my **Father**, my **Brother**, and my **Sister**, who have always encouraged me, and help me all my life.

Finally, I thank **Friends** with whom I shared so many enjoyable and nice moments during the pursuit of my Ph.D.

Thank everyone who aided me.

Alla Eddine TOUBAL MAAMAR

قال الله تعالى:

۞ وَوَصَّيْنَا الْإِنسَانَ بِوَالِدَيْهِ
حَمَلَتْهُ أُمُّهُ وَهْنًا عَلَى وَهْنٍ وَفِصَالُهُ فِي عَامَيْنِ
أَنِ اشْكُرْ لِي وَلِوَالِدَيْكَ إِلَيَّ الْمَصِيرُ (14) ۞ سورة لقمان - الآية 14

۞ **And We have enjoined upon man [care] for his parents. His mother carried him, [increasing her] in weakness upon weakness, and his weaning is in two years. Be grateful to Me and to your parents; to Me is the [final] destination (14) ۞. Sura Luqman, aya 14. [http://quran.ksu.edu.sa/].**

قال الله تعالى:

۞ فَتَعَالَى اللَّهُ الْمَلِكُ الْحَقُّ ۗ وَلَا تَعْجَلْ بِالْقُرْآنِ مِن قَبْلِ أَن يُقْضَى إِلَيْكَ وَحْيُهُ ۖ وَقُل رَّبِّ زِدْنِي
عِلْمًا (114) ۞ سورة طه- الآية 114

۞ **So high [above all] is Allah, the Sovereign, the Truth. And, [O Muhammad], do not hasten with [recitation of] the Qur'an before its revelation is completed to you, and say, "My Lord, increase me in knowledge (114) ۞. Sura Taa-Haa, aya 114. [http://quran.ksu.edu.sa/].**

I thanking and dedicate my work to:

- *My Dear Parents & My family*

Abstract

Contribution to the Modeling and Advanced Control of a Multilevel Resonant Inverter

By

Mr. Alla Eddine Toubal Maamar

Directed by: Professor M'hamed HELAIMI and Professor Rachid TALEB

Electrical Engineering Department, Laboratoire Génie Electrique et Energies Renouvelables (LGEER) Laboratory, Faculty of Technology, Hassiba Benbouali University of Chlef, 02180, Algeria

The current study addresses the topic "Contribution to the modeling and advanced control of a multilevel resonant inverter". This study introduces new circuits in the power electronics field: the improved asymmetrical Twenty-one level inverter and the five-level resonant inverter. The proposed circuit of the five-level resonant inverter combines the advantages of the multi-level inverter and the abilities of the resonant inverter. The importance of the subject has been that it is one of the recent studies that provide the latest valuable information that researchers have achieved in the field of mathematical modeling of converters and advanced control techniques. The main achievements of this study are: The mathematical model of the five-level resonant inverter using small-signal modeling technique; Modulation of the five-level resonant inverter with the artificial neural network (ANN) based on selective harmonic elimination (SHE) scheme; Design and implementation of a closed-loop control system using reliable and high-efficient methods including the Coefficient Diagram Method (CDM), the Model Reference Adaptive Control (MRAC), the control method based on the intelligent algorithm as the fractional regulator (PI^{λ}) based on Genetic Algorithm (GA) and the fractional regulator (PI^{λ}) based on Particle Swarm Optimization (PSO).

Keywords: Power electronics, DC-AC converter, Multilevel inverter, Five-level series resonant inverter, Small-signal model, Selective harmonic elimination SHE modulation, Artificial neural network ANN, Coefficient diagram method CDM, Adaptive control, Intelligent algorithms control, Genetic algorithm GA, Particle swarm optimization PSO.

الملخص باللغة العربية

المساهمة في النمذجة والتحكم المتقدم في عاكس متعدد المستويات الرنان

من اعداد
السيد: طوبال معمر علاء الدين
تحت إشراف: الأستاذ. حلايمي امحمد و الأستاذ. طالب رشيد
قسم الإلكتروتقني، مخبر الهندسة الكهربائية و الطاقات المتجددة، كلية التكنولوجيا، جامعة حسيبة بن بوعلي بالشلف، 02180، الجزائر.

تتناول الدراسة الحالية موضوع "المساهمة في النمذجة و التحكم المتقدم في عاكس متعدد المستويات الرنان". تسمح هذه الدراسة بتقديم دوائر جديدة في مجال إلكترونيات الطاقة ، وهي العاكس غير المتماثل المحسن ذو واحد وعشرون مستوى، والعاكس ذي الخمس مستويات الرنان. تجمع الدائرة المقترحة للعاكس ذي الخمس مستويات الرنان بين مزايا العاكس متعدد المستويات بالإضافة إلى قدرات العاكس الرنان. تكمن أهمية الموضوع في أنه من الدراسات الحديثة التي توفر أحدث المعلومات القيمة التي حققها الباحثون في مجال النمذجة الرياضية لمحولات الطاقة وأيضًا في مجال تقنيات التحكم المتقدمة في الأنظمة. الإنجازات الرئيسية لهذه الدراسة هي: النموذج الرياضي للعاكس ذي المستويات الخمسة الرنان باستخدام تقنية نمذجة الإشارة الصغيرة؛ تعديل العاكس ذي الخمس مستويات بواسطة الشبكة العصبية الاصطناعية (ANN) بناءً على مخطط الإزالة التوافقي الانتقائي (SHE) ؛ كذلك تم تصميم وتنفيذ نظام التحكم في الحلقة المغلقة باستخدام طرق موثوقة وعالية الكفاءة وهي: طريقة الرسم البياني للمعامل (CDM)، والتحكم التكيفي على أساس نموذج مرجعي (MRAC) ، وطريقة التحكم الذكي القائم على الخوارزمية الوراثية(GA) ، و طريقة التحكم الذكي على أساس تحسين سرب الجسيمات (PSO).

الكلمات الرئيسية: إلكترونيات الطاقة ، محول DC-AC ، عاكس متعدد المستويات، العاكس ذو خمسة مستويات الرنان، نموذج الإشارة الصغيرة، التعديل بالحذف الإنتقائي المتناسق SHE، شبكة عصبية اصطناعية ANN، طريقة مخطط المعامل CDM، التحكم التكيفي، التحكم الذكي بإستعمال الخوارزميات، الخوارزمية الجينية GA ، خوارزمية تحسين سرب الجسيمات PSO.

Contents

List of acronyms

NPC: Neutral Point Clamped.

FC: Flaying Capacitor.

THMI: Trinary Hybrid Multilevel Inverter.

DC: Direct Current.

AC: Alternating Current.

MLI: Multilevel Inverter.

f_s: Switching *f*requency.

f_0: Resonance *f*requency.

M: Modulation index.

ANN: Artificial Neural Network.

SHE: Selective Harmonic Elimination.

PI: Proportional Integral.

CDM: Coefficient Diagram method.

MRAC: Model Reference Adaptive Control.

GA: Genetic Algorithm.

PSO: Particle Swarm Optimization.

DPS: Distributed Power Systems.

SRI: Series Resonant Inverter.

PRI: Parallel Resonant Inverter.

S-PRI: Series-Parallel Resonant Inverter.

ZVS: Zero Voltage Switching.

ZCS: Zero Current Switching.

GAM: General Average Model.

AGM: Average Generator Model

HBs: Half-bridges.

NL: Nearest Level.

SVM: Space Vector Modulation.

THD: Total Harmonic Distortion.

NR: Newton-Raphson.

PWM: Pulse Width Modulation.

OHSW: Optimized Harmonic Stepped Waveform

SVPWM: Space Vector Pulse Width Modulation.

LS-PWM: Level shifted-PWM.

PS-PWM: Phase shifted-PWM.

PD-PWM: Phase Disposition-PWM.

POD: Phase Opposition Disposition.

APOD: Alternate Phase Opposition Disposition.

HVDC: High Voltage Direct Current.

TGV: Trains Grande Vitesse.

PI: Proportional-Integral.

PD: Proportional-Derivative.

PID: Proportional-Integral-Derivative.

PI^{λ}: Fractional Order PI.

$PI^{\lambda}D^{\delta}$: Fractional Order PID.

Z-N: Ziegler-Nichols.

IMC: Internal Model Control**.**

SMN: Single Memory Neuron.

GSA: Gravitational search algorithm.

MPC: Model Predictive Control.

OSV: Optimal Switching Vector.

OSS: Optimal Switching Sequence.

AI: Artificial Intelligence.

BA: Bat Algorithm.

ACO: Ant Colony Optimization.

GWO: Grey Wolf Optimizer.

ABC: Artificial Bee Colony.

SSA: Salp Swarm Algorithm.

GSA: Gravitational Search Algorithm.

LTI: Linear Time-Invariant.

PC: Linear Time-Invariant.

DSP: Digital Signal Processor

MIT: Massachusetts Institute Technology.

List of figures

List of tables

Chapter 01:
GENERAL INTRODUCTION

CHAPTER 1 GENERAL INTRODUCTION

1.1 Introduction

The activities in the power electronics industry are interesting and beneficial because it opens the opportunity for experimentation and knowledge, and it is a perfect way to develop new systems. ‘‘The global power electronics market size was valued at 23.25 billion dollars in 2019 and is expected to reach 36.64 billion dollars by 2027’’ [1]; the money figure in the previous sentence provides the importance of power electronics in our daily life. On Wednesday, October 31, 2021, A.E. Toubal Maamar was granted access to the Scopus-Elsevier database by ***CERIST-SNDL*** to search the sentence "**power electronic**," and the word "**inverter**", where the search was done within the article title option, and the data was selected from 1990 to 2021. The Scopus database shows that 5,208 documents use the sentence "power electronic" and 43,701 documents use the sentence "inverter" in several subjects’ areas. Table 1 displays the data about the use of the sentence "**power electronic**" as part of the document's title in the Scopus database from 1990 to 2021, and Table 2 displays the data on the use of the word "**inverter**". Figure 1 shows the line graph of the data that use the sentence "**power electronic**" and word "**inverter**" in the document's title.

Table 1: Data on the use of the sentence “power electronic” in documents’ title -Scopus database

Year	***2021***	***2020***	***2019***	***2018***	***2017***	***2016***	***2015***	***2014***	***2013***	***2012***	***2011***
Documents	278	341	338	338	267	269	235	241	225	216	240
	2010	***2009***	***2008***	***2007***	***2006***	***2005***	***2004***	***2003***	***2002***	***2001***	***2000***
	182	222	166	157	132	145	127	101	115	117	100
	1999	***1998***	***1997***	***1996***	***1995***	***1994***	***1993***	***1992***	***1991***	***1990***	***Total***
	84	125	77	93	49	51	61	38	25	53	5208

Table 2: Data on the use of the word “inverter” in documents’ title -Scopus database

Year	***2021***	***2020***	***2019***	***2018***	***2017***	***2016***	***2015***	***2014***	***2013***	***2012***	***2011***
Documents	2584	3692	3937	3793	3243	3051	2514	2656	2300	2035	1831
	2010	***2009***	***2008***	***2007***	***2006***	***2005***	***2004***	***2003***	***2002***	***2001***	***2000***
	1500	1338	1083	1087	835	770	683	556	529	447	390
	1999	***1998***	***1997***	***1996***	***1995***	***1994***	***1993***	***1992***	***1991***	***1990***	***Total***
	377	365	354	323	277	277	289	206	156	187	43701

From Tables 1 and 2, we can see that “**power electronic**” and “**inverter**” are popular in the research scientific; also from Figure 1, we can obviously note the increase of research in power electronic and inverter subjects from 1990-2019, generally. Moreover, there is a decrease in scientific research documents from 2020-2021 due to the

COVID-19 pandemic and its influence on humanity in all areas.

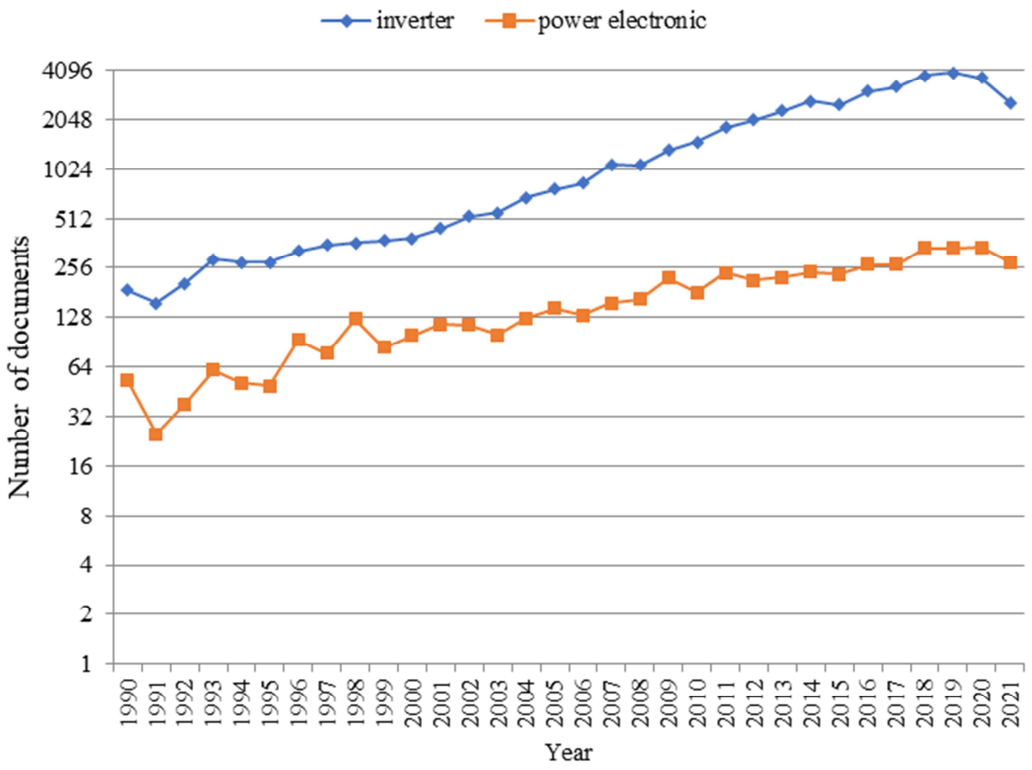

Figure 1: Line graph based on the data of use the sentence "power electronic" and word "inverter" in documents title [Scopus database from 1990-2021].

Scientists' research on improving the efficiency and production of electronic converters will increase to meet the tremendous worldwide demand for electricity in the coming years. This forecast is based on the data of energy consumption worldwide from 2000 to 2018, with a forecast until 2050 [2], and the information that the inverter is an essential part of the distributed power generation systems (*DPGS*) for integrating the popular renewable energy sources, such as Hydropower, Wind, and Solar [3].

Table 3 illustrates the data of the worldwide energy consumption with exajoules unit [Statista Data-2021], and Figure 2 shows the bar graph of the data. From figure 2, we can see the increasing demand of renewable energy. The data presented in Tables 1, 2, and 3 notes that power electronics play an important role in sustainable energy systems.

Table 3: Data of the worldwide energy consumption with exajoules unit [Statista Data-2021]

	Nuclear	*Natural gas*	*Oil*	*Coal*	*Renewable energy*	*Hydropower*
2000	26	86	155	99	3	27
2005	27	99	169	130	4	28
2010	26	114	173	151	10	32
2015	23	125	184	158	18	35
2018	24	138	190	158	27	38
2025	26	154	191	155	48	43
2030	27	166	190	149	70	46
2035	28	175	187	145	89	47
2040	29	180	182	138	114	49
2045	30	184	177	131	137	50
2050	31	187	172	123	161	51

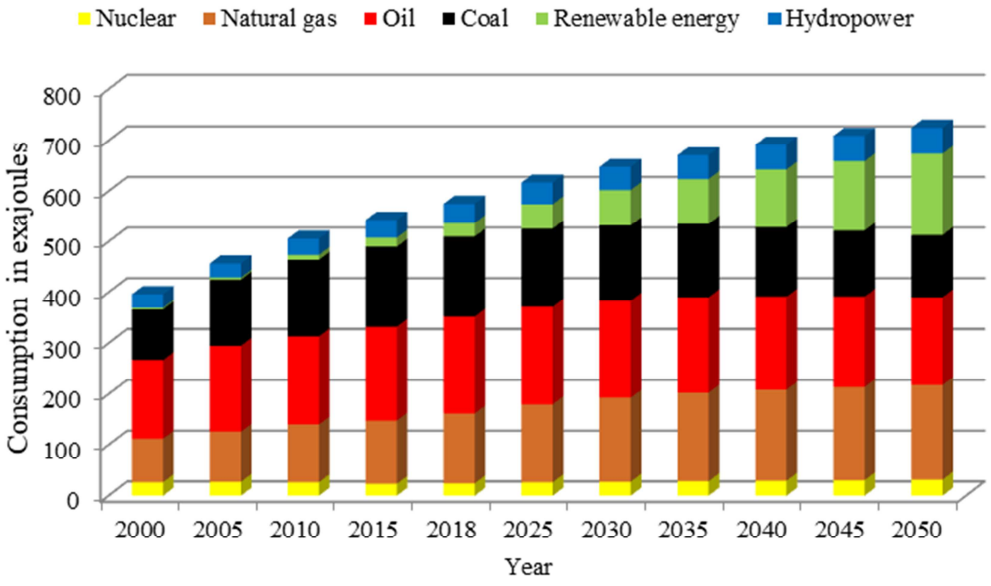

Figure 2: Bar graph based on the data of the worldwide energy consumption [Statista Data-2021].

In the power electronics domain, the switching converter is the main component for processing electric power. Currently, four primary switching converters exist. One of the most used converters is the *DC–AC* converter; it is an inverter because the *DC* input voltage is modulated to produce an *AC* output voltage with controllable magnitude, duty cycle, and frequency [4]. If the inverter can produce more than two levels of output voltage, then it can be called a multilevel inverter (*MLI*). In recent decades, several emerging *MLI* topologies have been proposed to overcome the conventional inverters' problems [5]–[9]. The resonant inverter is a particular type of converter; this type is invented to achieve a high-efficiency conversion and address specific industrial applications [10]–[12]. The implementation of multilevel inverter needs the use of modulation technique; the modulation techniques are classified into two categories: high-

switching modulation techniques and low (also known as fundamental) switching modulation techniques [13]-[15].

On the other hand, mathematical presentation of the inverter is an essential step for control design; some theoretical and practical studies present the modeling of inverters and resonant inverters. The general average model, the average generator model, the average state model method, and small-signal modeling are the most used modeling methods in dynamic system analysis [16]-[20]. Currently, there is several control methods proposed to overcome the classical control problems. The coefficient diagram method, the model reference adaptive control, the model predictive control, and the fractional controller based intelligent algorithms (Genetic algorithm, Particle swarm optimization PSO, …etc.) attracted the attention of many researchers in control theory, where has a lot of theoretical and practical studies been done [21]-[27].

From the review and analysis of previous studies, there is a gap in knowledge about applying a small-signal method for modeling multilevel power converters. Also, none of the earlier works attempted to use a six-switch five-level topology to realize a series resonant inverter and model the circuit using small-signal *AC* analysis. Furthermore, it isn't easy to design a classical or advanced controller for nonlinear switching converters, where the analysis of the dynamic behavior of such nonlinear systems is very complex.

The current study addresses the topic "Contribution to the modeling and advanced control of a multilevel resonant inverter".

1.2 Objectives and specific aims

The importance of the subject "Contribution to the modeling and advanced control of a multilevel resonant inverter" has been that it is one of the recent studies that provide a new contribution in the field of power electronics, and provide the latest valuable information that researchers have achieved in the field of mathematical modeling and also in the field of system control. This study introduces a new circuit, which is the five-level resonant inverter. The proposed circuit combines the advantages of the multilevel inverter and the abilities of the resonant inverter. The latest mathematical modeling techniques of the inverter have been presented through the previous studies, and we focused on the small-signal method. Furthermore, in this research, some recent advanced control techniques have been discussed. We have chosen four high-efficient methods for

implementing the proposed small-signal model of the multilevel resonant inverter. The suggested control methods in this research are: the Coefficient Diagram Method (*CDM*), the Model Reference Adaptive Control (*MRAC*), the Fractional controller based on the intelligent algorithm as PI^{λ}-based on Genetic Algorithm (*GA*) and PI^{λ}-based on Particle Swarm Optimization (*PSO*).

In our research on the topic "Contribution to the modeling and advanced control of a multilevel resonant inverter", we used the analytical approach to present the previous works and summarize the basic information derived from them. Also, the analytical approach has been used throughout the analysis of the proposed circuit of the five-level-series resonant inverter. Moreover, the experimental approach has been used to investigate the proposed circuit and display the achieved data using simulation software and be applied using several electronic devices. In this research, four highly efficient control methods have been implemented for controling the proposed small-signal model of the multilevel resonant inverter. Hence, the study required the comparative approach, which we have employed to compare the achieved results.

The study objectives can be summarized as follows: Objective I: Establish new circuits in the field of power electronics, which are the improved asymmetrical Twenty-one level inverter, and the five-level resonant inverter. Objective II: Analysis of the proposed five-level resonant inverter. Objective III: Establish a small-signal model for the proposed five-level resonant inverter. Objective IV: Design and implementation of the closed-loop system using reliable and high-efficient advanced control methods.

1.3 Thesis outline

This thesis is addressed in six chapters to present all aspects of the subject well. Each chapter begins with a brief introduction, followed by subsections contains comprehensive information, discussion, and analysis, eventually a short chapter summary. This thesis is organized as follows:

Chapter 1 general introduction: The current chapter seeks to introduce the subject of the research and its significance, taking into account the perspectives of the previous work. Also, this chapter aims to present and discuss the study problem based on the many scientific gaps in similar previous works and identify the endorsed curriculum to study the subject. Furthermore, the current chapter presents the organization of a thesis.

Chapter 2 state of the art about the inverters and the electrical control systems: we have divided this chapter into two main parts for the precise positioning of our work according to state-of-the-art. PART. I Overview of the resonant inverters & the multilevel inverters; this part introduces the basic types of resonant inverters and discusses their current modeling techniques. Also, identify the emerging topologies of multilevel inverters and presents their modulation strategies. The part is concluded by a discussion of the well-known application fields of inverters. This part aims to give comprehensive information about the resonant inverters and multilevel inverter topologies, select the appropriate topology of the multilevel inverter, the resonant inverter type, and the modeling technique for implementing our research study. PART. II Overview of controller actions and control techniques for electrical power systems. This part introduces the controller actions for closed-loop systems and discusses the popular control techniques, classical and advanced. This part aims to present comprehensive information about the control of electrical systems, and subsequently, we select the control techniques to be implemented in our research study.

Chapter 3 analysis of the proposed five-level series resonant inverter: this chapter introduces a new circuit of the five-level series resonant inverter; the circuit combines the multilevel inverter advantages and the advantages of the physical phenomenon “the resonance”. We have presented the topology and the operating mode of the five-level series resonant inverter. Furthermore, we have discussed a piece of excellent comprehensive information about the system and mathematical expressions.

Chapter 4 small-signal modeling of a five-level series resonant inverter: the fourth chapter focuses on the mathematical description of the proposed circuit of a five-level series resonant inverter. We have validated the small-signal model of the circuit in the frequency domain for later use in the design of the control system. Also, we have discussed the results of simulation and experiments in this chapter.

Chapter 5 control techniques for a five-level series resonant inverter: we divided this chapter into three main parts; each part presents a specific control technique and their implementation procedures for controling a five-level series resonant inverter. The control techniques are designed based on the validated small-signal model. ***Part A: Implementation of the classical control technique: CDM-based PI control***; this part introduces the Coefficient Diagram Method (*CDM*) and design procedure of the CDM-

based PI controller for a five-level series resonant inverter. ***Part B: Implementation of the advanced control technique: adaptive control***; this part presents the adaptive control techniques and implementation procedure of the Model Reference Adaptive Control (*MRAC*) for controling the proposed circuit of five-level series resonant inverter. ***Part C: Implementation of the advanced control techniques: PI^{λ}-based on Genetic Algorithm (GA) and PI^{λ}-based on Particle Swarm Optimization (PSO)***; in this part, we have introduced the fractional-order controllers and the intelligent algorithms. Also, this part discusses the implementation procedure of the GA-based PI^{λ} and the implementation procedure of the PSO-based PI^{λ} for controling a five-level series resonant inverter. Furthermore, we have compared the obtained results by applying the four control techniques.

Chapter 6 conclusion: the sixth chapter summarizes the contribution and the most important results of this thesis and proposes future works based on this topic.

Chapter 02:

STATE OF THE ART ABOUT THE INVERTERS AND THE ELECTRICAL CONTROL SYSTEMS

CHAPTER 2 STATE OF THE ART ABOUT THE INVERTERS AND THE ELECTRICAL CONTROL SYSTEMS

2.1 Introduction

Resonance *DC-AC* inverter is a type of electric power converter designed to develop high-frequency with a high-efficiency power converter. Resonant inverter technology is becoming a very important subject of research in the field of power electronics for several industrial applications because of the ability and the efficiency to generate high-quality power. On the other hand, Multilevel Inverter (MLI) technology is becoming a very important subject of research in the field of power electronics for several industrial applications because of the simplicity of control and the ability to generate high output voltage levels with high quality. A static Direct Current to Alternating Current (*DC/AC*) converter can be called a "Multilevel Inverter" when it generates a chopped output voltage composed of a minimum of three levels. We can find Resonant inverters and Multilevel inverters in power transmission systems, induction heating applications, distributed power systems (*DPS*), telecom and network applications, wireless power transfer systems, traction systems, active filtering, motor drives, high-voltage and medium-voltage applications, renewable energy station, and many other new technologies. The recent advancement in power control by developing high-speed calculators and the development of effective semiconductor devices is increasing the demand for electrical energy. Therefore many resonant inverter and multilevel inverter structures have been proposed in the literature to address this demand. This chapter presents a Background on the Resonant Inverters, Topologies, and modeling methods. Also, discuss the Multilevel Inverters, Fundamental Circuits, and emerging technologies.

PART. I Overview about the resonant inverters & the multilevel inverters

I.1 Fundamental types of single-phase resonant inverters

The resonant converters are used for efficient and powerful applications. The conversion of electrical energy is realized by a single-phase, non-modulated *DC-AC* converter where the converter structure depends on the nature of the *DC* source. This converter is a voltage inverter or a current switch. In these converters, the resonance is exploited to reduce the electrical stress on the electrical switches, maximize the output power, and reduce the harmonics. In the literature, there are several types of resonance converters, including series resonant inverter (*SRI*), parallel resonant inverter (*PRI*), series-parallel resonance inverter (*S-PRI*) [1], [2].

I.1.1 Series resonant inverter (SRI)

The Series resonant inverter: is an inverter delivering power to a series resonant circuit with low damping. The capacitor is placed in series with the load; the inverter delivers on a current receiver, so a voltage source must power it. In this type of compensation, the output power produced varies with frequency and has a maximum peak value close to the resonance frequency. In addition, the current flowing through the load is quasi-sinusoidal. The used switches of the voltage inverter have only one type of switching to be ensured (*ZVS*), and this will reduce the switching losses, reduces the electrical stress, and allows frequency rise [1], [3]. If taking into account the number 1 as a frequency rapport, then the series compensation is characterized by:

1. For: $f_s < 1$, the circuit is capacitive.

2. For: $f_s > 1$, the circuit is inductive.

3. For: $f_s = 1$, the circuit is resistive.

Figure 3 shows the schematic diagram of the series resonant half-bridge inverter. This topology is frequently used in low power applications. It consists of a *DC* source, a series *RLC* circuit, and one switching cell (S_1, S_2); by using an appropriate control, the source will be modulated to obtain an alternating signal of the desired frequency and duty cycle.

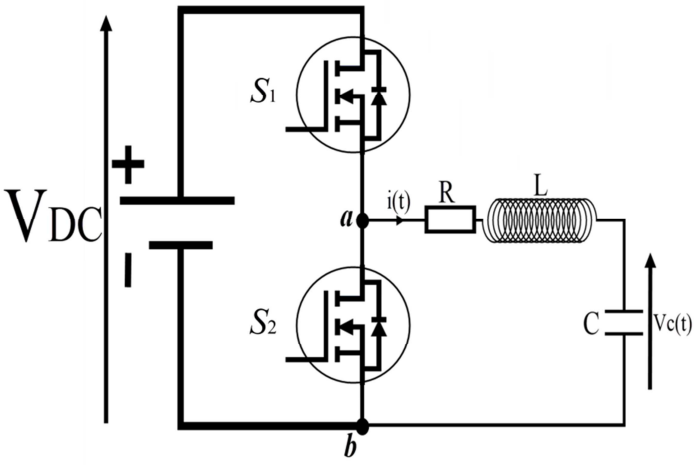

Figure 3: Topology of Half-bridge series resonant inverter

Figure 4 shows the schematic diagram of the series resonant H-bridge inverter. It consists of a DC source, a series *RLC* circuit, and two switching cells connected in parallel (S_1, S_2) and (S_3, S_4); by using an appropriate control, the source will be modulated to obtain an alternating signal of the desired frequency and duty cycle.

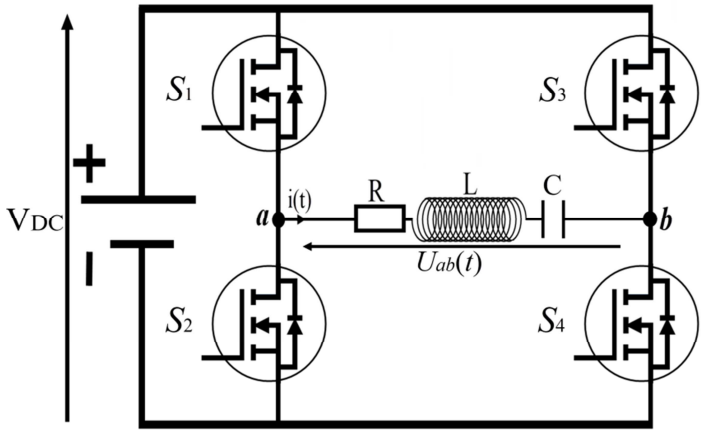

Figure 4: Topology of Full-bridge series resonant inverter

I.1.2 Parallel resonant inverter (PRI)

Parallel resonant inverter: is an inverter delivering on a parallel resonant circuit with low damping. The load has a capacitance directly connected between the outputs terminals; a *DC* source must power the inverter. The inverter switching has only one type of switching to be ensured (*ZCS*), which reduces switching losses [1]-[3]. In contrast to series compensation, parallel compensation is characterized by:

1. For: $f_s < 1$, the circuit is inductive.

2. For: $f_s > 1$, the circuit is capacitive.

3. For: $f_s = 1$, the circuit is resistive.

Figure 5 shows the schematic diagram of the parallel resonant Half-bridge inverter. Figure 6 shows the schematic diagram of the parallel resonant Full H-bridge inverter.

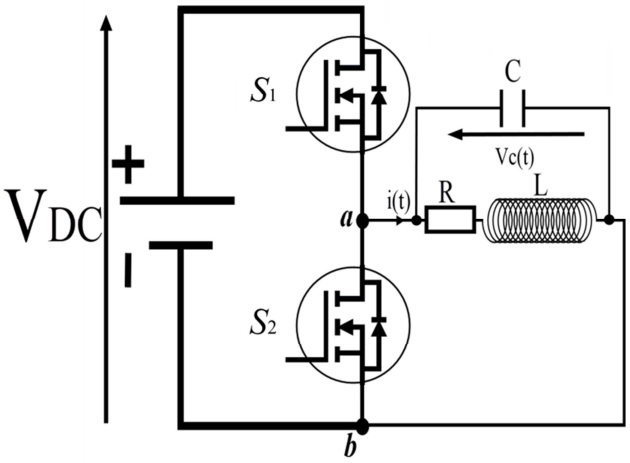

Figure 5: Topology of Half-bridge parallel resonant inverter

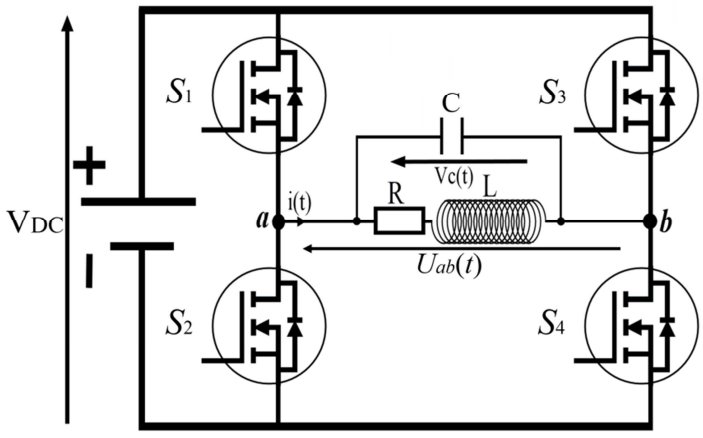

Figure 6: Topology of Full-bridge parallel resonant inverter

I.1.3 Series-Parallel resonant inverter (S-PRI)

This topology is based on a series-parallel oscillating circuit type *LLC* formed by inductances and capacitors connected with the terminals of the load. This structure presents two resonance points and combines the advantages of the series resonant inverter,

such as Zero Voltage Switching (*ZVS*) and current gain. Furthermore, this topology has the advantage of Inverter Self-Protection [1], [4]. Figure 7 shows the topology of a Series-Parallel resonant inverter (S-PRI) type half-bridge *LCC*. In this structure, the oscillating circuit consists of a capacitance C_s placed in series with a parallel resonant circuit.

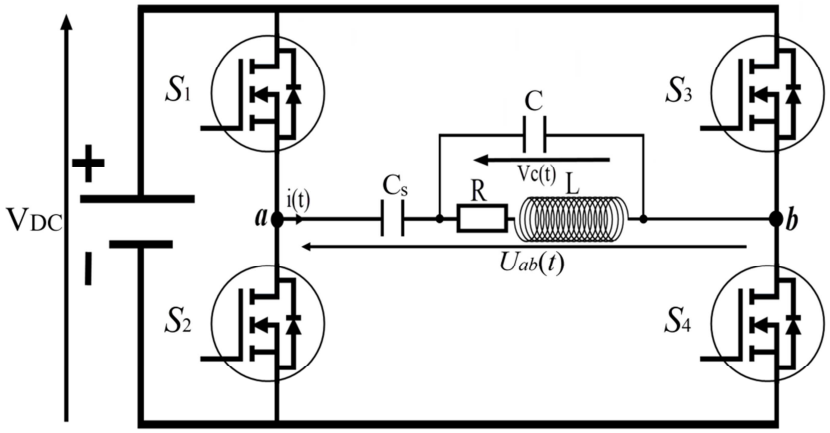

Figure 7: Topology of Half-bridge series-parallel LCC resonant inverter

Figure 8 shows the topology of a Series-Parallel resonant inverter (S-PRI) type half-bridge *LLC*. This topology is composed of an inductance L_s placed in series with a parallel resonant circuit.

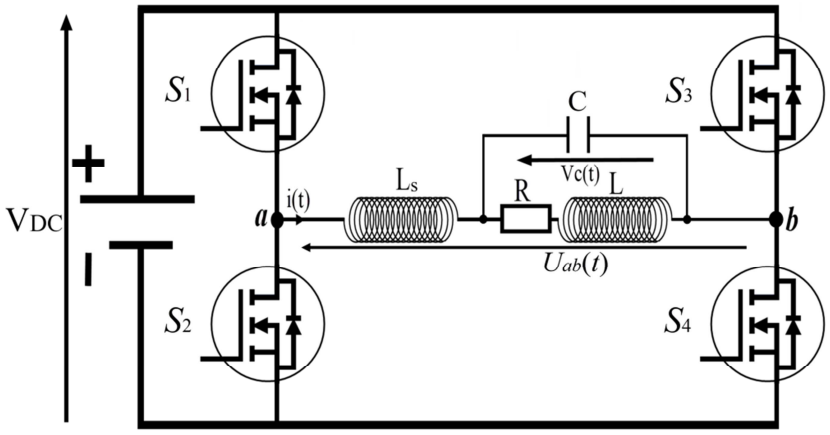

Figure 8: Topology of Half-bridge series-parallel LLC resonant inverter

I.2 Classification of the modeling techniques of resonant inverters

Develop an appropriate mathematical model of the resonant inverter is the first step in the control design, where the model may be derived from electrical laws or

experimental data. The model of a resonant inverter is usually elaborated from an analysis of the operating sequences, generally, a state model, continuous, non-linear, multi-variable, and varying in time. The dynamics of orders higher than the switching frequency due to disturbances and electromagnetic interactions are generally neglected. Various approaches have been proposed [5]-[8]. This section introduces the general average model, the average generator model, the average state model method, and small-signal approach representations.

I.2.1 The general average model

The General Average Model (GAM) is a flexible generalization of linear regression. GAM generalizes linear regression by providing the linear model to be related to the variable response via a relationship function and by allowing the magnitude of the variance of each measure to be a function of its expected value. The generalized average model is applied specifically to converters having one or more alternating stages (s). It makes the relationship between the dynamics of alternating and continuous variables. As in general, the modeling is conducted only with fundamentals and average values, so let's limit ourselves to harmonics of rank (k=1) and average values (M=0). Therefore, in this modeling technique, the period T is supposed to be constant or varies slightly in time [9], [10].

I.2.2 The average generator model

The average generator model method (AGM), which is also called the VORPÉRIAN model [11], [12], aims to find an equivalent circuit in the average regime of the converter. The principle consists of replacing the power switches with dummy generators; a generator is either a voltage source or a current source depending on the topological position of the corresponding switch over a switching period [7], [13], [14]. In this context, the average generator model is a good compromise between complexity, computation time, and acceptable accuracy for studying simple power electronics systems. However, this technique becomes excessively difficult for the complex converters when the structures of the converters are complexes and their control involves complicated mathematical expressions.

I.2.3 The average state space model

The principle of the state-space averaging model is based on the expression of the state model for each state of the control vector $U(t)$. This method offers a systematic approach that makes it easy to implement. Compared to the average generator technique, the average state model method is a standardized or even systematized modeling approach that applies to a wide variety of high-frequency switching topologies. The state-space averaging model consists of two steps. In the First step, the elementary state models corresponding to the different stable configurations of the converter. Second step: The average state model will be deduced by a linear combination of the previous models. The weighting of each elementary model is related to its duration of appearance of a switching period [8], [13].

I.2.4 The small-signal model

The average and large-signal techniques previously discussed are non-linear models. Therefore, they can't be used to synthesize a continuous or a sampled linear regulator of the studied system. In this context, it is necessary to build a linearization of the model called the tangent model, valid around an operating point. These models make it possible to get rid of non-linearity problems. The construction of such models requires a Taylor series development limited to the first order. The resulting model is linear, invariant in time, and regulates the inverter's dynamic behavior in a small variation regime around its equilibrium point. The small-signal model offers the possibility to design various linear control methods [15]-[17].

I.3 Topologies of single-phase multilevel inverters

Recently, the multilevel inverter has been proposed for many industrial applications; there are conventional categories of single-phase multilevel inverters and novel technologies of single-phase multilevel inverters.

I.3.1 Conventional categories of single-phase multilevel inverters

There are three conventional categories of single-phase multilevel inverters in applied power engineering fields: cascaded H-bridge, neutral point clamped, and flying capacitor. The diode-clamped multilevel inverter, also known as the neutral-point clamped (*NPC*) multilevel inverter, was first presented in 1981 by A.Nabae and H. Akagi. The

capacitor clamped, also known as flying capacitor multilevel inverter, was first introduced in 1992 by T.A. Meynard and H. Foch. The cascaded multilevel inverter was first proposed in 1975 by Baker Richard H. and Bannister Lawrence H. [18].

I.3.1.1 Diode Clamped Multilevel Inverter

Figure 9 shows the N-level diode clamped structure. The topology uses series switching devices and series capacitors to generate multiple voltage levels. The inner voltage points are clamped by the two extra diodes. The clamping diode needs different voltage ratings for different inner voltage levels. N-level diode clamped inverter has: 2(N–1) power electronic switches, 2(N–2) clamped diodes, (N–1) DC-link capacitors, where the voltage across each DC-link capacitor = (Vdc/ N-1), and Vdc is the DC-link voltage [18].

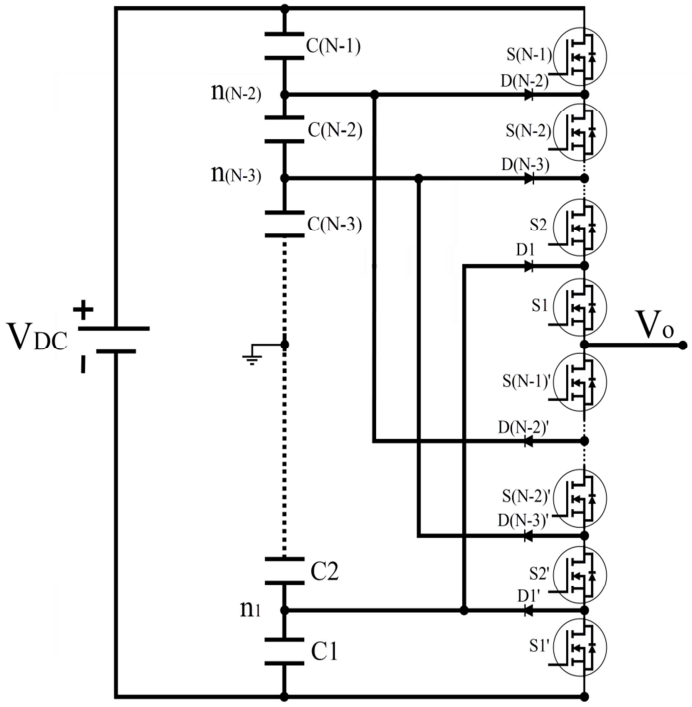

Figure 9: One leg of an NPC inverter has N-levels output voltage

Figure 10 shows the five-level diode-clamped inverter topology. In the five-level circuit, the DC-bus voltage is split into five levels by four series- DC-link capacitors, C1, C2, C3, and C4. For DC bus voltage (V_{DC}), the voltage across each capacitor is (V_{DC}/4). The key components are (D1, D1'), (D2, D2'), and (D3, D3'). These diodes clamp the switch voltage to a quarter or half of the DC-link voltage. For output voltage level (Vo = V_{DC}/2), turn on all upper switches (S1–S4). For output voltage level (Vo = V_{DC}/4), turn on

three upper switches (S1–S3) and one lower switch S4'. For output voltage level (Vo = 0), turn on two upper switches (S1–S2) and two lower switches (S3'–S4'). For output voltage level (Vo = $-V_{DC}/4$), turn on one upper switch (S1) and three lower switches (S2'–S4'). For output voltage level (Vo = $-V_{DC}/2$), turn on all lower switches (S1'–S4').

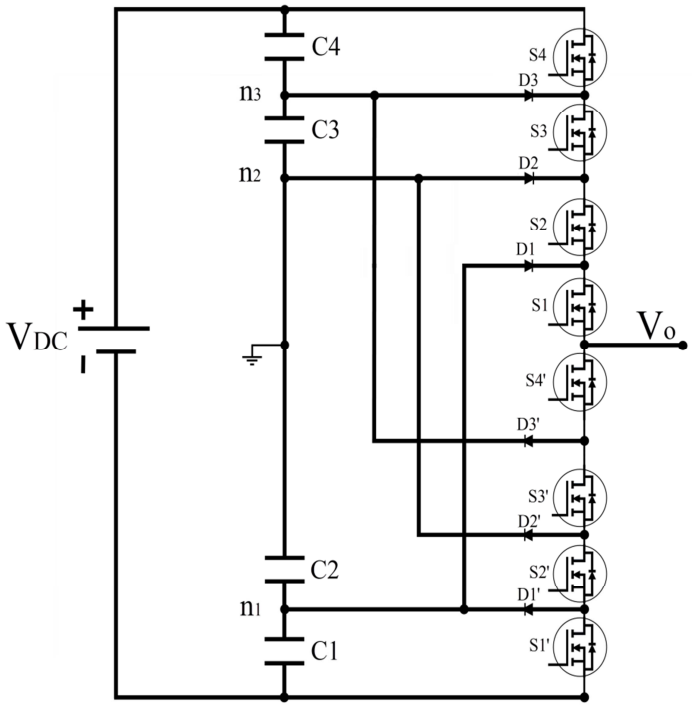

Figure 10: Topology of five-level NPC inverter

I.3.1.2 Flying Capacitor Multilevel Inverter

Figure 11 shows the N-level flying capacitor structure. The structure of the flying capacitor inverter is similar to the NPC inverter except that instead of using clamp diodes, capacitors are used instead of clamp diodes to act as floating voltage sources from which it derives the name floating capacitor inverter. N-level flying capacitor inverter has: 2(N – 1) power electronic switches, (N – 2) floating capacitors, (N – 1) DC-link capacitors, where the voltage across each DC-link capacitor = (V_{DC}/ N-1) [18].

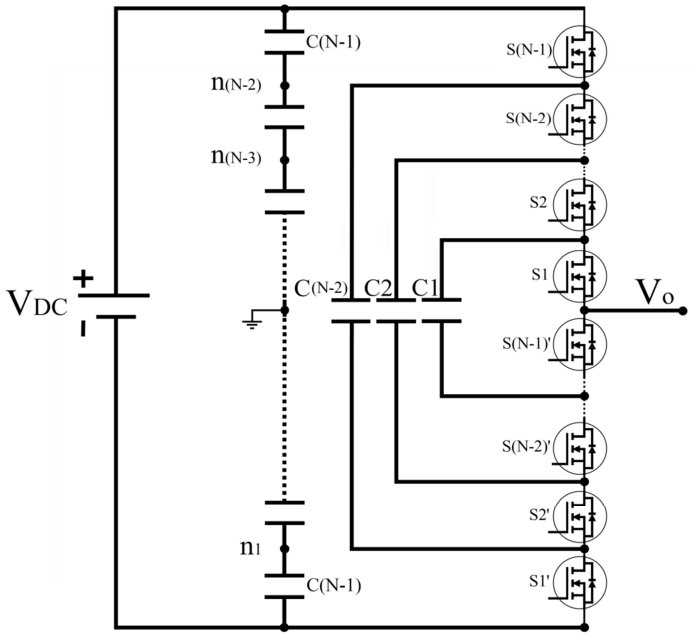

Figure 11: One leg of an FC inverter has N-levels output voltage

Figure 12 shows the five-level flying capacitor inverter topology. In the five-level circuit, the DC-bus voltage is split into five levels by four series- DC-link capacitors, C1, C2, C3, and C4. For DC bus voltage (V_{DC}), the voltage across each capacitor equal to ($V_{DC}/4$).

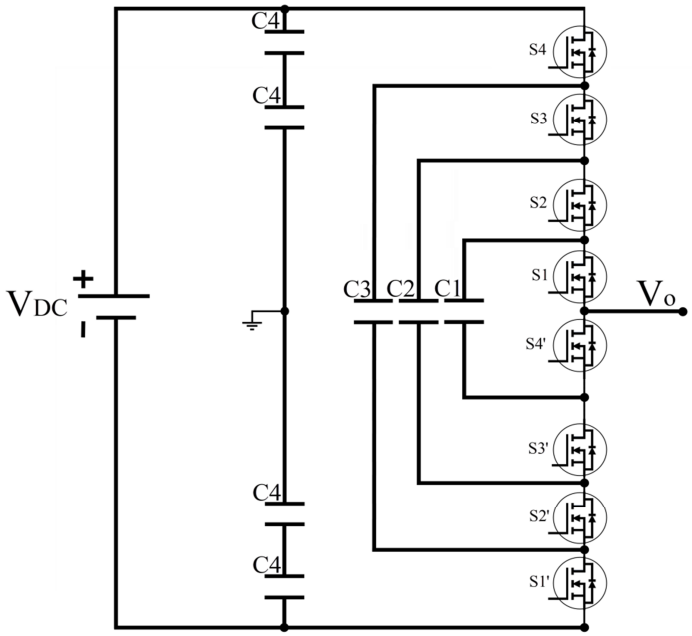

Figure 12: Topology of five-level FC inverter

I.3.1.3 Cascade H Bridge Multilevel Inverter

The N-level cascaded H-bridge inverter has: 2(N – 1) power electronic switches, ((N–1)/2) DC source [18]. Figure 13 shows the 5-level cascaded H-bridge structure.

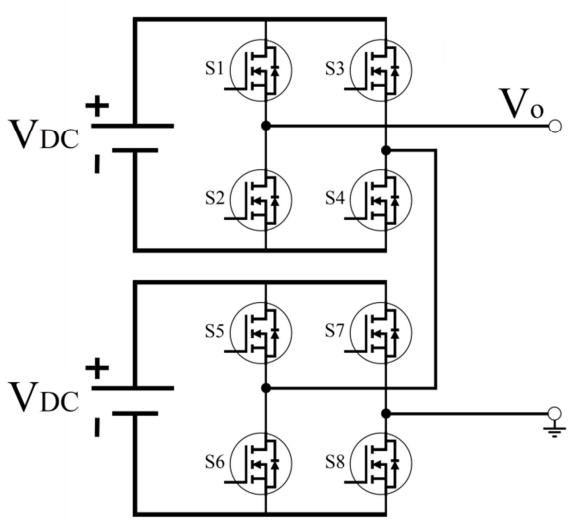

Figure 13: Topology of five-level cascaded H-bridge inverter

I.3.2 Emerging technologies of a single-phase multilevel inverters

Emerging inverters attracted a lot of attention from researchers, especially with the increasing demand of electrical energy. There are many advanced topologies [19]. The recently discussed topologies in the literature are mentioned in this section.

I.3.2.1 Modular multilevel inverters

The modular multilevel inverter is an interesting topology for High-quality, high-power applications due to simplicity and easy control. Also, using the High-switching modulation technique for driving the modular multilevel inverter is quite simple and offers many advantages; a historical review of the modular multilevel inverter is presented in [20]-[21]. The connection of Half-bridges or Full-bridges in cascade is the most preferred method for designing a modular multilevel inverter.

I.3.2.2 Reduced device count multilevel inverters

Recently decades, this structure is developed to overcome the conventional inverters problems, and the purpose is to achieve specified-levels output voltage using less

number of power electronic components (less number of switching devices, less number of gate drivers, less number of *DC* power supplies, less number of power capacitors,…etc.) [18], [22]. Figure 14 shows an example of a single-phase reduced device count multilevel inverter, composed of 10 *MOSFETs* switches, 04 *DC* power supplies, and ten gate drivers. The values of DC-link voltages are 1:2:3:4, and the maximum synthesized voltage equals 21-Levels [18].

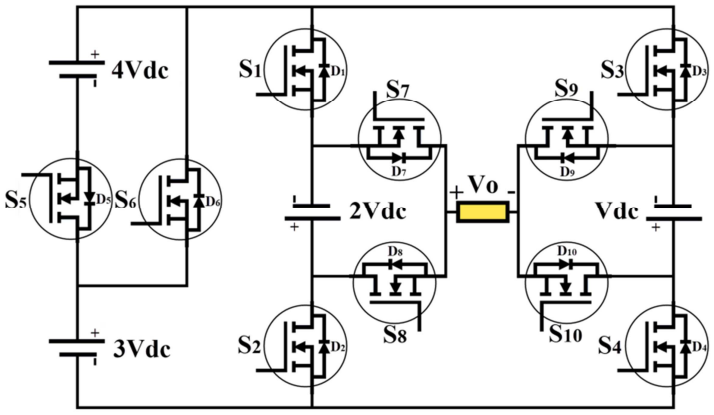

Figure 14: 21-levels inverter structure with less number of devices

I.3.2.3 Single source multilevel inverters

Single source multilevel inverters are suitable for renewable and sustainable energy systems; this structure has many advantages over the Multiple-DC-Source multilevel inverter. The lower cost is one of the most benefits. For generating specified-levels voltages, the single source multilevel inverter is based on some DC-link capacitors. The most critical challenges are the design of DC-link capacitors and control of charge/discharge [23], [24].

I.3.2.4 Trinary Hybrid Multilevel Inverters (THMI)

Trinary hybrid multilevel inverter (*THMI*) is a particular type of cascaded N-level inverter, where the values of DC-link voltages are $1:3:\ldots:3^{a-1}$, *a*: is the number of Half-bridges HBs. The maximum voltage achieved by this type of inverters is 3^a [25]. Figure 15 shows an example of single-phase *THMI* with *3*-HBs. The values of DC link voltages are 1:3:9, and the maximum synthesized voltage equals 3^3= 27-Levels.

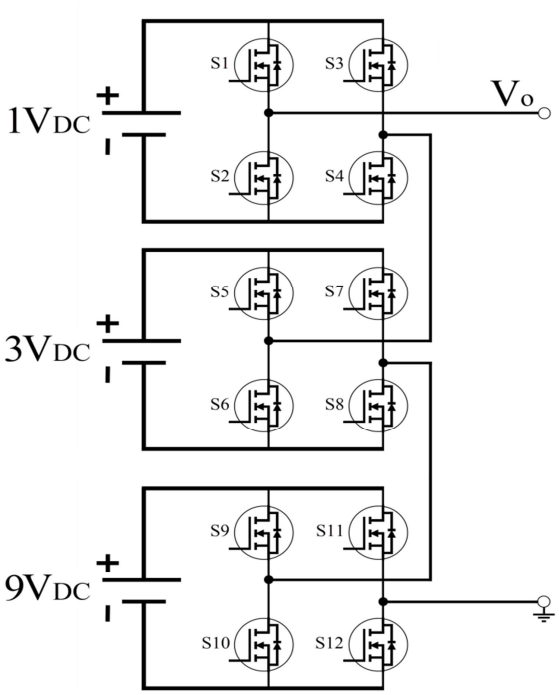

Figure 15: 27-levels Trinary Hybrid Multilevel Inverter (THMI) structure

I.3.2.5 Softs witched multilevel inverters

Switching is (turn-on/turn-off) of electronic devices; it plays a critical part in the power electronics field. Soft-switching means reducing losses associated with the switching operation; it can be achieved during turn-on or turn-off or during both (turn-on/turn-off). The differences between the switching types are shown in Figure 16. In (a): The hard switching is traditional; in this case, the switches are turn-off with a full-load current and turn-on with full-voltage; this type creates high power losses and heat of switches; this type can damage the power switches. (b): Soft-switching is a high-quality technique; its aim was to overlap the voltage and current waveforms using an external circuit. These techniques of soft-switching take their place in the emerging multilevel inverter because of the mentioned advantages, where many soft-switching control studies have been proposed [26]-[28].

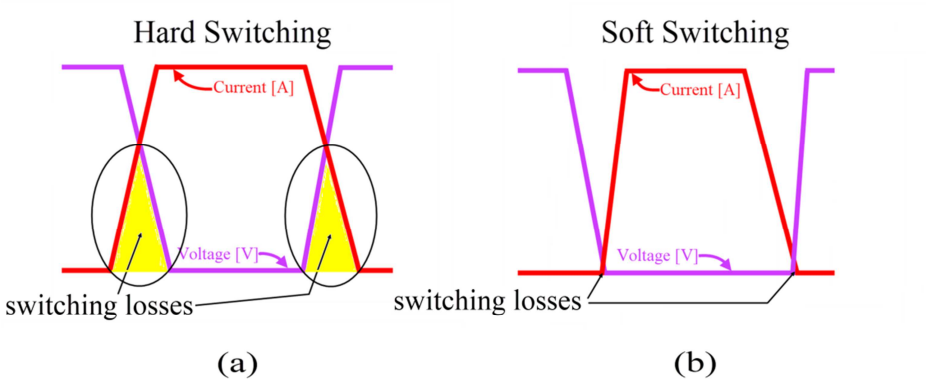

Figure 16: The switching of electronic devices. (a): Hard switching, (b): Soft switching.

I.3.2.6 Symmetrical and asymmetrical multilevel inverters

Symmetrical and asymmetrical multilevel inverters have been developed for achieving a high-power and high-level voltage in electrical power systems. These inverters offer many advantages compared to the conventional 2-level inverters. There is one essential element for differences between the asymmetrical inverter from the symmetrical, i.e., *DC* sources. In the symmetrical multilevel inverter structure, the magnitude of the DC-link is identical for each source. However, in the asymmetrical multilevel inverter structure, values of DC links are unequal [29].

I.4 Modulation Strategies for single-phase multilevel inverters

The modulation is defined as a methodology or technique to generate the gating pulses for semiconductor devices; two operation modes exist, ON and OFF states. Under the ON state, the switch is in the saturation region (conducting mode). On the other hand, during the OFF state, the switch is in the cutoff region (stops conducting). The output voltage is proportional to the pulse width value, where the pulse width is the elapsed time between the rising and falling edges of a single pulse. In this section, the basic modulation strategies for single-phase multilevel inverters are mentioned. There are two types of modulation based on switching frequency, the fundamental-switching frequency modulation and the High-switching frequency modulation [30]. Figure 17 illustrates the classification of modulation strategies.

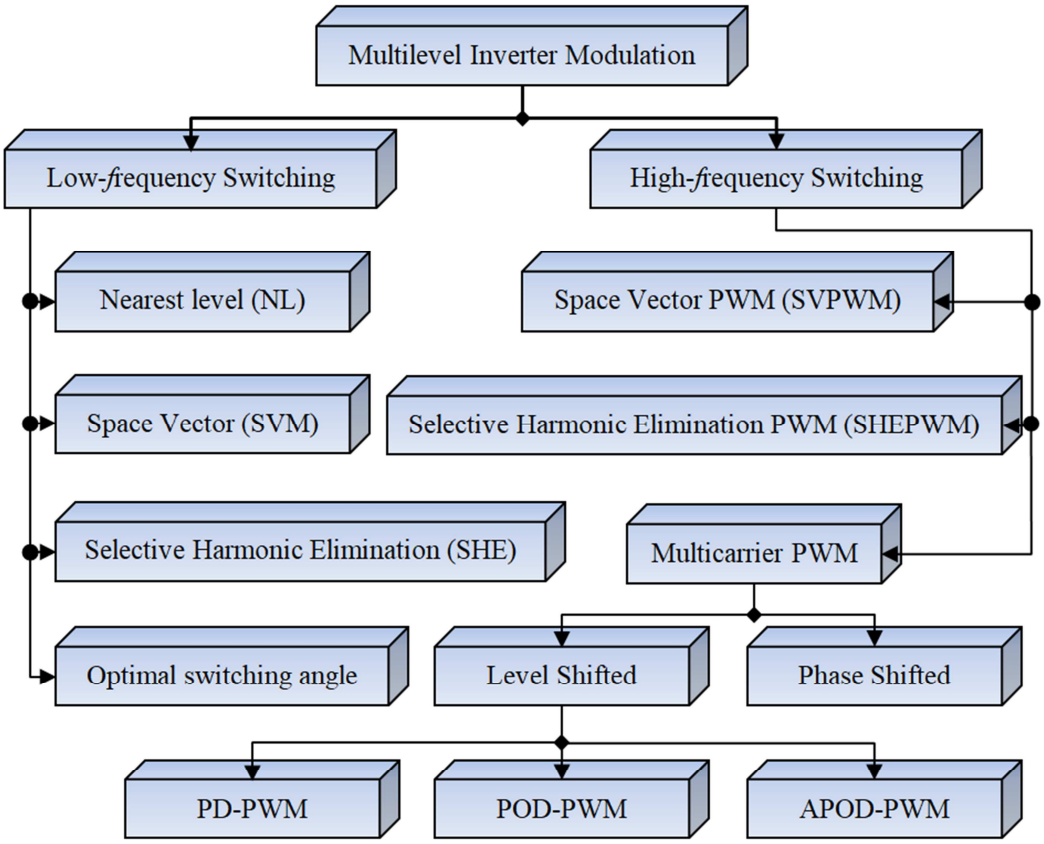

Figure 17: Modulation strategies of Multilevel Inverters

I.4.1 Fundamental frequency switching modulation

The low-frequency modulation techniques based on the Fundamental-switching frequency (60 Hz or 50 Hz) are the most preferred methods for driving high-power multilevel inverters, such as nearest level (*NL*) modulation, space vector modulation, selective harmonic elimination (*SHE*) modulation, and optimal switching angles modulation [30], [31].

I.4.1.1 Nearest level (NL) modulation

Nearest-level modulation is a popular technique used in multilevel inverters; due to its flexibility and ease of implementation, it is suitable for any N-level inverter. The nearest level modulation is rounding the nearest voltage level, which compares the reference wave with inverter output voltage levels. For implementing this modulation technique, we can define three stages. (1): In the first stage, the reference wave is compared and sampled. (2): In the second stage, the result value is rounded near the

nearest voltage level. (3): Third stage, the design of the lookup table for switching the inverter. Figure 18 illustrates the principle for working the *NL* technique.

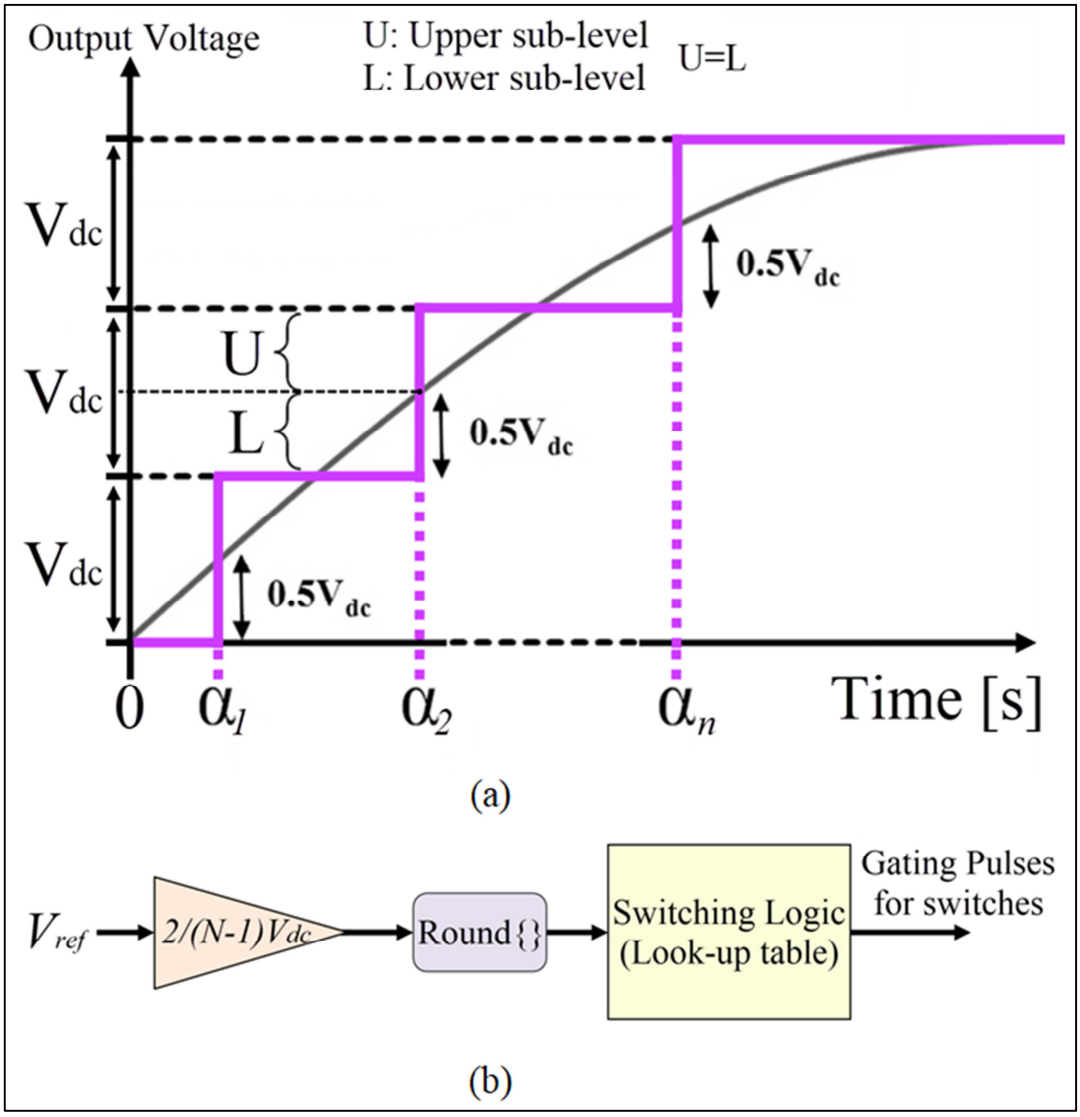

Figure 18: Nearest level modulation scheme

I.4.1.2 Space vector modulation (SVM)

Space Vector Modulation (*SVM*) is a modulation technique used to apply a given voltage vector to a load. The principle of this technique is to determine the duty cycles for controlling the switches of an inverter and synthesize a required modulated output voltage without the use of a carrier waveform. *SVM* offers easy digital implementation and better performance of an optimal output voltage/current to reduce total harmonic distortion *THD* [32].

I.4.1.3 Selective harmonic elimination (SHE)

The principle of the Selective harmonic elimination (*SHE*) technique is based on the calculation of switching angles for driving a multilevel inverter, thus are determined by solving a transcendental system of non-linear equations. Moreover, *SHE* requires many mathematical acknowledgments for solving non-linear equations, which is usually very difficult. Various approaches can solve the equations, including algebraic methods, Newton-Raphson (*NR*) algorithm, genetic algorithm (*GA*) … etc. The switching time required to achieve the desired switching angle is stored in the lookup table in the memory of the digital controller, and output pulses are generated using standard *PWM* modules. The complexity of *SHE* depends on the number of inverter levels [33].

I.4.1.4 Optimal switching angle modulation

Optimal switching angle modulation technique also called Optimized Harmonic Stepped Waveform (*OHSW*). The principle of the *OHSW* method is searching for the best switching angles to drive the multilevel inverter, with the primary objective of minimization of the total harmonic distortion or reduce specified order harmonics. The *THD* value can be established as an objective function and transcendental nonlinear equations. Various algorithms can be used to calculate the optimal switching angles, where the metaheuristic algorithms are proved their high effectiveness, including genetic algorithm (*GA*), Particle Swarm Optimization (*PSO*) [34].

I.4.2 High frequency switching modulation

The high-frequency modulation techniques based on the switching frequency (>1kHz) are popular methods for driving multilevel inverters, wherein these techniques have several switching angles at each level. The popular high-frequency modulation techniques are space vector pulse width modulation (*SVPWM*), selective harmonic elimination pulse width (*SHEPWM*) modulation, and Multi Carrier-based pulse width modulation (*SPWM*) [30].

I.4.2.1 Space vector pulse width modulation (SVPWM)

The principle of Space vector pulse width modulation (*SVPWM*) is the same as the low-switching *SVM*. Still, The *SVPWM* is very complex for multilevel inverters; the complexity is associated with the number of levels. *SVPWM* is high-quality modulation

because it enables efficient use of *DC* voltages. The most benefits of using this technique are the low *THD* and Low switching losses in high-frequency [32].

I.4.2.2 Selective harmonic elimination pulse width modulation (SHEPWM)

Selective harmonic elimination pulse width modulation (*SHEPWM*) is a high-frequency modulation technique. The objective is to eliminate unwanted harmonics as the low switching *SHE* method, but *SHEPWM* is complex; there are many switching angles to be calculated. Each output level voltage has many switching angles in one period cycle [33].

I.4.2.3 Multi Carrier based pulse width modulation (SPWM)

Multicarrier *PWM* modulation is the popular technique to produce the gating pulses of the multilevel inverter. The principle of this technique is the comparison of reference waveform (generally sine wave) with carrier waveforms to produce the gating pulses. Multicarrier *PWM* modulation can generate a high-quality signal, where the output voltage/current waveform appears as close as the sinusoidal. There are two types of Multicarrier *PWM* modulation depending upon the position of the carrier waveforms, namely: (1): Level shifted (*LS-PWM*). (2): Phase shifted PWM (*PS-PWM*). Also, there are three alternative *PWM* strategies for shifting of level: (a): Phase disposition (*PD*). (b): Phase opposition disposition (*POD*). (c): Alternate phase disposition (*APOD*) [32], [35].

(1): Level shifted (*LS-PWM*), in the *LS-PWM* technique, the carriers are equal in amplitude (peak to peak amplitude), same frequency, and phase, but they differ in their levels of biasing. (2): Phase shifted PWM (*PS-PWM*), in *PS-PWM* technique, the carriers are equal in amplitude and frequency, but they have phase differences with each other. (a): Phase disposition (*PD*), all carriers waveforms are in phase. (b): Phase opposition disposition (*POD*), all carriers waveforms above zero reference are in phase, and all carriers waveforms below the zero reference are 180 degrees out of phase. (c): alternate phase dispositions (*APOD*), all carrier waveforms (above and below zero) reference are 180 degrees out of phase compared to their neighboring carrier [35]. Figure 19 illustrates the discussed 04 cases of Multicarrier *PWM* modulation techniques for a five-level inverter. (a): Phase shifted PWM (*PS-PWM*) modulation. (b): waveform of the Five-level output voltage using (*PS-PWM*). (c): Level shifted (*LS-PWM*) modulation based on Phase disposition (*PD*). (d): waveform of the five-level output voltage using (*PD-LS-PWM*). (e):

Level shifted (*LS-PWM*) modulation based on phase opposition disposition (*POD*). (f): waveform of the five-level output voltage using (*POD-LS-PWM*). (g): Level shifted (*LS-PWM*) modulation based on alternate phase opposition disposition (*APOD*). (h): waveform of the five-level output voltage using (*APOD-LS-PWM*).

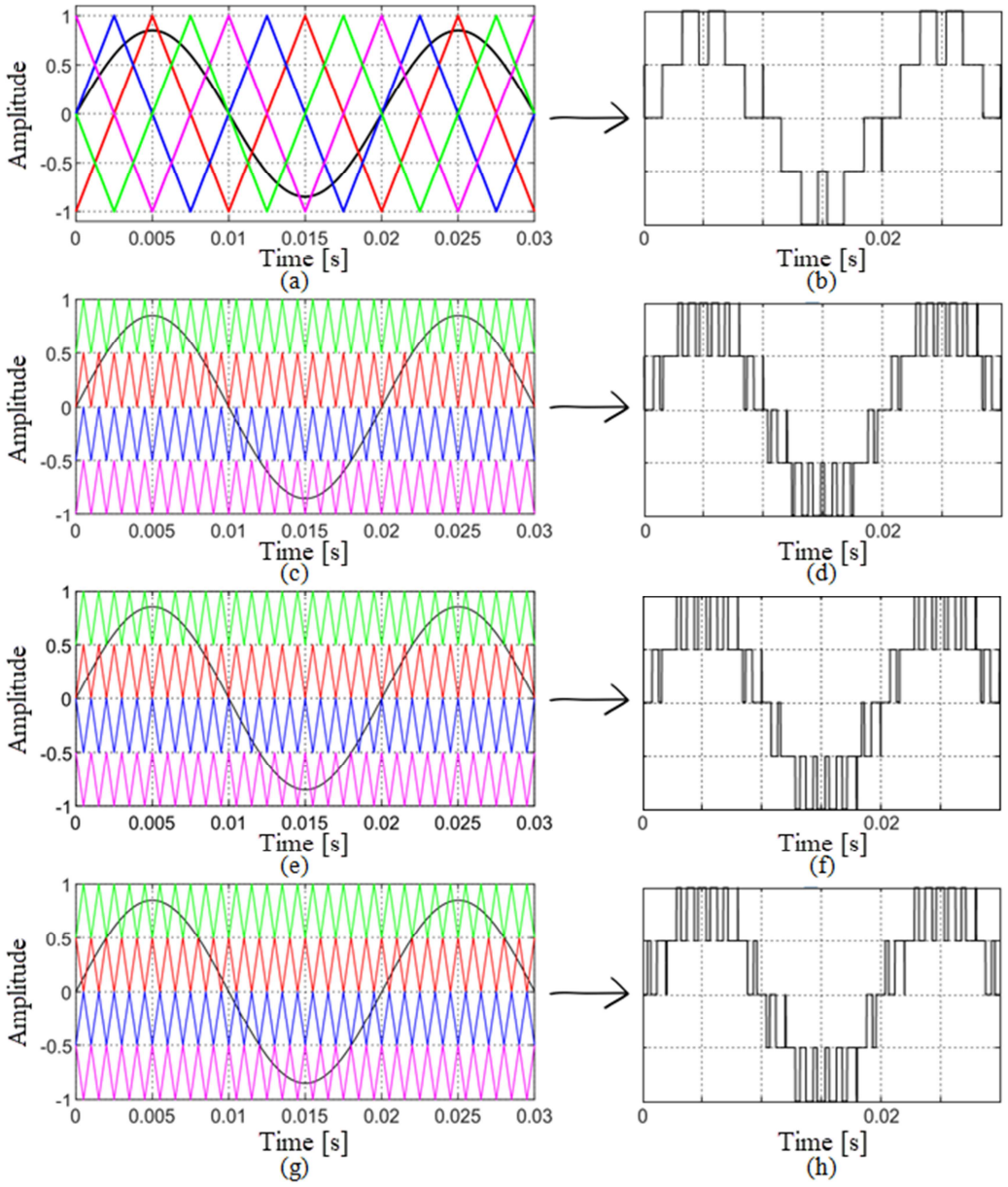

Figure 19: Multicarrier PWM modulation techniques

I.5 Well known application fields of inverters

Recently, the multilevel inverter has been proposed for many industrial applications and electrical systems, including the transmission of energy, robotic domain,

power supplies (*PS*) technologies, Wireless power transfer, *AC* motor drives, Emergency power supplies, *HVDC* transmission line, and Speed control of electrical machines. … etc.

I.5.1 Renewable energy systems

The most renewable energy sources are solar energy, wind energy, hydro energy, geothermal energy, biomass energy. The multilevel inverter finds its diverse uses in most renewable energy systems as well as produces Direct Current (*DC*), which then needs to be converted to Alternating current (*AC*) mode because most systems work in *AC* mode; this task of inverters [36]. Figure 20 shows solar panels with *DC-DC-AC* converter and batteries for household appliances. (1): Solar panels. (2): *MPPT DC/DC* converter and *DC/AC* converter regulator. (3): Battery. (4): Example of household appliances.

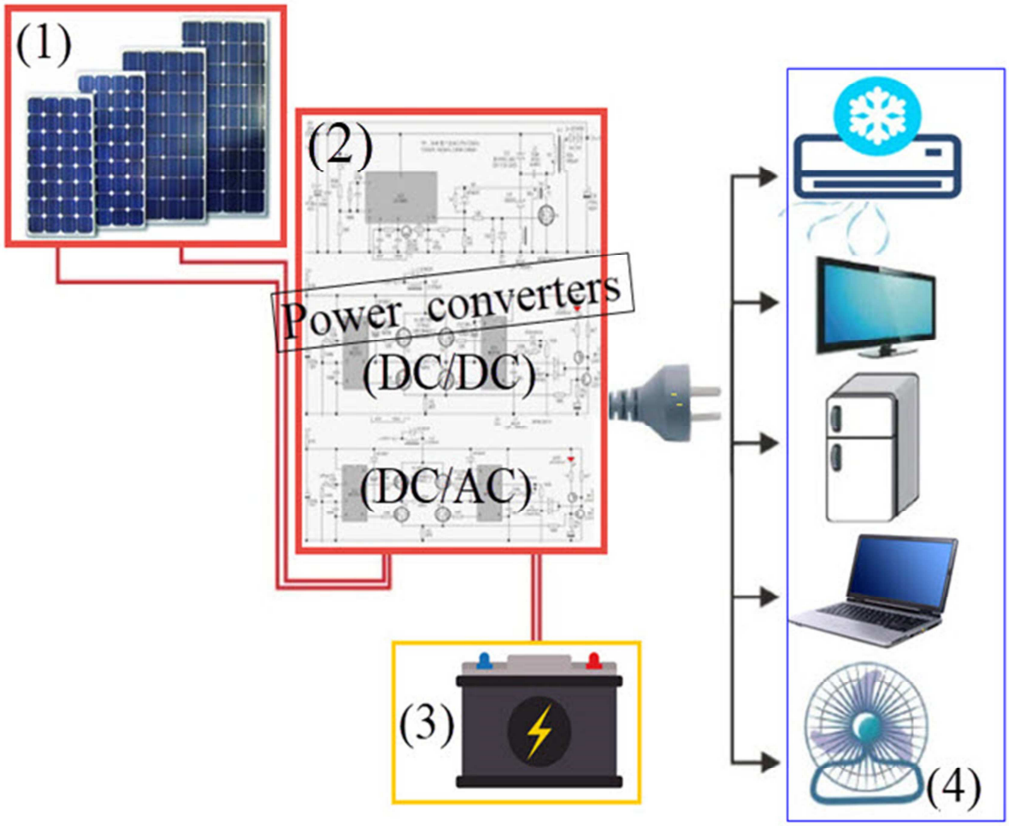

Figure 20: Solar panels with DC-DC-AC converter and batteries for household appliances [15].

I.5.2 Applications related to the transport sector

An inverter is a device used to convert direct current *DC* into alternating current *AC*; it can adjust the speed of motors by controlling the frequency of the alternating

current. So, the inverter is suitable for transport applications, electric vehicles, railway transport such as *TGV* or tramways [37].

I.5.3 Distributed generation systems (DGS)

The distributed generation systems (*DGS*), also known as district/decentralized energy systems. Distributed generation means a combination of various technologies that generate electricity at or close to the location of its use. The common *DGS* include solar panels, small wind turbines, fuel cells, *DC-DC* converters, *DC-AC* converters, Filters. *DC-AC* converter plays a significant role in the *DG* system. The *DGS* has been attracted a lot of attention from researchers because of its advantages, such as stability of electrical energy production, fewer power losses, and less cost compared to centralized generation systems [38].

I.5.4 Industrial manufacturing process

The multilevel inverter is suitable for many industrial applications, and some examples include induction heating systems, heat treatment of metals by melting and welding [39]. Also, the multilevel inverter can be used in robot arm drive, pumps, compressors, conveyors, extruders, crushers, fans, grinding, mixers, rolling mills, mine hoists [40], [41].

PART. II Overview about controller actions and control techniques for power electrical systems

II.1 Classification of controller actions for closed-loop systems

Controllers are a fundamental part of control engineering; it aims to reduce the difference between the actual value and the desired value of the system, there are 03 main controller actions and other type actions can be designed based on these mains. With the correct design of the converter elements, PI controller has been widely used in the industry for its simplicity and low cost. Each controller action has a specific use case. You cannot just insert any controller type at any system and expect good results; there are some conditions that must be respected.

II.1.1 The proportional (P) action controller

Proportional action refers to the term given to a controller's action when the output signal is proportional to the difference between the desired and measured values. The proportional controller can reduce the steady-state error, reduce the rise time, have small effects on settling time, and increase the overshoot. The proportional controller has one adjustable parameter, i.e. *Kp*. If (*Kp* is small) then (the controller is sluggish), else (the controller is aggressive). The aggressive controller is causing the oscillation of the system. The sluggish controller is causing the lags and dead time. The transfer function of the proportional (*P*) action controller is: $\boldsymbol{G}(s)=Kp$ [42], [43].

II.1.2 The integral (I) action controller

The integral *(I)* action controller makes it possible to consider the control history of the system by performing the integral of the variation of the difference between the measured output and the set-point over time. An integral controller can decrease the steady-state error that occurs with a proportional controller, decrease the rise time, increase the overshoot, increase the settling time. Integral *(I)* control action is expressed with transfer function as follows: $G(s)=Ki/s$ [44], [45].

II.1.3 The derivative (D) action controller

The derivative *(D)* controller action makes the system more stable. It can make a small change to the rise time, decrease the settling time, and decrease the overshoot, but it does not affect the steady-state error. Derivative action cannot be used by itself. The transfer function of the derivative *(D)* action controller is: $G(s)=K_D S$ [46].

II.1.4 Other types of controller actions PI, PD, PID, I-PD, PI-PD, PI^{λ}, $PI^{\lambda}D^{\delta}$

Proportional, integral, and derivative controller actions are used both singly and in combination with each other. Other types of controller actions can be implemented, such as *PI*, *PD*, *PID*, *I-PD*, and *PI-PD* controllers [47], [48]. Furthermore, fractional-order controllers PI^{λ}, $PI^{\lambda}D^{\delta}$ are based on the fractional calculus. Fractional calculus is a purely mathematical problem dealing with integrals and derivatives of non-integer orders. The modeling of natural physical systems by differential equations based on fractional derivatives is becoming the focus of many studies. Developing efficient methods to solve these equations numerically has been getting more and more attention during recent years. Various methods based on Grünwald-Letnikov, Caputo, or Riemann-Liouville definitions have been suggested and investigated. The simulation and the implementation of a fractional-order physical system require its approximation by a transfer function of integer-order finite-dimension. In recent years, several approximation methods have been developed using continuous rational models, including Carlson's approach, Oustaloup's method, Matsuda's method, Charef's method. In 1999, Podlubny proposed a Fractional Order Proportional Integral Derivative *FOPID* to improve the controller actions performances by adding two extra real parameters, α to the integral-action controller and β to the derivatives-action controller [49], [50].

II.2 List of a popular classical-control techniques

Classical-control techniques have been widely used for its simplicity and low cost. These Classical techniques require a full knowledge of the model for good efficiency and maintain control performance in the case of small variations in the nominal values of the system elements [51].

II.2.1 The Ziegler-Nichols method

In the industry, Ziegler-Nichols (Z-N) method is the most known and the most

widely used method for tuning of controllers, also known as an ultimate gain tuning method; Ziegler and Nichols first proposed it in 1942. The Z-N method is based on the trial-and-error principle. The advantage of the Z-N method is that it's performant and easy for simple process control. The disadvantages of this technique are: tuning quality is very sensitive to the non-linearities of the system, computing time because the principle is trial and error calculation [52], [53].

II.2.2 The Cohen-Coon method

The Cohen-Coon method is based on the Z-N method, with uses of more information from the system to tuning the controller parameters. This method has significantly better control performance compared to Z-N method [52].

II.2.3 Internal Model Control (IMC) technique

The internal Model Control (*IMC*) technique is a well-known and widely used method for tuning controllers in the industrial process. Morari and Garcia have developed IMC in 1982. The *IMC* presents a methodology for designing Q-parameterized controllers. Note that the Q-parameterization concept plays an essential part in the design of many modern control techniques. *IMC* technique has acceptable performance for controlling the common processes but requires a sufficiently accurate system model [54], [55].

II.2.4 Coefficient Diagram Method (CDM)

In dynamic system control, the coefficient diagram method (*CDM*) is an algebraic approach used to design the controller parameters; Prof. Shunji Manabe developed this method in 1991 [56]. The most considerable advantages of the *CDM* technique are: (1): Straightforward and easily understandable. (2): Useful method for control any system. (3) There are relations between the desired performances (the time response, stability, and robustness) and the coefficients of the controller polynomials; for this reason, this technique can be combined with any optimization search algorithm for adjusting the controller parameters. In literature, many control systems have been designed successfully using the coefficient diagram method.

II.3 List of a popular advanced-control techniques

In literature, many advanced-control techniques have been proposed to improve the

efficiency of systems and to overcome the problem of finding the optimal values of the classical-control techniques under real operating conditions. Robust control, adaptive control, predictive control and fuzzy logic control techniques are commonly utilized to handle modeling parameter uncertainties and changing system properties [50], [57]. Also, the genetic algorithm [58], a Single Memory Neuron (*SMN*) to adapt parameters of the *PID* [59], Robust adaptive *PI* controller [60], PI controller optimization through various metaheuristic algorithms [61], a hybrid particle swarm optimization and gravitational search algorithm (*PSO–GSA*) to tune the parameters of (*PI*) controller [62], Fuzzy logic [63], Artificial Neural Networks for the *PID* using a single neuron [64] and others.

II.3.1 Adaptive techniques

The high-quality techniques for designing control systems are based on a good analysis of the system under various step changes and disturbances of its environment. In the control theory area, adaptive is one of the advanced control techniques; adaptive controls denote the ensemble of methods allowing the real-time automatic adjustment of the controller parameters. There are several schemes for designing an adaptive control system, yet for the same aim, to achieve or maintain a desired level of performance by making the model output follow the desired trajectory. Adaptation occurs at the level of the controller parameters (adjustments of parameters) or directly at the level of the command signal to satisfy or enhance a predefined performance index through an adaptation mechanism [57], [60].

II.3.2 Model Predictive Control (MPC) techniques

The Model Predictive Control (*MPC*) techniques are well-known and widely accepted methods for process control in the industry. In the *MPC* technique, the model of the system is required to predict the future behavior of the variables, where the predictions are evaluated using a configured cost function for obtaining the future control actions. The most popular *MPC* techniques are Generalized Model Predictive Control (*GMPC*), Explicit Model Predictive Control (*EMPC*), Optimal Switching Vector *MPC* (*OSV-MPC*), Optimal Switching Sequence *MPC* (*OSS-MPC*). Model predictive techniques are beneficial for multivariable processes, and it is also found wide acceptance for treating dead time of systems. As a drawback, some predictive model techniques are complex for their formulation and implementation design; also, *MPC* is sensitive to errors of the

process model [55], [57], [65].

II.3.3 Intelligent control techniques

Intelligent control techniques use various Artificial Intelligence (*AI*) computing approaches to control a dynamic system. Currently, Intelligent control techniques received many attentions of researcher because there advantages and benefices for process control. Intelligent control techniques have good performance and maintain control performance in the case of large variations. In literature, many techniques have been proposed, the popular are: artificial neural networks, fuzzy logic, genetic algorithms [66]-[68].

II.3.4 Swarm intelligence and optimization algorithms

Swarm intelligence and optimization algorithms are part of the artificial intelligence (*AI*) area. These *AI* algorithms are used in huge applications domain because there advantages, like the high efficiency for solving complex and non-linear systems, decentralized and robust control because the objective is always completed, and these techniques do not require the order of execution. In the control theory, the (*AI*) techniques guide the search process; it aims to find the optimal parameters for controlling a system with an efficient exploration of the defined search space. In the literature, we can find many developed algorithms as Particle Swarm Optimization (*PSO*), Bat Algorithm (*BA*), Ant Colony Optimization (*ACO*), Grey Wolf Optimizer (*GWO*), Artificial Bee Colony (*ABC*), Salp Swarm Algorithm (*SSA*), and Gravitational Search Algorithm (*GSA*) [69], [70].

II.3.5 Hybrid advanced techniques

Hybrids advanced techniques refer to the combination of the previous intelligence methods and techniques. Hybrids advanced techniques are preferment and optimal control techniques; it combines the advantages of the used algorithms and techniques. In literature, many Hybrid advanced techniques have been proposed; the popular are Neuro-fuzzy algorithms, Adaptive neural network control, a hybrid particle swarm optimization and gravitational search algorithm (PSO–GSA), fractional-order controller based on swarm intelligent technique like the $PI^{\lambda}D^{\delta}$-based on *PSO* control technique, $PI^{\lambda}D^{\delta}$-based on *GWO* control technique, $PI^{\lambda}D^{\delta}$-based on *GA* control technique [71]-[73].

2.4 Positioning of our work according to the state of the art

The literature review permitted us to select: (1): The five-level inverter topology with a low number of switching devices. (2): a series resonant *RLC* circuit for implementing a new converter, i.e. the five-level series resonant inverter. (3): Small signal modeling for the mathematical presentation of the inverter. (4): The selective harmonic elimination (*SHE*) for the modulation strategy. (5): The *CDM* method, the adaptive technique, the fractional-order controller (PI^{λ}) based on *GA*, and the fractional-order controller (PI^{λ}) based on *PSO* algorithm are selected control techniques for implementing the proposed small-signal model of the five-level series resonant inverter. We discussed the selected topology, the modulation strategy, the small-signal modeling, and the different control techniques in detail in the next chapters.

(1): Criteria for choosing a five-level topology: The half-bridge and Full-bridge are the conventionally implemented topologies of resonant inverters. In our study, we have chosen a multilevel topology for implementing resonant inverter, i.e., the five-level reduced switches topology. The five-level inverter topology with a reduced number of switches is an emerging type of multilevel inverter (*MLI*) with several advantages compared to conventional topologies. The benefits include the low *THD* and the low total standing voltage *TSV*; complementary switches can also increase the voltage easily.

(2): Criteria for choosing a series resonant circuit: As mentioned in state of the art, there are 03 basic types of the resonant circuit: the series, the parallel, and the series-parallel. In the series resonant type, the controllable state is the output capacitor voltage; in the other part, the controllable state is the current in the parallel and series-parallel types. Moreover, the resonance is an attractive physical phenomenon, where the controllable state will be amplified, so the experimental implementation of a resonant circuit requires a specified efficiency and quality of power electronic components, capacitance, and inductance. In our study, we are choosing the series resonant inverter because we are limited with the available equipment's and electronic components for the experimental tests, where the work with a voltage-mode control using the controllable state "voltage" is easy compared to the work with a current-mode control using the controllable state "current".

(3): Criteria for choosing small-signal modeling: The resonant inverters,

including our proposed five-level series resonant inverter, are special converters types. The analysis and the modeling of the resonant converter are not easy. On the other hand, a small-signal technique transforms the non-linear model of the circuit to a large signal model and then linearizes around an operating point. After that, the developed small-signal model will be validated in frequency and time domains. So, the small-signal technique is a very efficient and practical method for generating a linear time-invariant (*LTI*) model of any non-linear circuit. The validation step of the *LTI* model concludes the accuracy of the small-signal technique.

(4): Criteria for choosing the selective harmonic elimination (SHE) modulation: selective harmonic elimination is a popular modulation strategy; we use *SHE* to eliminate the third-order harmonic because of their drawback and influence in the system. The third-order harmonic is the most unwanted harmonic order because it is responsible for the over-current generation and overheating of the circuit.

(5): Criteria for choosing the control techniques: Based on the literature overview, we suggest the following control methods: the Coefficient Diagram Method (*CDM*), the Model Reference Adaptive Control (*MRAC*), the GA-based PI^{λ} controller, the PSO-based PI^{λ} controller. The *CDM* and *MRAC* methods are easy and simple methods, which proved their efficiency, stability, and usability in several closed-loop systems. The two methods require the known of the plant model for design the control system. The control methods based on the intelligent algorithms are advanced control techniques that provide high-performances; they can be implemented with less information about the plant and do not require the plant model for tuning the control parameters. Currently, the intelligent algorithms are very interesting and effective methods for solving many simple or complex optimization problems in several subject areas. The *GA* and *PSO* are the popular algorithms as shown in Tables 1, 2 and Figures 19, 20.

On Wednesday, October 27, 2021, A.E. Toubal Maamar was granted access to Scopus-Elsevier database by *CERIST-SNDL* for searching of the sentences “genetic algorithm; ant colony algorithm; particle swarm optimization; simulated annealing; differential evolution; artificial bee colony; firefly algorithm; harmony search, cuckoo search; jaya algorithm; grey wolf optimization”, where the search was done within article title option and the data are selected from 1990 to 2021. In several subjects’ areas, the Scopus database shows 64929 document results use the sentence “**genetic algorithm**”,

5413 document results use the sentence "**ant colony algorithm**", 24928 document results use the sentence "**particle swarm optimization**", 8080 document results use the sentence "**simulated annealing**", 9564 document results use the sentence "**differential evolution**", 3692 document results use the sentence "**artificial bee colony**", 2121 document results use the sentence "**firefly algorithm**", 2099 document results use the sentence "**harmony search**", 2038 document results use the sentence "**cuckoo search**", 841 document results use the sentence "**grey wolf optimization**", 369 document results use the sentence "**jaya algorithm**". Table 4 illustrates the data of algorithms from 1990-2021, and Figure 21 shows a line graph based on the extracted data.

Table 4: Data of some popular algorithms from 1990-2021

Year	*GA*	*ACA*	*PSO*	*SA*	*DE*	*ABC*	*FA*	*HS*	*CS*	*JA*	*GWO*
2021	2417	230	1467	305	570	256	227	104	205	74	210
2020	3134	353	1808	326	678	364	240	157	274	106	232
2019	3190	349	1890	338	773	418	307	143	283	81	173
2018	3025	301	1655	349	737	406	307	171	306	67	127
2017	2759	276	1590	302	629	335	227	159	259	30	55
2016	2800	268	1536	319	689	360	237	195	230	11	32
2015	2689	257	1533	323	671	336	191	181	192	0	12
2014	3058	350	1703	330	679	329	170	191	140	0	0
2013	3136	379	1607	343	742	330	124	188	85	0	0
2012	3377	395	1831	363	672	269	57	179	39	0	0
2011	3429	362	1624	396	641	185	24	137	19	0	0
2010	3614	478	1745	373	562	71	7	135	3	0	0
2009	3438	394	1564	372	439	25	2	87	1	0	0
2008	3084	341	1126	327	300	3	1	26	0	0	0
2007	2793	193	862	286	203	4	0	17	0	0	0
2006	2895	214	687	303	161	0	0	7	0	0	0
2005	2457	116	364	283	94	0	0	7	0	0	0
2004	2207	80	194	224	61	0	0	2	0	0	0
2003	1738	35	72	166	48	0	0	1	1	0	0
2002	1494	29	44	168	34	0	0	2	0	0	0
2001	1293	4	8	171	34	0	0	3	0	0	0
2000	1252	4	5	187	30	0	0	0	0	0	0
1999	1117	3	5	170	20	1	0	1	0	0	0
1998	1040	2	6	160	15	0	0	0	0	0	0
1997	888	0	1	158	15	0	0	1	0	0	0
1996	880	0	0	207	10	0	0	1	0	0	0
1995	704	0	1	158	15	0	0	0	0	0	0
1994	493	0	0	165	10	0	0	2	0	0	0
1993	270	0	0	150	11	0	0	0	0	0	0
1992	139	0	0	136	10	0	0	2	1	0	0
1991	87	0	0	121	7	0	0	0	0	0	0
1990	32	0	0	101	4	0	0	0	0	0	0

Genetic Algorithm (***GA***), Ant Colony Algorithm (***ACO***), Particle Swarm Optimization (***PSO***), Simulated Annealing (***SA***), Differential Evolution (***DE***), Artificial Bee Colony (***ABC***), Firefly Algorithm (***FA***), Harmony Search (***HS***), Cuckoo Search (***CS***), Jaya Algorithm (***JA***), Grey Wolf Optimization (***GWO***).

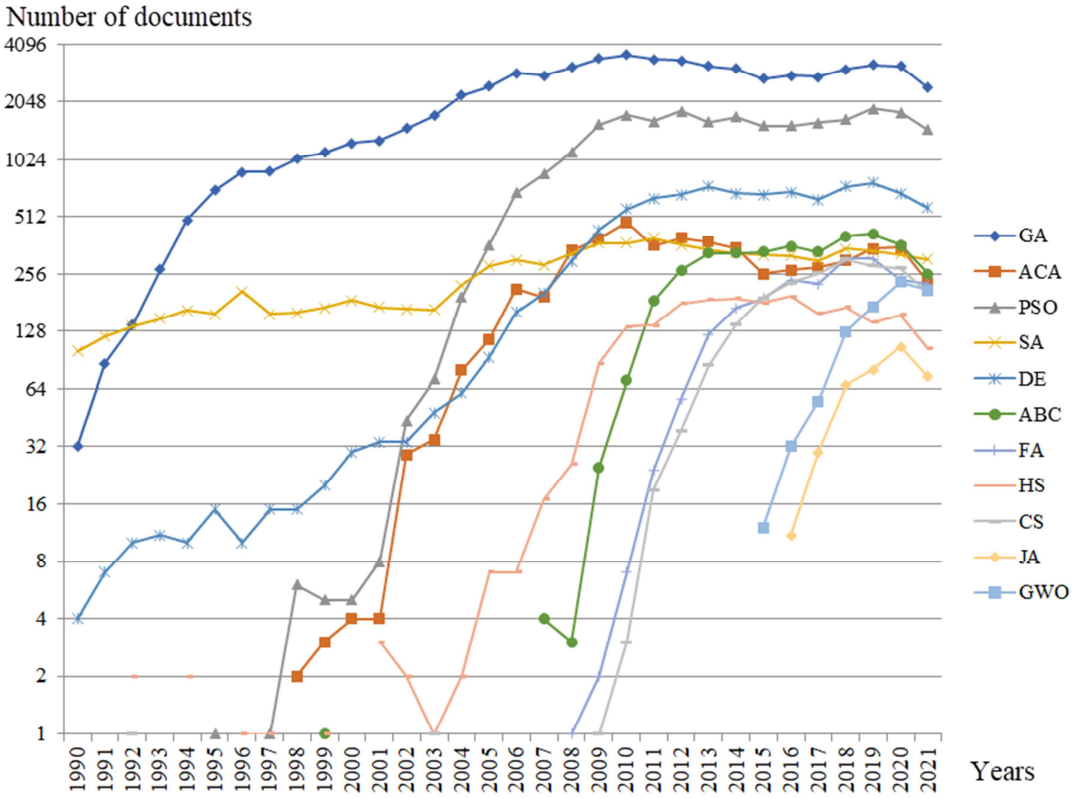

Figure 21: Line graph based on the data of some common algorithms

Table 5 illustrates the total data of some popular algorithms from 1990-2021, and Figure 22 shows a pie chart based on the total extracted data.

Table 5: The total data of some popular algorithms from 1990-2021

total	*GA*	*ACA*	*PSO*	*SA*	*DE*	*ABC*	*FA*	*HS*	*CS*	*JA*	*GWO*
1990-2021	64929	5413	24928	8080	9564	3692	2121	2099	2038	369	841

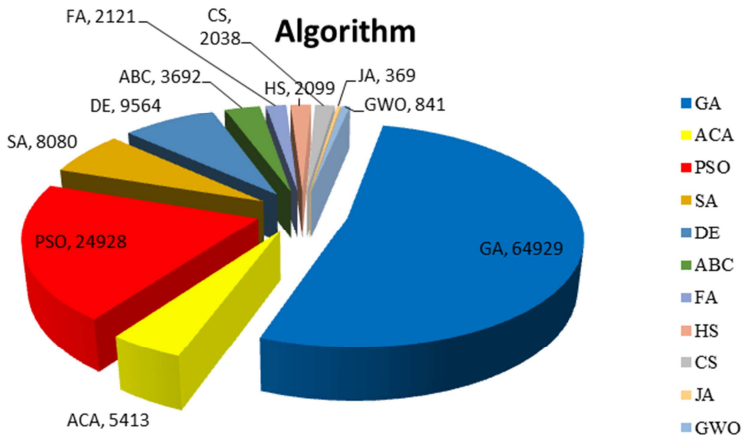

Figure 22: Pie chart based on the total data of some common algorithms

From the line graph and pie chart of the algorithm's data, we can obviously note that the genetic algorithm and particle swarm optimization are the popular optimization algorithms. Please, go to chapter 5, part c, to have an idea and know why these algorithms are popular in the evolutionary computation domain.

2.5 Summary

This chapter was focused on the literature review about resonant inverters' topologies and their modeling methods. Also, the conventional and emerging multilevel inverter topologies and the popular modulation strategies have been discussed. Then, some applications of multilevel inverters were given to highlight the industrial applications. The resonant inverters' topologies can be divided into three main categories: the resonant circuit, series, parallel, and series-parallel. The series resonant inverter is the simplest topology that generates multiple voltage levels with high-efficiency quality based on recent research. There are several modulations strategies for implementing multilevel inverters, classified into the low-frequency switching modulation strategies and the high-frequency switching modulation strategies. The SHE is a low-frequency modulation strategy, has many advantages, including the simplest, and allows the user to simultaneously control the inverter and eliminate unwanted harmonics. On the other hand, an overview of controller actions and control techniques for electrical power systems has been discussed. P, I, and D are the main controller actions, and other types of actions can be designed based on these 03 mains. The control techniques are divided into classical-control and advanced-control techniques based on their performances and efficiencies. The most classical-control techniques require complete knowledge of the system model and maintain control performance in the case of small variations in the nominal values of the system elements. If the material properties vary significantly during a line scan, the controller performance can become inadequate or unstable. Many advanced-control techniques have been proposed to improve the efficiency of systems. Controller actions-based intelligent technique is an excellent hybrid method for the control of systems because of their advantages.

Chapter 03:

ANALYSIS OF THE PROPOSED FIVE-LEVEL SERIES RESONANT INVERTER

CHAPTER 3 ANALYSIS OF THE PROPOSED FIVE-LEVEL SERIES RESONANT INVERTER

3.1 Introduction

Analysis, modeling, and controller design are the three main processes for developing any power system converter. Here, in this chapter, we will mainly focus on analyzing the proposed five-level series resonant inverter. The resonant inverter is usually analyzed using electrical lows as Kirchhoff's laws.

First, the physical phenomena: resonance is defined to explain what happens in this phenomenon and how it is achieved. Next, the three operating modes based on resonance-frequency of a series resonant circuit are discussed, and characteristics of a series resonant circuit. Furthermore, a description of the proposed Five-level series resonant inverter is presented. The electrical circuit, the switching configuration, and the simplified circuit of the system with the state-space model are given. Eventually, the fundamental electrical quantities for controlling the system are compared, the voltage quantity, the frequency quantity, and the switching-angles quantity.

3.2 The physical phenomena: resonance

In nature, the energy of a system exists in many different forms, including Mechanical Energy, Chemical Energy, Gravitational Energy, Electrical Energy,….etc. Each form can be converted or changed into other forms. Figure 23 shows energy conversion between two forms. Resonance is a physical phenomenon, occurs when a system can store and transfer energy between two or more different storage modes, such as kinetic and potential [1]. When a system has functioned near a resonance frequency, maximum physical characteristics can be obtained (current, voltage, or power). Inductance and capacitor are the popular used components in resonant circuits because they can store energy in kinetic and potential forms, respectively. At resonance, the inductive reactance equals the capacitive reactance (X_L=X_C), so the effects of the reactances are canceled in the system [2].

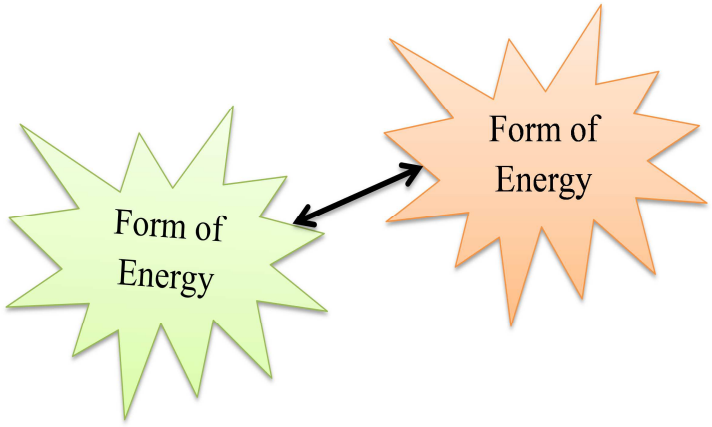

Figure 23: Diagram of the energy conversion and flow between two forms

3.3 Operating modes of a series resonant circuit

Based on the resonant frequency, three operating modes can be achieved, operation below the resonance frequency, operation above the resonance frequency, and operation at resonance frequency [3]. Figure 24 resumes the three operating modes of the series resonant circuit.

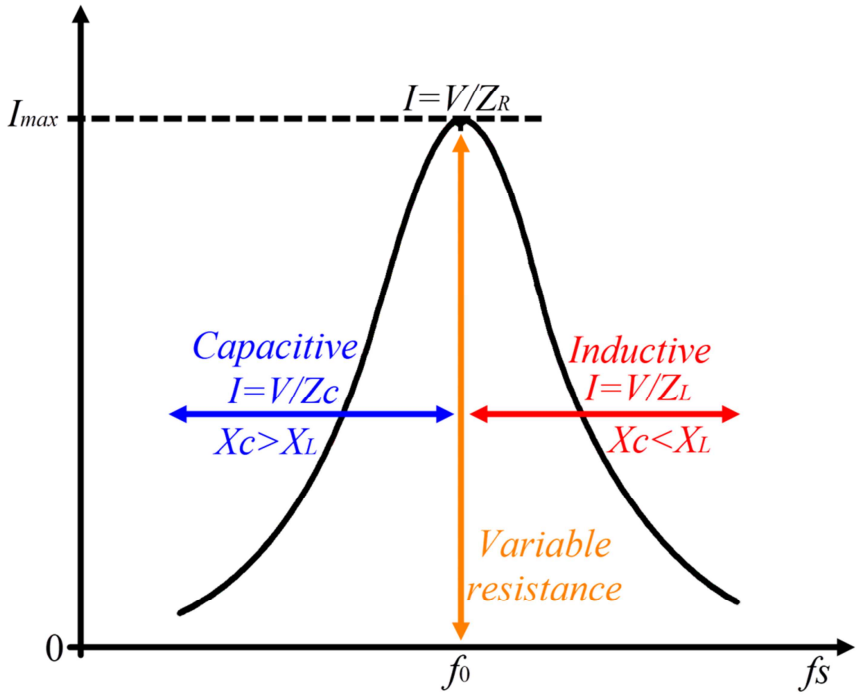

Figure 24: The bandwidth of current versus switching-frequency

3.3.1 Operation below the resonance frequency

In this operation mode, the inverter switching-frequency (f_s) is inferior to the resonant circuit frequency (f_0). The series resonant circuit (*RLC*) is operating as a capacitive circuit. The current waveform leads the voltage waveform by a phase angle equal to $\theta°$ because, in this operating mode, the capacitive reactance (X_C) is superior to the inductive reactance (X_L), (X_C>X_L). Figure 25 illustrates the current and voltage waveforms of the series resonant circuit (*RLC*) in the operating mode: Below the resonance frequency (f_s <f_0).

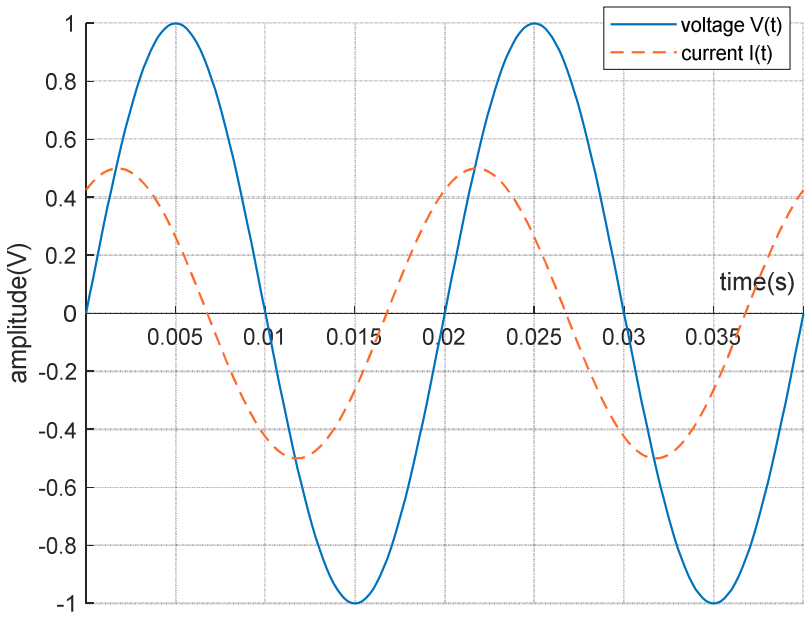

Figure 25: Current and voltage waveforms for operating mode: Below the resonance frequency (f_s <f_0).

3.3.2 Operation above the resonance frequency

In this operation mode, the inverter switching-frequency (f_s) is superior to the resonant circuit frequency (f_0). The series resonant circuit (*RLC*) is operating as an inductive circuit. The current waveform lags the voltage waveform by a phase angle equal to $\theta°$ because, in this operating mode, the capacitive reactance (X_C) is inferior to the inductive reactance (X_L), (X_C<X_L). Figure 26 illustrates the current and voltage waveforms of the series resonant circuit (*RLC*) in the operating mode: Below the resonance frequency

($f_s > f_0$).

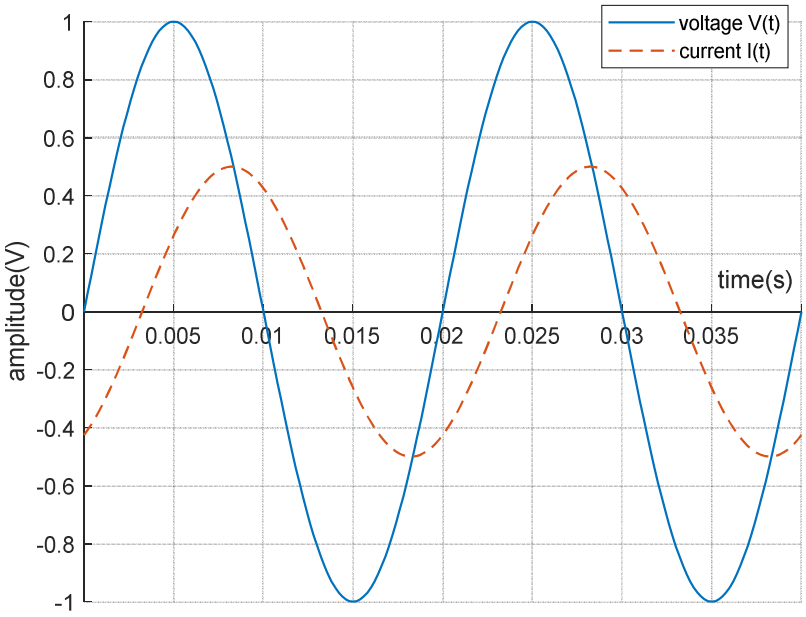

Figure 26: Current and voltage waveforms for operating mode: Above the resonance frequency ($f_s > f_0$).

3.3.3 Operation at resonance frequency

In this operation mode, the inverter switching-frequency (f_s) equals the resonant circuit frequency (f_0). The series resonant circuit (*RLC*) is operating as a resistive circuit. The current waveform is in phase with the voltage waveform because, in this operating mode, the capacitive reactance (X_C) is equal to the inductive reactance (X_L), (X_C=X_L). Figure 27 illustrates the current and voltage waveforms of the series resonant circuit (*RLC*) in the operating mode: At the resonance frequency ($f_s = f_0$).

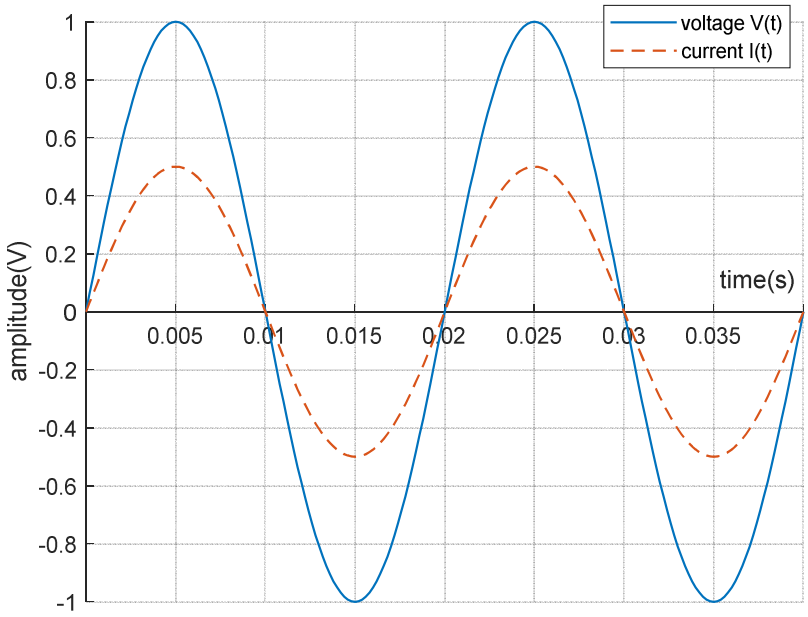

Figure 27: Current and voltage waveforms for operating mode: At the resonance frequency ($f_s = f_0$).

3.4 Characteristics of a series resonant circuit

As mentioned in the above section 2, the inductance (L) and the capacitor (C) are the popular used components for realizing the resonant circuits; if these two components are associated in series with or without resistor (R), a series resonant circuit (RLC) is realized. The series resonant circuit can be used to model several physical phenomena, such as the induction heating process [4], the wireless power transfer systems [5]. This type of circuit is characterized by the resonance frequency and the power factor.

3.4.1 Resonance frequency

In the complex presentation, the series resonant circuit (RLC) is expressed by the impedance values of each component. $\underline{I}$, $\underline{U}$, Z_R, Z_L, Z_C are the current, voltage, resistor impedance, inductor impedance, capacitor impedance, respectively [6]. The ohmic resistance, the inductance reactance, the capacitor reactance are R, X_L, X_C, respectively. Figure 28 shows the complex presentation of the series resonant circuit. Figure 29 shows the equivalent circuit of the complex presentation of the series resonant circuit. $\underline{Z}$ is the total impedance of the circuit; its unit is the ohm [Ω].

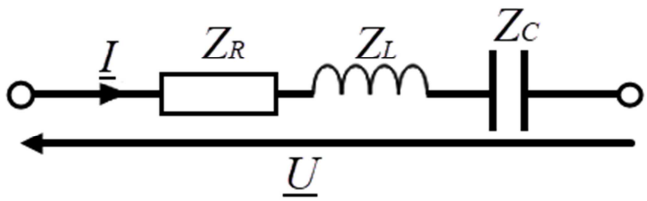

Figure 28: The complex presentation of the series resonant circuit.

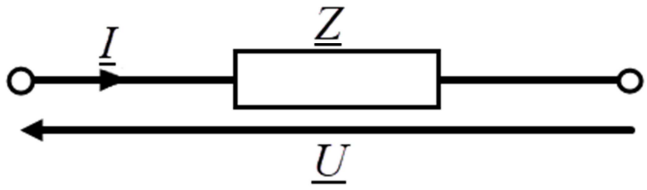

Figure 29: Equivalent circuit of the complex presentation of the series resonant circuit.

Where:

$$\begin{cases} \underline{Z}_R = R \\ \underline{Z}_L = jL\omega \\ \underline{Z}_C = -\dfrac{j}{C\omega} \end{cases} ; \quad \begin{cases} X_R = R \\ X_L = L\omega \\ X_C = \dfrac{1}{C\omega} \end{cases}$$

The total circuit impedance ($\underline{Z}$) can be calculated using the voltage ($\underline{U}$) and the current ($\underline{I}$); it indicates the opposition made to the passage of the current ($\underline{I}$) through the components of the circuit (*RLC*). Using Kirchhoff's laws, the complex circuit equations can be developed as:

$$\underline{U} = \underline{Z}_R\underline{I} + \underline{Z}_L\underline{I} + \underline{Z}_C\underline{I} = \left(\underline{Z}_R + \underline{Z}_L + \underline{Z}_C\right)\underline{I} \tag{1}$$

$$\underline{U} = \left(R + jL\omega - \frac{j}{C\omega}\right)\underline{I} \tag{2}$$

$$\underline{Z} = \frac{\underline{U}}{\underline{I}} \tag{3}$$

Through the previous equations, we can calculate the total impedance ($\underline{Z}$), the impedance module (Z), and the circuit current (I) of the series circuit (*RLC*) as:

$$\underline{Z} = \left(R + jL\omega - \frac{j}{C\omega} \right) = R + j\left(L\omega - \frac{1}{C\omega} \right) \tag{4}$$

$$Z = |\underline{Z}| = \sqrt{R^2 + \left(L\omega - \frac{1}{C\omega} \right)^2} \tag{5}$$

$$I = \frac{U}{\sqrt{R^2 + \left(L\omega - \frac{1}{C\omega} \right)^2}} \tag{6}$$

From the circuit, if the value of the inductive reactance equals that of the capacitance reactance ($X_L = X_C$), we observe a resonance phenomenon, the effects of the reactance's are canceled, and the total circuit impedance is equal to the resistance ($Z=R$). Therefore, the voltage applied to the circuit is equal to the voltage at the resistance. Also, the current in the circuit is at its maximum and the voltage at the capacitor and inductance are also at their maximum because the resonance impedance is at a minimum value.

$$X_L = X_C \tag{7}$$

$$L\omega_0 = \frac{1}{C\omega_0} \tag{8}$$

$$LC\omega_0^2 = 1 \tag{9}$$

$$\omega_0 = \frac{1}{\sqrt{LC}} \tag{10}$$

The resonance frequency of the series resonant circuit (RLC) is determined by the product of the inductance and the capacitance with the following relationship:

$$f_0 = \frac{1}{2\pi\sqrt{LC}} \tag{11}$$

3.4.2 Quality factor

From the resonance frequency equation, it is noted that different values of (L) and (C) can give the same resonance frequency respecting the resonance condition ($X_L = X_C$),

so the series resonant circuit (*RLC*) is characterized by a quality factor (Q) at the resonance. The quality factor is determined by the division of the inductance or capacitance and the resistance with the following relationships:

$$\begin{cases} Q_0 = \dfrac{X_L}{R} = \dfrac{L\omega_0}{R} \\ or \\ Q_0 = \dfrac{X_C}{R} = \dfrac{1}{RC\omega_0} \end{cases} \tag{12}$$

$$Q_0 = \frac{1}{R}\sqrt{\frac{L}{C}} \tag{13}$$

3.5 Description of the proposed Five-level series resonant inverter

In this section, the proposed Five-level series resonant inverter structure is discussed, where the electrical circuit, the operating principle, and simplified electrical circuit are given, respectively.

3.5.1 The electrical circuit

The Five-level inverter topology consists of six electronic switches and two separate DC sources; if compared with the conventional topology of cascaded five-level H-bridge inverter, this structure consists of fewer switches [7]. Figure 30 illustrates the electrical circuit of the proposed series resonant five-level inverter. This inverter can produce five different voltage levels: $+V_{dc}$, $+2V_{dc}$, 0, $-V_{dc}$, and $-2V_{dc}$ with the appropriate switching angles technique.

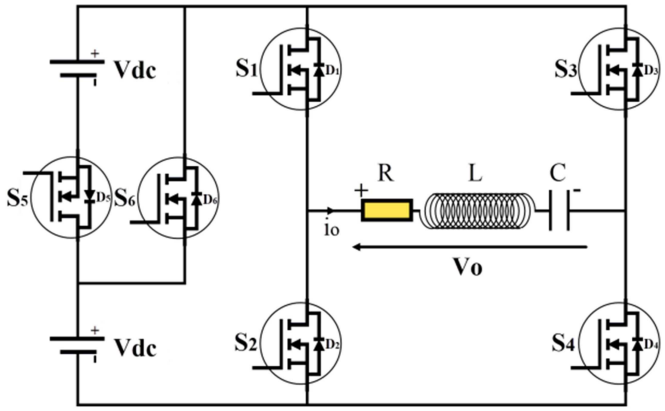

Figure 30: Circuit of the five-level series resonant inverter.

3.5.2 The switching devices configuration

Figure 31 shows the desired output voltage waveform of the five-level inverter, where in a complete switching period (T) there are 12 switching transitions.

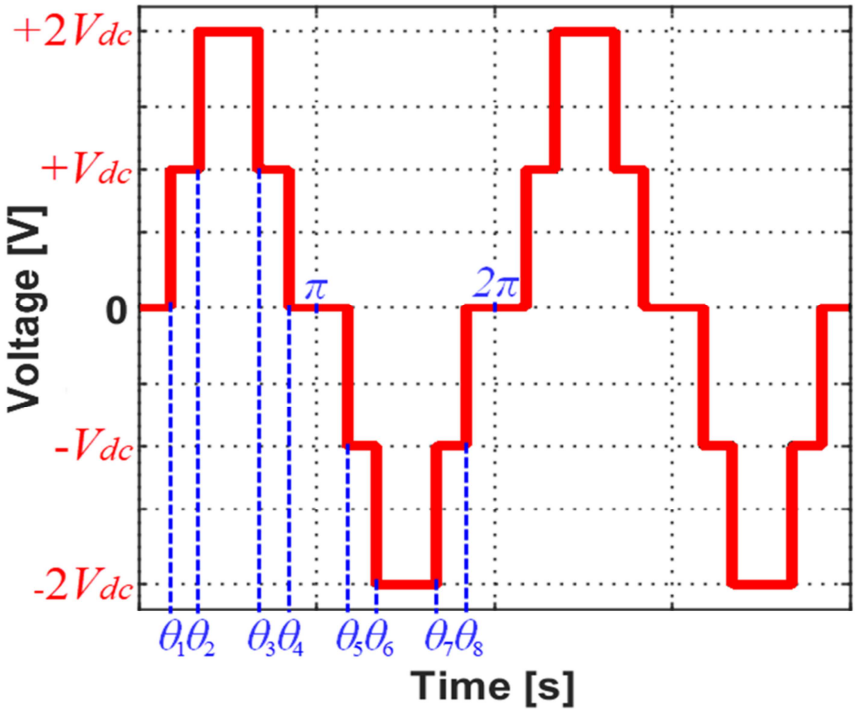

Figure 31: The desired Five-level output voltage: full-waveform.

Figure 32 illustrates the equivalent circuits for producing the desired five-level voltages. The output voltage ($V_o = U_{RLC} = 0$) as shown in Figure 32(a), the switch (S_2 and S_4) are closed, and switches (S_1, S_3, S_5, S_6) are opened, in this scenario ($V_o = 0$), the

positive current circulates in the components (S_4 and D_2) and the negative current passes in the components (D_4 and S_2). Figure 32(b) shows the scenario ($V_o = +V_{dc}$), in this situation (S_1, S_4, S_6) are closed, and the switches (S_2, S_3, S_5) are opened, the positive output current across (S_4, D_6, and S_1) components, and the negative current passes through (D_4, S_6, D_1) components. Figure 32(c) shows the scenario ($V_o = +2V_{dc}$), in this situation (S_1, S_4, and S_5) are closed, and the switches (S_2, S_3, S_6) are opened, the positive current circulates through (S_4, S_5, and S_1) components, and the negative current circulates in (D_4, D_5, and D_1) components. Figure 32(d) shows the scenario ($V_o = -V_{dc}$), in this situation (S_2, S_3, and S_6) are closed, and the switches (S_1, S_4, S_5) are opened, the positive current circulates in the components (S_3, D_6, and S_2) and the negative current passes in the components (D_3, S_6, and D_2). Figure 32(e) shows the scenario ($V_o = -2V_{dc}$), in this situation (S_2, S_3, S_5) are closed, and the switches (S_1, S_4, S_6) are opened, the positive output current across (S_3, S_5, and S_2) components, and the negative current passes through (D_3, D_5, and D_2) components. Figure 32(f) shows the scenario ($V_o = 0$), in this situation (S_1 and S_3) are closed, and the switches (S_2, S_4, S_5, S_6) are opened, the positive current circulates through (S_3 and D_1) components, and the negative current circulates in (D_3 and S_1) components.

Table 6 shows the summary of the switching modes of the five-level inverter topology.

Table 6: Switching states of the five-level inverter topology

Interval	***V_o***	***ON Switches***	***OFF Switches***
$[0, \theta_1]$	0	S_2, S_4	S_1, S_3, S_5 S_6
$[\theta_1, \theta_2]$	$+V_{dc}$	S_1, S_4, S_6	S_2, S_3, S_5
$[\theta_2, \pi/2]$	$+2V_{dc}$	S_1, S_4, S_5	S_2, S_3, S_6
$[\pi/2, \theta_3]$	$+2V_{dc}$	S_1, S_4, S_5	S_2, S_3, S_6
$[\theta_3, \theta_4]$	$+V_{dc}$	S_1, S_4, S_6	S_2, S_3, S_5
$[\theta_4, \theta_5]$	0	S_2, S_4	S_1, S_3, S_5 S_6
$[\theta_5, \theta_6]$	$-V_{dc}$	S_2, S_3, S_6	S_1, S_4, S_5
$[\theta_6, 3\pi/2]$	$-2V_{dc}$	S_2, S_3, S_5	S_1, S_4, S_6
$[3\pi/2, \theta_7]$	$-2V_{dc}$	S_2, S_3, S_5	S_1, S_4, S_6
$[\theta_7, \theta_8]$	$-V_{dc}$	S_2, S_3, S_6	S_1, S_4, S_5
$[\theta_8, 2\pi]$	0	S_1, S_3	S_2, S_4, S_5 S_6

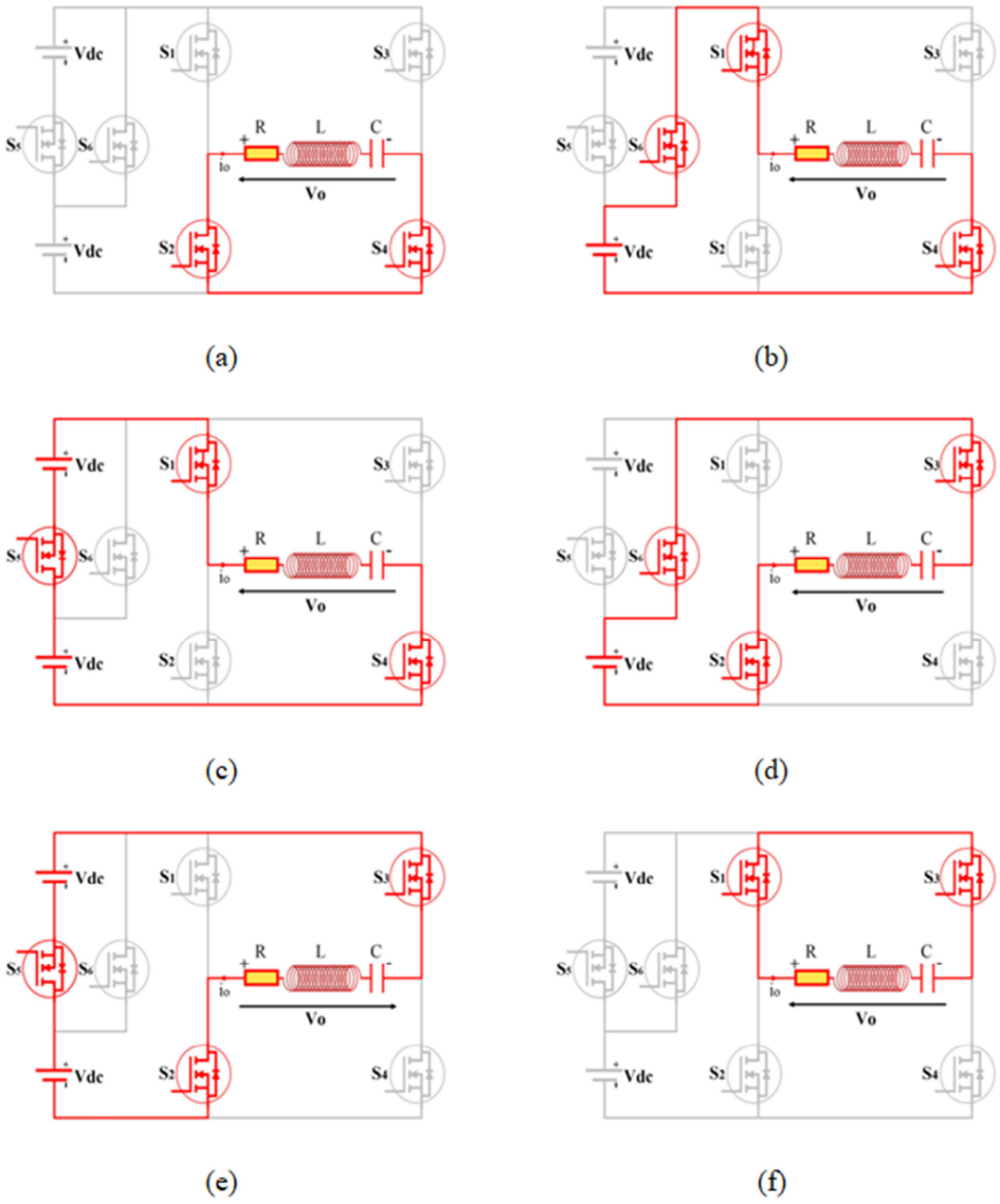

Figure 32: The equivalent electrical circuits to produce the desired Five-level output voltage.

3.5.3 The simplified circuit

The modeling of the inverter requires the simplification of the circuit, there are some assumptions that must be verified for the simplification, which are the following: The electronic switches are ideal: instantaneous switching, zero voltage drop, the reactive elements of the inverter are ideal; the input voltage *U* is constant [2]. Under these simplification assumptions, our circuit can be reduced to the form shown in Figure 33. R,

L, and C are the elements of the resonant circuit.

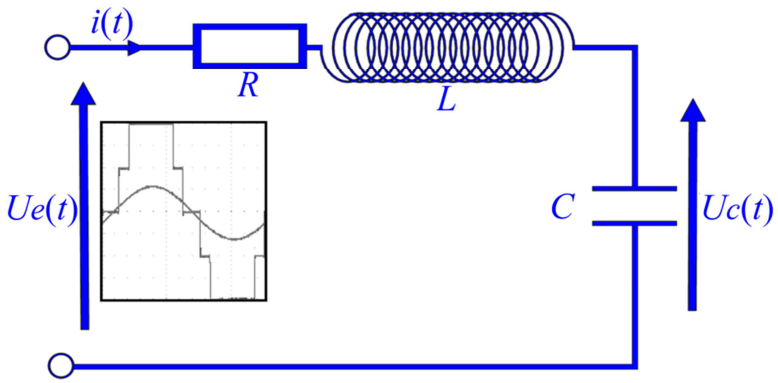

Figure 33: Simplified circuit of the series resonant Five-level inverter.

Using Kirchhoff's laws, the simplified circuit can be expressed with the following relations:

$$U_e(t) = V_o(t) = Ri(t) + L\frac{di(t)}{dt} + U_c(t) \tag{14}$$

$$U_c(t) = \frac{1}{C}\int i(t)\,dt \tag{15}$$

$$i(t) = C\frac{dU_c(t)}{dt} \tag{16}$$

The transfer function of the circuit from output capacitor voltage $U_c(t)$ to input voltage $U_e(t)$ in complex mathematical form can be written as:

$$H(j\omega) = \frac{U_c}{U_E} = \frac{\frac{1}{jC\omega}}{R + jL\omega + \frac{1}{jC\omega}} = \frac{1}{1 + jRC\omega - LC\omega^2} \tag{17}$$

3.5.4 The state-space model of the simplified circuit

The state-space model of the simplified circuit can be written with the following equations:

$$\begin{cases} U_c(t) = \dfrac{1}{C}\int i(t)\,dt \\ U_e(t) = Ri(t) + L\dfrac{di(t)}{dt} + U_c(t) \end{cases} \tag{18}$$

$$\begin{cases} \dfrac{dU_c(t)}{dt} = \dfrac{1}{C}i(t) \\ \dfrac{di(t)}{dt} = -\dfrac{1}{L}U_c(t) - \dfrac{R}{L}i(t) + \dfrac{1}{L}U_e(t) \end{cases} \tag{19}$$

In the simplified form of state presentation, the equations system can be written as:

$$\begin{cases} \dot{x} = Ax + Bu \\ y = Cx + Du \end{cases} \tag{20}$$

$$\begin{bmatrix} \dfrac{dU_c(t)}{dt} \\ \dfrac{di(t)}{dt} \end{bmatrix} = \begin{bmatrix} 0 & 1/C \\ -1/L & -R/L \end{bmatrix} \begin{bmatrix} U_c(t) \\ i(t) \end{bmatrix} + \begin{bmatrix} 0 \\ 1/L \end{bmatrix} U_e(t)$$

$$y(t) = \begin{bmatrix} 1 & 0 \end{bmatrix} \begin{bmatrix} U_c(t) \\ i(t) \end{bmatrix} \;\; ; \; D = 0$$

Where: $x(t)$: The state vector, $U_e(t)$: The control vector, and $y(t)$: The output vector.

$$x(t) = \begin{bmatrix} U_c(t) \\ i(t) \end{bmatrix}$$

$$A = \begin{bmatrix} 0 & 1/C \\ -1/L & -R/L \end{bmatrix}; \; B = \begin{bmatrix} 0 \\ 1/L \end{bmatrix}; \; C = \begin{bmatrix} 1 & 0 \end{bmatrix}; \; D = 0$$

3.6 Mathematical expressions example of series resonant circuit

In this example, a series resonance circuit consisting of resistor R equal to 200 Ω, capacitor C equal to 3 nF, and inductance L equal to 300 mH. The series RLC circuit is connected to a sinusoidal supply, assuming that this power supply is delivering a constant

Root-Mean-Square RMS voltage of *V*=5 V.

A. The resonant frequency of circuit f_0

$$f_0 = \frac{1}{2\pi\sqrt{LC}} = \frac{1}{2\pi\sqrt{300\ (e-3)3(e-9)}} \approx 5.3\ \text{kHz}$$

B. The circuit current at resonance *I*

$$I = \frac{V}{R} = \frac{5}{200} = 25\ \text{mA}$$

C. The inductive reactance at resonance X_L

$$X_L = 2\pi f_0 L = 2(\pi)5300(0.3) \approx 10\ \text{k}\Omega$$

D. The capacitive reactance at resonance X_C

$$X_L = \frac{1}{2\pi f_0 C} = \frac{1}{2(\pi)5300(3e-9)} \approx 10\ \text{k}\Omega$$

E. The voltages across each reactive component, inductor and the capacitor, V_L, V_C

$$V_L = V_C = 10(e^3)25(e^{-3}) = 250\ \text{V}$$

F. the Quality factor *Q*

$$Q = \frac{X_L}{R} = \frac{10000}{200} \approx 50$$

G. the Bandwidth *Bw*

$$Bw = \frac{f_0}{Q} = \frac{5300}{50} \approx 106\ \text{Hz}$$

H. The upper and lower -3dB frequency points, f_{H} and f_{L}

$$\begin{cases} f_L = f_0 - \frac{1}{2}Bw = 5300 - \frac{1}{2}(106) \approx 5.2\ \text{kHz} \\ f_H = f_0 + \frac{1}{2}Bw = 5300 + \frac{1}{2}(106) \approx 5.4\ \text{kHz} \end{cases}$$

Figure 34 illustrates the max current, the resonance frequency with upper and lower -3dB frequency points, f_{H} and f_{L}.

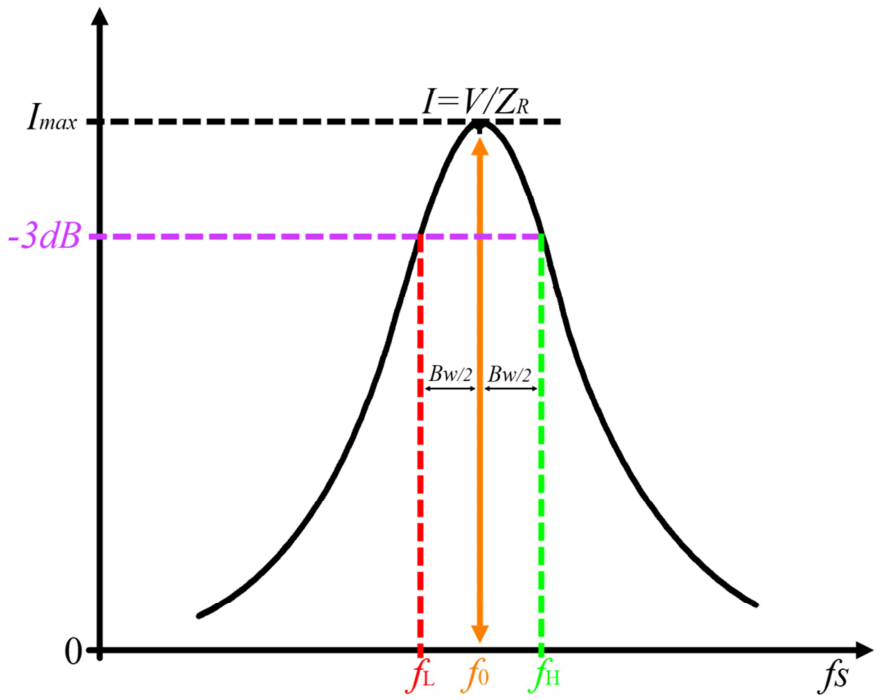

Figure 34: The resonance frequency with upper and lower -3dB frequency points, f_H and f_L.

3.7 The basic electrical quantities for controlling the system

In power engineering systems, the control problems naturally divided into the voltage control issues and the frequency control problems [8], [9]. Our system, a five-level series resonant inverter has outputs (capacitor voltage, current, or power) and inputs (DC-link voltage, switching-angles, frequency-switching), where each one of the mentioned inputs can be used for controlling the outputs electrical quantities.

3.7.1 The voltage

Voltage is an electrical quantity indicating the potential difference between two points. Mathematically, the voltage between two points can be expressed as the change in energy undergone by a charge. The unit for measuring the voltage is known as a volt (symbol: V).

3.7.2 The frequency

Frequency is the quantity designating the number of direction changes; it is the number of times that an AC sine wave repeats a positive-to-negative cycle. In the International System of Units, frequency is measured in Hertz (symbol: Hz).

3.7.3 The switching-angles

The switching angle is the actual time of changing the output voltage level of the inverter or changing the state of the switch between ON and OFF modes [10]. The unit for defining the switching angle is radian (symbol: rad) or can be presented on the degree. System outputs can be controlled by variation of the switching angles value, i.e. the output capacitor voltage, the circuit current.

3.8 Summary

This chapter is related to the mathematical analysis and design of the proposed five-level series resonant inverter. The operating modes of a series resonant circuit are presented; there are three modes of operation: operation below the resonance frequency, operation above the resonance frequency, operation at the resonance frequency. Also, the characteristics of a series resonant circuit are given. Then, the proposed five-level series resonant inverter structure is discussed, where the electrical circuit, the operating principle, and the simplified electrical circuit are detailed. All mathematical expressions were presented with calculation examples of series resonant circuit parameters.

The proposed five-level series resonant inverter combines the advantages of emerging multilevel inverter topologies as the reduced devices count, low THD compared to the conventional half-bridge and full-bridge resonant inverters, low power losses and high-quality output voltage, simplicity of the operating principle; and the advantages of resonant inverters such as High efficiency, where at switching frequency near the resonance frequency, the capacitor voltage and the circuit current are in maximal values, so the power supplied to the load is maximum.

Chapter 04:

SMALL SIGNAL MODELING OF A FIVE-LEVEL SERIES RESONANT INVERTER

CHAPTER 4 SMALL SIGNAL MODELING OF A FIVE-LEVEL SERIES RESONANT INVERTER

4.1 Introduction

The five-level series resonant inverter is a nonlinear system; the complexity of this type of resonant converter requires a mathematical model that can represent their static and dynamic behavior. Therefore, modeling has become a very interesting step. A small-signal model is an analysis technique used to approximate the behavior of electrical circuits containing nonlinear devices with linear equations [1]-[4]. The objective is the determination of an AC equivalent circuit which is linear. So this search focused on the study of alternating quantities, including the current $i(t)$ in the circuit *RLC* and the voltage in the capacitor $V_c(t)$. So in this chapter, we're going to determine:

- The exact model of the system.
- The Large-Signal Model (L-SM) of the system.
- The Small-Signal Model (S-SM) of the system.

4.2 Small-signal model of the five-level series resonant inverter

Small-signal model of the proposed five-level series resonant inverter based on the following steps [5]:

1. Fourier analysis of the inverter output-voltage.

2. Extraction of state vector $x(t)$, control vector $u(t)$, and output vector $y(t)$.

3. First harmonic approximation of the state variables.

4. Construction and validation of the Large-Signal Model.

5. Determination of the operating points (X_0, U_0, Y_0) by putting the $\left\{\frac{dx(t)}{dt} = 0\right\}$.

6. Disruption and linearization of the model developed in step 4 using (X_0, U_0, Y_0).

7. Extraction of the matrices A_s, B_s, C_s, D_s of the linear model with small signals.

4.2.1 Fourier analysis of the inverter output-voltage

Figure 35 shows the desired output-voltage $V_o(t)$ of the five-level inverter. $V_o(t)$ is a periodic function and continue by parts, their mathematical expression can be constructed using the following Fourier transformation:

$$V_o(t) = a_0 + \sum_{n=1}^{\infty} a_n \cos(n\omega_s t) + \sum_{n=1}^{\infty} b_n \sin(n\omega_s t) \tag{21}$$

Where:

n: are whole numbers: 0, 1, 2, …n.

$$\omega_s = \frac{2\pi}{T}; \qquad \theta = \omega_s t$$

ω_s: The pulsation.

θ: The switching angle.

a_0, a_n, b_n: are the Fourier coefficients, they given by the following integrals:

$$\begin{cases} a_0 = \dfrac{1}{T}\int_0^T V_o(t)\,dt \\ a_n = \dfrac{2}{T}\int_0^T V_o(t)\cos(n\omega_s t)dt \\ b_n = \dfrac{2}{T}\int_0^T V_o(t)\sin(n\omega_s t)dt \end{cases} \tag{22}$$

The desired output-voltage $V_o(t)$ is an odd function and periodic, so:

$$a_0 = 0; \;\; a_n = 0; \;\; b_n = \frac{2}{T}\int_0^T V_o(t)\sin(n\omega_s t)dt$$

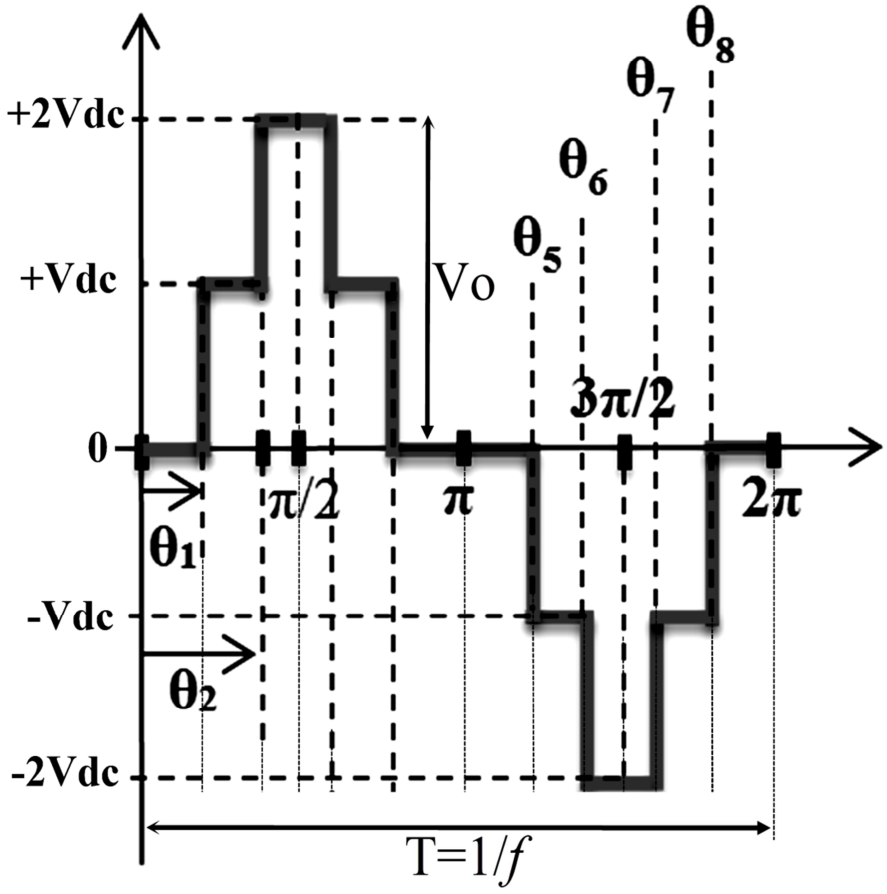

Figure 35: The desired output-voltage $V_o(t)$ of the five-level inverter

By putting ($V_{dc} = V$), b_n can be calculated as following:

$$b_n = \frac{2}{T}\left(\begin{array}{l} \int_{\theta_1}^{\theta_2}\left(+V\sin(n\omega_s t)\right)dt + \int_{\theta_2}^{\theta_3}\left(+2V\sin(n\omega_s t)\right)dt + \\ \int_{\theta_3}^{\theta_4}\left(+V\sin(n\omega_s t)\right)dt + \int_{\theta_5}^{\theta_6}\left(-V\sin(n\omega_s t)\right)dt + \\ \int_{\theta_6}^{\theta_7}\left(-2V\sin(n\omega_s t)\right)dt + \int_{\theta_7}^{\theta_8}\left(-V\sin(n\omega_s t)\right)dt \end{array}\right) \quad (23)$$

- In the interval $[\theta_1, \theta_2]$, $V_o(t) = +V$, so b_n is calculated as:

$$b_n = \frac{2}{T}\int_{\theta_1}^{\theta_2}\left(+V\sin(n\omega_s t)\right)dt = \frac{2V}{T}\times\frac{1}{n\omega_s}\left(-\cos(n\omega_s t)\Big|_{\theta_1}^{\theta_2}\right)$$
$$= -\frac{2V}{T}\times\frac{T}{2\pi n}\left(\cos(n\theta_2)-\cos(n\theta_1)\right) \quad (24)$$
$$= -\frac{V}{n\pi}\left(\cos(n\theta_2)-\cos(n\theta_1)\right)$$

- In the interval $[\theta_2, \theta_3]$, $V_o(t) = +2V$, so b_n is calculated as:

$$b_n = \frac{2}{T}\int_{\theta_2}^{\theta_3}\left(+2V\sin(n\omega_s t)\right)dt = \frac{4V}{T}\times\frac{1}{n\omega_s}\left(-\cos(n\omega_s t)\Big|_{\theta_2}^{\theta_3}\right)$$
$$= -\frac{4V}{T}\times\frac{T}{2\pi n}\left(\cos(n\theta_3)-\cos(n\theta_2)\right)$$
$$= -\frac{2V}{n\pi}\left(-\cos(n\theta_2)-\cos(n\theta_2)\right) \quad (25)$$
$$= +\frac{4V}{n\pi}\left(\cos(n\theta_2)\right)$$

- In the interval $[\theta_3, \theta_4]$, $V_o(t) = +V$, so b_n is calculated as:

$$b_n = \frac{2}{T}\int_{\theta_3}^{\theta_4}\left(+V\sin(n\omega_s t)\right)dt = \frac{2V}{T}\times\frac{1}{n\omega_s}\left(-\cos(n\omega_s t)\Big|_{\theta_3}^{\theta_4}\right)$$
$$= -\frac{2V}{T}\times\frac{T}{2\pi n}\left(\cos(n\theta_4)-\cos(n\theta_3)\right) \quad (26)$$
$$= -\frac{V}{n\pi}\left(-\cos(n\theta_1)+\cos(n\theta_2)\right)$$

- In the interval $[\theta_5, \theta_6]$, $V_o(t) = -V$, so b_n is calculated as:

$$b_n = \frac{2}{T}\int_{\theta_5}^{\theta_6}\left(-V\sin(n\omega_s t)\right)dt = \frac{-2V}{T}\times\frac{1}{n\omega_s}\left(-\cos(n\omega_s t)\Big|_{\theta_5}^{\theta_6}\right)$$
$$= +\frac{2V}{T}\times\frac{T}{2\pi n}\left(\cos(n\theta_6)-\cos(n\theta_5)\right) \quad (27)$$
$$= +\frac{V}{n\pi}\left(-\cos(n\theta_2)+\cos(n\theta_1)\right)$$

- In the interval $[\theta_6, \theta_7]$, $V_o(t) = -2V$, so b_n is calculated as:

$$b_n = \frac{2}{T}\int_{\theta_6}^{\theta_7}\left(-2V\sin(n\omega_s t)\right)dt = \frac{-4V}{T}\times\frac{1}{n\omega_s}\left(-\cos(n\omega_s t)\Big|_{\theta_6}^{\theta_7}\right)$$
$$= +\frac{4V}{T}\times\frac{T}{2\pi n}\left(\cos(n\theta_7)-\cos(n\theta_6)\right) \quad (28)$$
$$= +\frac{2V}{n\pi}\left(\cos(n\theta_2)+\cos(n\theta_2)\right)$$
$$= +\frac{4V}{n\pi}\left(\cos(n\theta_2)\right)$$

- In the interval $[\theta_7, \theta_8]$, $V_o(t) = -V$, so b_n is calculated as:

$$b_n = \frac{2}{T}\int_{\theta_7}^{\theta_8}\left(-V\sin(n\omega_s t)\right)dt = \frac{-2V}{T}\times\frac{1}{n\omega_s}\left(-\cos(n\omega_s t)\Big|_{\theta_7}^{\theta_8}\right)$$
$$= -\frac{2V}{T}\times\frac{T}{2\pi n}\left(\cos(n\theta_8)-\cos(n\theta_7)\right) \quad (29)$$
$$= +\frac{V}{n\pi}\left(\cos(n\theta_1)-\cos(n\theta_2)\right)$$

By sum of equations 24, 25, 26, 27, 28, 29, then some mathematical simplification, the expression of b_n can be written as:

$$b_n = +\frac{4V}{n\pi}\left(\cos(n\theta_1)+\cos(n\theta_2)\right) \quad (30)$$

The expression of $V_o(t)$ can be written as:

$$V_o(t)=\sum_{n=1}^{\infty} b_n \sin(n\omega_s t)=\sum_{n=1}^{\infty}\left(+\frac{4V}{n\pi}\left(\cos(n\theta_1)+\cos(n\theta_2)\right)\right)\sin(n\omega_s t) \tag{31}$$

For the first harmonic (n=1), The expression of $V_o(t)$ can be written as:

$$V_o(t)=+\frac{4V}{\pi}\left(\cos(\theta_1)+\cos(\theta_2)\right)\sin(\omega_s t) \tag{32}$$

4.2.2 Extraction of state vector *x*(*t*), control vector *u*(*t*), and output vector *y*(*t*)

Figure 36 shows the equivalent circuit of a five-level series resonant inverter. Kirchhoff's laws are applied to the equivalent circuit to give the mathematical expressions of the output capacitor voltage $V_c(t)$, and the input voltage $V_o(t)$, where $V_c(t) = U_c(t)$ and $V_o(t) = U_e(t)$:

$$\begin{cases} V_c(t)=\dfrac{1}{C}\int i(t)\,dt \\ V_o(t)=Ri(t)+L\dfrac{di(t)}{dt}+V_c(t) \end{cases} \tag{33}$$

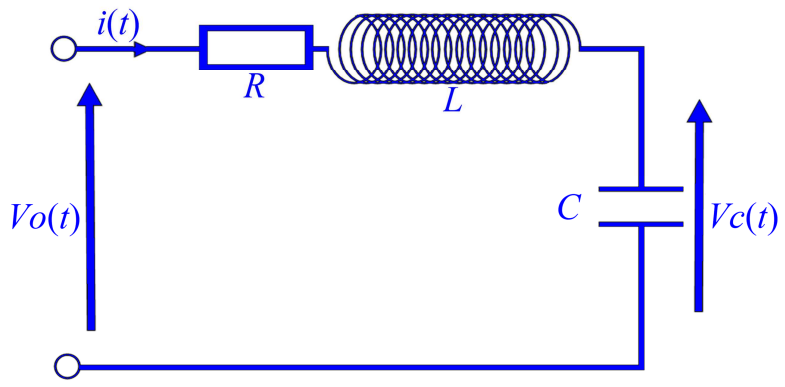

Figure 36: The equivalent circuit of a five-level series resonant inverter

The state vector $x(t)$ is defined with the currents $i(t)$ and the capacitor voltage $V_c(t)$ as:

$$x(t)=\begin{bmatrix} i(t) & V_c(t) \end{bmatrix}^t$$

The input variable $u(t)$ and the output variable $y(t)$ are :

$$\begin{cases} u(t) = V_o(t) \\ y(t) = V_c(t) \end{cases}$$

In the simplified form of state presentation, the system can be written as:

$$\begin{bmatrix} \frac{di(t)}{dt} \\ \frac{dV_c(t)}{dt} \end{bmatrix} = \begin{bmatrix} -R/L & -1/L \\ 1/C & 0 \end{bmatrix} \begin{bmatrix} i(t) \\ V_c(t) \end{bmatrix} + \begin{bmatrix} 1/L \\ 0 \end{bmatrix} u(t)$$

$$y(t) = \begin{bmatrix} 0 & 1 \end{bmatrix} \begin{bmatrix} i(t) \\ V_c(t) \end{bmatrix} \quad ; \; D = 0$$

4.2.3 First harmonic approximation of state variables

The system state variable $i(t)$ and $V_c(t)$ are complex values, which can be approximated by (34), where $i_c(t)$, $i_s(t)$ are the real and imaginary parts of the current $i(t)$ and $V_{cc}(t)$, $V_{cs}(t)$ are the real and imaginary parts of the voltage $V_c(t)$:

$$\begin{cases} i(t) \approx i_c(t)\cos(\omega_s t) + i_s(t)\sin(\omega_s t) \\ V_c(t) \approx V_{cc}(t)\cos(\omega_s t) + V_{cs}(t)\sin(\omega_s t) \end{cases} \tag{34}$$

The system state variable derivatives are given by:

$$\begin{cases} \dot{i}(t) \approx \dot{i}_c(t)\cos(\omega_s t) - i_c(t)\,\omega_s \sin(\omega_s t) + \dot{i}_s(t)\sin(\omega_s t) + i_s(t)\,\omega_s \cos(\omega_s t) \\ \dot{V}_c(t) \approx \dot{V}_{cc}(t)\cos(\omega_s t) - V_{cc}(t)\,\omega_s \sin(\omega_s t) + \dot{V}_{cs}(t)\sin(\omega_s t) + V_{cs}(t)\,\omega_s \cos(\omega_s t) \end{cases} \tag{35}$$

By simplification, the system state variable derivatives are described as:

$$\begin{cases} \dot{i}(t) \approx \left(\dot{i}_c(t) + i_s(t)\,\omega_s\right)\cos(\omega_s t) + \left(\dot{i}_s(t) - i_c(t)\,\omega_s\right)\sin(\omega_s t) \\ \dot{V}_c(t) \approx \left(\dot{V}_{cc}(t) + V_{cs}(t)\,\omega_s\right)\cos(\omega_s t) + \left(\dot{V}_{cs}(t) - V_{cc}(t)\,\omega_s\right)\sin(\omega_s t) \end{cases} \tag{36}$$

4.2.4 Construction and validation of the Large Signal Model

The use of the first harmonic approach gives us the opportunity to pass from the exact model to the first harmonic model by replacing the variables $i(t)$ and $V_c(t)$ by its

expressions and θ_1 , θ_2. In this case, the non-linear Large-signal model of the five-level series resonant inverter is achieved.

Based on equations (33), the state variables derivatives are given as:

$$\begin{cases} \dot{i}(t) &= -\dfrac{R}{L}i(t) - \dfrac{1}{L}V_c(t) + \dfrac{1}{L}V_o(t) \\ \dot{V}_c(t) &= +\dfrac{1}{C}i(t) \end{cases} \tag{37}$$

Using the equations (32) and (34) of the variables $i(t)$, $V_c(t)$, and $V_o(t)$, the state variables derivatives are given as:

$$\begin{cases} \dot{i}(t) &= \left(\begin{array}{l} -\dfrac{R}{L}\left(i_c(t)\cos(\omega_s t) + i_s(t)\sin(\omega_s t)\right) - \\ \dfrac{1}{L}\left(V_{cc}(t)\cos(\omega_s t) + V_{cs}(t)\sin(\omega_s t)\right) + \\ \dfrac{1}{L}\left(+\dfrac{4V}{\pi}\left(\cos(\theta_1) + \cos(\theta_2)\right)\sin(\omega_s t)\right) \end{array} \right) \\ \dot{V}_c(t) &= +\dfrac{1}{C}\left(i_c(t)\cos(\omega_s t) + i_s(t)\sin(\omega_s t)\right) \end{cases} \tag{38}$$

By applying some mathematical manipulations, the equations (38) can be expressed as:

$$\begin{cases} \dot{i}(t) &= \left(\begin{array}{l} \left(-\dfrac{R}{L}i_c(t) - \dfrac{1}{L}V_{cc}(t)\right)\cos(\omega_s t) + \\ \left(-\dfrac{R}{L}i_s(t) - \dfrac{1}{L}V_{cs}(t) + \dfrac{4V}{L\pi}\left(\cos(\theta_1) + \cos(\theta_2)\right)\right)\sin(\omega_s t) \end{array} \right) \\ \dot{V}_c(t) &= +\dfrac{1}{C}i_c(t)\cos(\omega_s t) + \dfrac{1}{C}i_s(t)\sin(\omega_s t) \end{cases} \tag{39}$$

By identification between equations (36) and (39), we find:

$$\begin{cases} \dot{i}_c(t) + i_s(t)\,\omega_s & = -\dfrac{R}{L} i_c(t) - \dfrac{1}{L} V_{cc}(t) \\ \dot{i}_s(t) - i_c(t)\,\omega_s & = -\dfrac{R}{L} i_s(t) - \dfrac{1}{L} V_{cs}(t) + \dfrac{4V}{L\pi}\left(\cos(\theta_1) + \cos(\theta_2)\right) \\ \dot{V}_{cc}(t) + V_{cs}(t)\,\omega_s & = +\dfrac{1}{C} i_c(t) \\ \dot{V}_{cs}(t) - V_{cc}(t)\,\omega_s & = +\dfrac{1}{C} i_s(t) \end{cases} \tag{40}$$

The Large-signal model of the system is developed to be:

$$\begin{cases} \dot{i}_c(t) & = -\dfrac{R}{L} i_c(t) - \dfrac{1}{L} V_{cc}(t) - i_s(t)\,\omega_s \\ \dot{i}_s(t) & = -\dfrac{R}{L} i_s(t) - \dfrac{1}{L} V_{cs}(t) + \dfrac{4V}{L\pi}\left(\cos(\theta_1) + \cos(\theta_2)\right) + i_c(t)\,\omega_s \\ \dot{V}_{cc}(t) & = +\dfrac{1}{C} i_c(t) - V_{cs}(t)\,\omega_s \\ \dot{V}_{cs}(t) & = +\dfrac{1}{C} i_s(t) + V_{cc}(t)\,\omega_s \end{cases} \tag{41}$$

The system input controls $u(t)$, the new state variables $x(t)$, and the output variable $y(t)$ are defined as:

$$\begin{cases} u(t) = \begin{bmatrix} v & \theta_1 & \theta_2 & \omega_s \end{bmatrix}^t \\ x(t) = \begin{bmatrix} i_c & i_s & V_{cc} & V_{cs} \end{bmatrix}^t \\ y(t) = V_c(t) = \sqrt{V_{cc}^2(t) + V_{cs}^2(t)} \end{cases} \tag{42}$$

The large-signal model is a nonlinear equations because it contains the product ($i_s.\omega_s$), ($i_c.\omega_s$), ($V_{cs}.\omega_s$), and ($V_{cc}.\omega_s$), where ω_s, i_s, i_c, V_{cs} and V_{cc} are independent variables. It isn't easy to use this model to design the control system.

After achieving the large-signal model of the system, the nonlinear equations can be linearized around the operating point in order to construct the generalized small-signal transfer function from any desired input (v, θ_1, θ_2, ω_s) to any desired output (i, V_c).

4.2.5 Determination of the operating points (X_0, U_0, Y_0) by putting the {dx(t)/dt=0}

Setting the derivatives of the large-signal model equal to zero, the above equation can be solved to find the equilibrium operation point of the system (I_{c0}, I_{s0}, V_{cc0}, V_{cs0}).

$$\begin{cases} 0 = -\dfrac{R}{L} I_{c0} - \dfrac{1}{L} V_{cc0} - I_{s0}\,\omega_{s0} \\ 0 = -\dfrac{R}{L} I_{s0} - \dfrac{1}{L} V_{cs0} + \dfrac{4V}{L\pi}\left(\cos(\theta_{10}) + \cos(\theta_{20})\right) + I_{c0}\,\omega_{s0} \\ 0 = +\dfrac{1}{C} I_{c0} - V_{cs0}\,\omega_{s0} \\ 0 = +\dfrac{1}{C} I_{s0} + V_{cc0}\,\omega_{s0} \end{cases} \tag{43}$$

The equations (43) can be written as matrix forms ($Ax=B$) to found the equilibrium operating points (I_{c0}, I_{s0}, V_{cc0}, V_{cs0}).

$$A = \begin{bmatrix} -\dfrac{R}{L} & -\omega_{s0} & -\dfrac{1}{L} & 0 \\ +\omega_{s0} & -\dfrac{R}{L} & 0 & -\dfrac{1}{L} \\ +\dfrac{1}{C} & 0 & 0 & -\omega_{s0} \\ 0 & +\dfrac{1}{C} & +\omega_{s0} & 0 \end{bmatrix} \; ; \; x = \begin{bmatrix} I_{c0} \\ I_{s0} \\ V_{cc0} \\ V_{cs0} \end{bmatrix} \; ;$$

$$B = \begin{bmatrix} 0 & -\dfrac{4V}{L\pi}\left(\cos\left(\theta_{10}\right) + \cos\left(\theta_{20}\right)\right) & 0 & 0 \end{bmatrix}^{t}$$

4.2.6 Disruption and linearization of the model developed in step 4 using (X_0, U_0, Y_0)

Using Taylor series, the generalized small-signal model of the system is derived by perturbation and linearization of Large-signal model around the operating point (U_0, X_0, Y_0):

$$\begin{cases} x(t) = X_0 + \tilde{x}(t) \;\; ; \;\; where: \; \tilde{x}(t) \ll X_0 \\ u(t) = U_0 + \tilde{u}(t) \;\; ; \;\; where: \; \tilde{u}(t) \ll U_0 \\ y(t) = Y_0 + \tilde{y}(t) \;\; ; \;\; where: \; \tilde{y}(t) \ll Y_0 \end{cases}$$

Using Taylor series, the perturbation and linearization of the input controls is given as:

$$\begin{cases} v = V + \tilde{v} \\ \theta_1 = \theta_{10} + \tilde{\theta}_1 \\ \theta_2 = \theta_{20} + \tilde{\theta}_2 \\ \omega_s = \omega_{s0} + \tilde{\omega}_s \end{cases}$$

Using Taylor series, the perturbation and linearization of the Large-signal model of the system is developed to be:

$$\begin{cases} \dot{\tilde{i}}_c = -\dfrac{R}{L}\tilde{i}_c - \dfrac{1}{L}V_{cc} - I_{s0}\tilde{\omega}_s - \tilde{i}_s\omega_{s0} \\ \dot{\tilde{i}}_s = -\dfrac{R}{L}\tilde{i}_s - \dfrac{1}{L}\tilde{V}_{cs} + I_{c0}\tilde{\omega}_s + \tilde{i}_c\omega_{s0} + \dfrac{4}{L\pi}\cos(\theta_{10})\tilde{v} + \\ \qquad \dfrac{4}{L\pi}\cos(\theta_{20})\tilde{v} - \dfrac{4V}{L\pi}\sin(\theta_{10})\tilde{\theta}_1 - \dfrac{4V}{L\pi}\sin(\theta_{20})\tilde{\theta}_2 \\ \dot{\tilde{V}}_{cc} = +\dfrac{1}{C}\tilde{i}_c - V_{cs0}\tilde{\omega}_s - \tilde{V}_{cs}\omega_{s0} \\ \dot{\tilde{V}}_{cs} = +\dfrac{1}{C}\tilde{i}_s + V_{cc0}\tilde{\omega}_s + \tilde{V}_{cc}\omega_{s0} \end{cases} \tag{44}$$

Using Taylor series, the perturbation and linearization of the output variable of the system is given as:

$$\dot{\tilde{y}} = \frac{V_{cc0}}{\sqrt{V_{cc0}^2 + V_{cs0}^2}}\tilde{V}_{cc} + \frac{V_{cs0}}{\sqrt{V_{cc0}^2 + V_{cs0}^2}}\tilde{V}_{cs} \tag{45}$$

4.2.7 Extraction of the matrices A_s, B_s, C_s, D_s of the linear model with small signals

In matrix form, the state equations of the small-signal model are given as:

$$\begin{cases} \dot{\tilde{x}}(t) = A_s\tilde{x}(t) + B_s\tilde{u}(t) \\ \tilde{y}(t) = C_s\tilde{x}(t) + D_s\tilde{u}(t) \end{cases} \tag{46}$$

Furthermore, the state equations of the small-signal model can be described as:

$$\begin{cases} \dot{\tilde{x}}(t) = A_s\tilde{x}(t) + B_1\tilde{u}_1(t) + B_2\tilde{u}_2(t) + B_3\tilde{u}_3(t) + B_4\tilde{u}_4(t) \\ \tilde{y}(t) = C_s\tilde{x}(t) + D_s\tilde{u}(t) \end{cases} \tag{47}$$

Where:

$$\begin{cases} \tilde{x}(t) = \begin{bmatrix} \tilde{i}_c & \tilde{i}_s & \tilde{V}_{cc} & \tilde{V}_{cs} \end{bmatrix}^t \\ \tilde{u}(t) = \begin{bmatrix} \tilde{u}_1(t) & \tilde{u}_2(t) & \tilde{u}_3(t) & \tilde{u}_4(t) \end{bmatrix}^t = \begin{bmatrix} \tilde{v} & \tilde{\theta}_1 & \tilde{\theta}_2 & \tilde{\omega}_s \end{bmatrix}^t \\ \tilde{y}(t) = \tilde{V}_c \end{cases}$$

$$A_s = \begin{bmatrix} -\frac{R}{L} & -\omega_{s0} & -\frac{1}{L} & 0 \\ +\omega_{s0} & -\frac{R}{L} & 0 & -\frac{1}{L} \\ +\frac{1}{C} & 0 & 0 & -\omega_{s0} \\ 0 & +\frac{1}{C} & +\omega_{s0} & 0 \end{bmatrix};$$

$$B_1 = \begin{bmatrix} 0 & +\frac{4}{L\pi}\left(\cos(\theta_{10}) + \cos(\theta_{20})\right) & 0 & 0 \end{bmatrix}^t$$

$$B_2 = \begin{bmatrix} 0 & -\frac{4V}{L\pi}\sin(\theta_{10}) & 0 & 0 \end{bmatrix}^t$$

$$B_3 = \begin{bmatrix} 0 & -\frac{4V}{L\pi}\sin(\theta_{20}) & 0 & 0 \end{bmatrix}^t$$

$$B_4 = \begin{bmatrix} -I_{s0} & +I_{c0} & -V_{cs0} & +V_{cc0} \end{bmatrix}^t$$

$$C_s = \begin{bmatrix} 0 & 0 & \dfrac{V_{cc0}}{\sqrt{V_{cc0}^2 + V_{cs0}^2}} & \dfrac{V_{cs0}}{\sqrt{V_{cc0}^2 + V_{cs0}^2}} \end{bmatrix};$$

$$D_s = 0$$

In transfer functions form [5], the equations of the small-signal model for the five-level series resonant inverter are given as:

$$\begin{cases} G_{\tilde{v}}^{\tilde{V}_c}(s) = \dfrac{\tilde{V}_c(s)}{\tilde{v}(s)} = tf\left(A_s, B_1, C_s, D\right) \\ G_{\tilde{\theta}_1}^{\tilde{V}_c}(s) = \dfrac{\tilde{V}_c(s)}{\tilde{\theta}_1(s)} = tf\left(A_s, B_2, C_s, D\right) \\ G_{\tilde{\theta}_2}^{\tilde{V}_c}(s) = \dfrac{\tilde{V}_c(s)}{\tilde{\theta}_2(s)} = tf\left(A_s, B_3, C_s, D\right) \\ G_{\tilde{\omega}_s}^{\tilde{V}_c}(s) = \dfrac{\tilde{V}_c(s)}{\tilde{\omega}_s(s)} = tf\left(A_s, B_4, C_s, D\right) \end{cases} \quad (48)$$

Where:

$G_{\tilde{v}}^{\tilde{V}_c}(s)$: The transfer functions of input-voltage-to-capacitor-output-voltage.

$G_{\tilde{\theta}_1}^{\tilde{V}_c}(s)$: The switching-angle-θ_1-to-capacitor-output-voltage.

$G_{\tilde{\theta}_2}^{\tilde{V}_c}(s)$: The switching-angle-θ_2-to-capacitor-output-voltage.

$G_{\tilde{\omega}_s}^{\tilde{V}_c}(s)$: The switching-frequency-to-capacitor-output-voltage.

4.3 Validation of the small signal model and the five-level series resonant inverter

Currently, several tools exist for validating the small-signal model of any system, among them: SIMPLIS AC analysis [6], AC SWAP of PLECS, LTspice AC analysis, STREAM in Linearization manager tool of MATLAB [7]. In this study, two steps are

followed for validating the proposed small-signal model and the five-level series resonant inverter. The first step is the calculation of switching angles using the selective harmonic elimination modulation. The second step is frequency analysis of the small-signal model using the Linearization manager tool with sinestream as the perturbation signal and system identification toolbox.

4.3.1 Selective harmonic elimination modulation

The SHE technique offers several advantages when used to generate the gating signals of the multilevel inverter, where the switching angles are determined by solving a nonlinear transcendental system of equations. In literature, several methods have been proposed to find the best switching angles, including Newton-Raphson (N-R) Algorithm, Genetic Algorithm (GA), Artificial Neural Network (ANN) [8]-[11].

With the Fourier analysis, the first harmonic (n=1) of the inverter output voltage $V_o(t)$ is written as:

$$V_o(t) = \frac{4V}{\pi}\left(\cos(\theta_1) + \cos(\theta_2)\right)\sin(\omega_s t) \tag{49}$$

To eliminate the third harmonic and their multiple, we must search the switching angles θ_1, θ_2 versus the modulation index M. The switching angles must satisfy the subsequent algebraic system of the non-linear equations:

$$\begin{cases} \cos(\theta_1) + \cos(\theta_2) = \dfrac{\pi h_1}{4V} \\ \cos(3\theta_1) + \cos(3\theta_2) = 0 \end{cases} \tag{50}$$

This study used an MLP neural network with a (1:5:2) structure, as shown in Figure 37. The (1:5:2) structure is composed of an input layer (modulation index M) that receives data, a hidden layer comprising five-neuron, and an output layer (switching angles θ_1 and θ_2) formed of two-neuron.

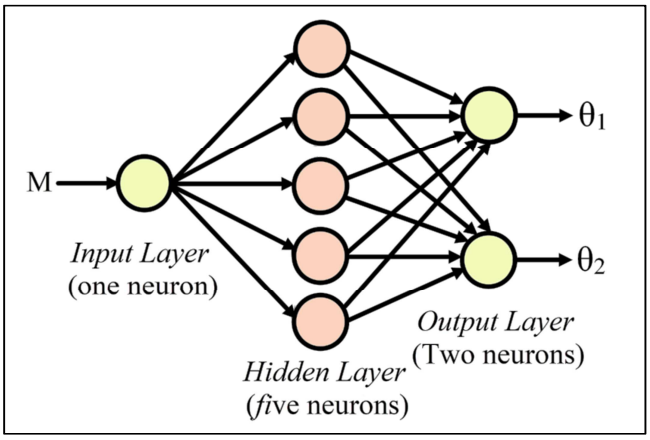

Figure 37: The MLP neural network with (1:5:2) structure.

Figure 38 illustrates the gating switching angles θ_1 and θ_2 generated using the ANN algorithm, considering the modulation index M values. Following the analytical analysis [12], the valid interval of modulation index is $M \in [0.45;0.85]$ to eliminate the third harmonic and their multiple.

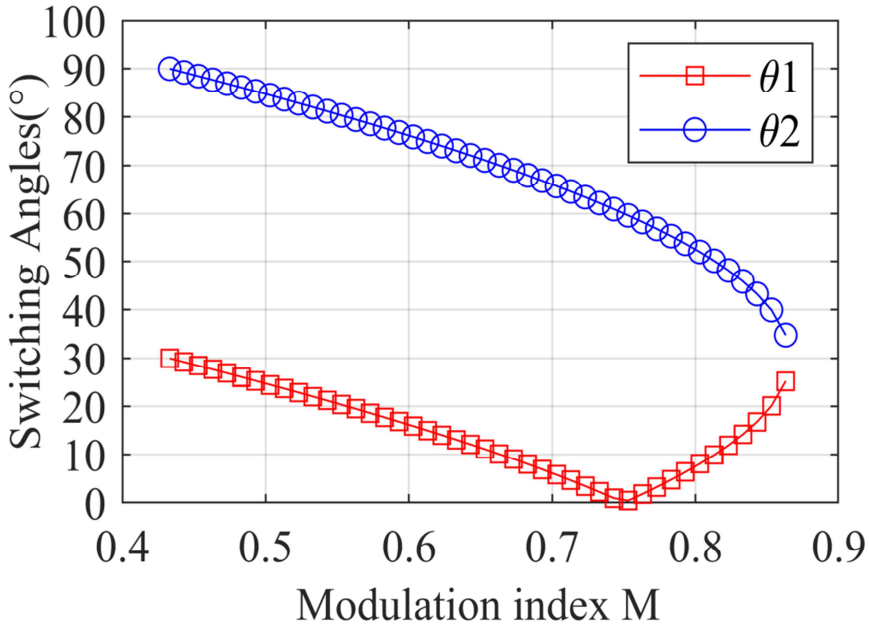

Figure 38: The switching angles θ_1 and θ_2 using ANN algorithm.

Table 7 illustrates the gating switching angles θ_1 and θ_2 versus the modulation index M with the artificial neural network-based selective harmonic elimination (ANN-SHE).

Table 7: Switching angles θ_1 and θ_2 versus modulation index M with ANN-SHE.

Modulation index	*Switching angles*	
	θ_1	θ_2
0.50	25	85
0.55	21	81
0.60	16	76
0.65	11	71
0.70	06	66
0.80	07	53
0.85	19	41

Modulation index M=0.85, and switching angles equal to θ_1=19°, θ_2=41° are selected for testing the system, where these parameters give maximum RMS voltage with the elimination of 3rd harmonic plus their multiples [5].

4.3.2 Validation of the small signal model with frequency analysis

After selecting the switching angles equal to θ_1=19°, θ_2=41° for selective harmonic elimination modulation, Table 8 illustrates the other required operating parameters for validation of the presented small-signal model in subsection 4-2-7.

Table 8: Operating parameters of the five-level series resonant inverter

Item.	*Ref.*	*Value*
Input Voltage	V_{dc}	5 Volts
Equivalent Resistance	R	200 Ω
Equivalent Inductance	L	300 mH
Resonant Capacitor	C	3 nF
Resonant frequency	f_0	5.3 kHz
Switching Angle	θ_1	19°
Switching Angle	θ_2	41°

The Editor of the MATLAB environment has been used to test the small-signal model; next, the Linearization manager tool and system identification toolbox of MATLAB are used to compare the small-signal model with the Simulink model [5].

In transfer functions form, the equations of the small-signal model are given as:

$$\begin{cases} G_{\tilde{v}}^{\tilde{V}_c}(s) = \dfrac{\tilde{V}_c(s)}{\tilde{v}(s)} = \dfrac{1.649e08\,S^2 + 1.129e14\,S + 3.794e16}{S^4 + 1333\,S^3 + 4.441e09\,S^2 + 2.96e12\,S + 4.975e14} \\ G_{\tilde{\theta}_1}^{\tilde{V}_c}(s) = \dfrac{\tilde{V}_c(s)}{\tilde{\theta}_1(s)} = \dfrac{-1.579e08\,S^2 - 1.08e14\,S - 3.632e16}{S^4 + 1333\,S^3 + 4.441e09\,S^2 + 2.96e12\,S + 4.975e14} \\ G_{\tilde{\theta}_2}^{\tilde{V}_c}(s) = \dfrac{\tilde{V}_c(s)}{\tilde{\theta}_2(s)} = \dfrac{-3.181e08\,S^2 - 2.177e14\,S - 7.319e16}{S^4 + 1333\,S^3 + 4.441e09\,S^2 + 2.96e12\,S + 4.975e14} \\ G_{\tilde{\omega}_s}^{\tilde{V}_c}(s) = \dfrac{\tilde{V}_c(s)}{\tilde{\omega}_s(s)} = \dfrac{-8.464e09\,S + 4.926e13}{S^4 + 1333\,S^3 + 4.441e09\,S^2 + 2.96e12\,S + 4.975e14} \end{cases}$$

Figure 39, Figure 40, Figure 41, and Figure 42 show the Bode diagram frequency responses of the input-voltage-to-capacitor-output-voltage $G_{\tilde{v}}^{\tilde{V}_c}(s)$, the switching-angle-$\theta_1$-to-capacitor-output-voltage $G_{\tilde{\theta}_1}^{\tilde{V}_c}(s)$, switching-angle-$\theta_2$-to-capacitor-output-voltage $G_{\tilde{\theta}_2}^{\tilde{V}_c}(s)$, and the switching-frequency-to-capacitor-output-voltage $G_{\tilde{\omega}_s}^{\tilde{V}_c}(s)$, respectively. The figures illustrate the simulation model (Measurement) and the small-signal model's transfer functions (Model). (Solid trace): the theoretical small-signal model (Model), and (blue cross): Measurement data from simulation model (Measurement).

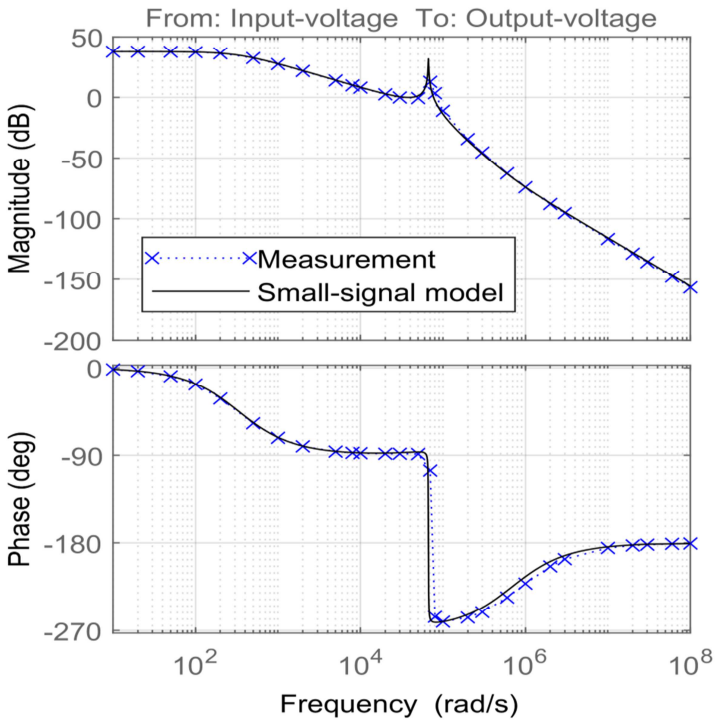

Figure 39: Comparisons of Bode plots related to the input-voltage-to-capacitor-output-voltage.

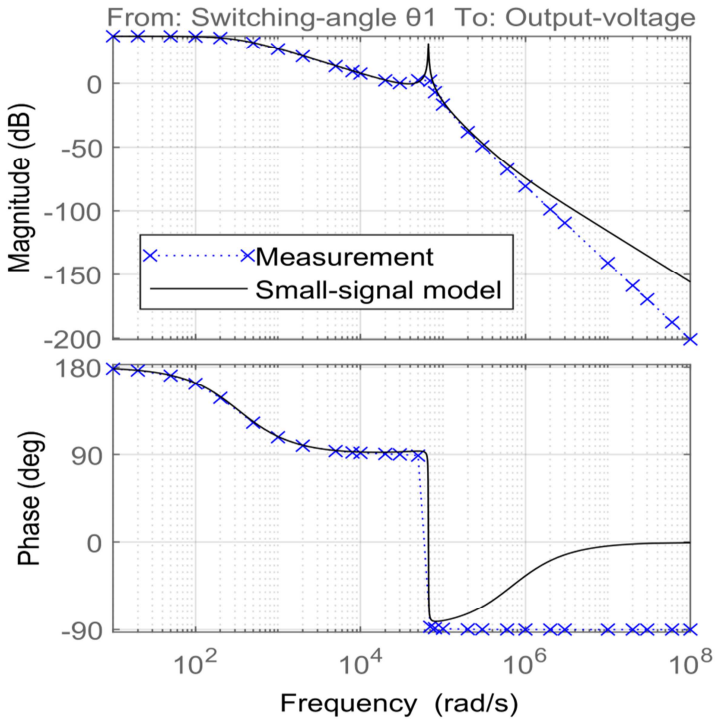

Figure 40: Comparisons of Bode plots related to the switching-angle-θ_1-to-capacitor-output-voltage.

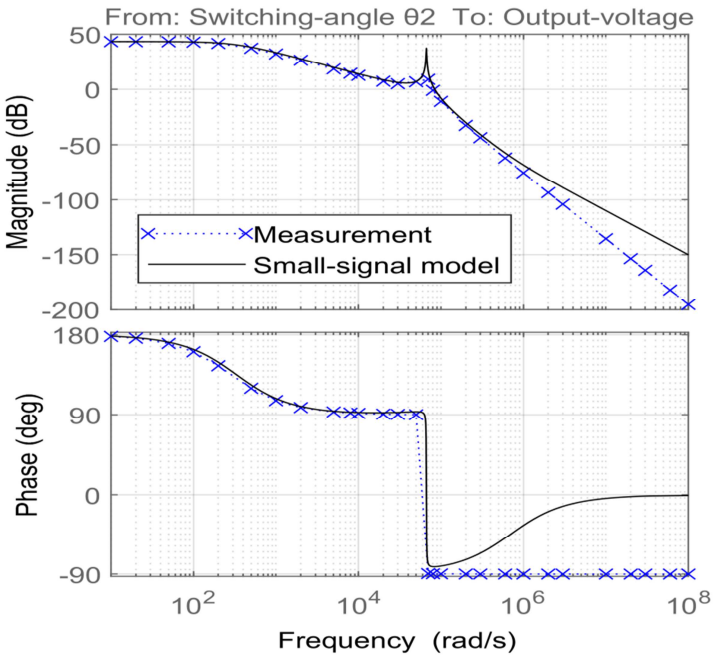

Figure 41: Comparisons of Bode plots related to the switching-angle-θ_2-to-capacitor-output-voltage.

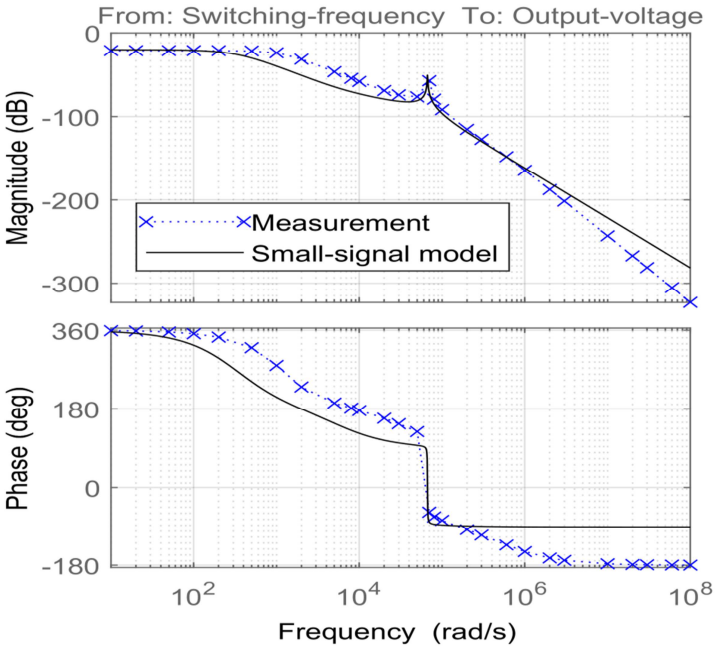

Figure 42: Comparisons of Bode plots related to the switching-frequency-to-capacitor-output-voltage.

As noted in Figures 39, 40, 41, and 42, the responses of both small-signal and the Simulink model are closely matching, where there are certain deviations because only the

fundamental component is considered in the small-signal modeling approach. These results validate the mathematical analysis and the proposed small-signal LTI model.

4.4 Results discussion & interpretations

The proposed circuit of a five-level series resonant inverter is evaluated using simulation and experimental tests. In this section, the results are presented with various switching frequency tests, less than the resonant frequency ($f_s<f_0$), equals the resonant frequency ($f_s=f_0$), and above the resonant frequency ($f_s>f_0$); where the system operating parameters are given in Table 8.

4.4.1 Simulation results

The simulation model of the five-level inverter with ANN-SHE modulation is built under a Matlab/Simulink environment. Figure 43 shows the Simulink model of the five-level series resonant inverter.

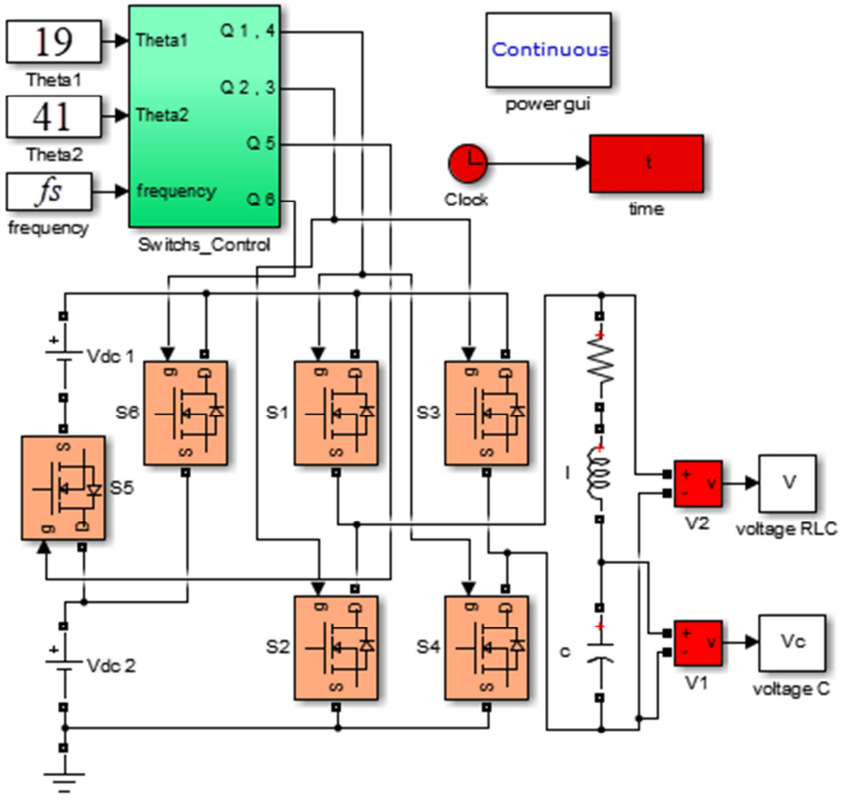

Figure 43: Simulink model of the five-level series resonant inverter.

Figure 44 shows the five-level output voltage waveform with ANN-SHE modulation, M=0.85, θ_1=19°, and θ_2=41°, and f=5 kHz. Their associated harmonic spectrums are presented in Figure 45, where the $THDv$=16.34 % and the 3rd harmonic with their multiples have been eliminated.

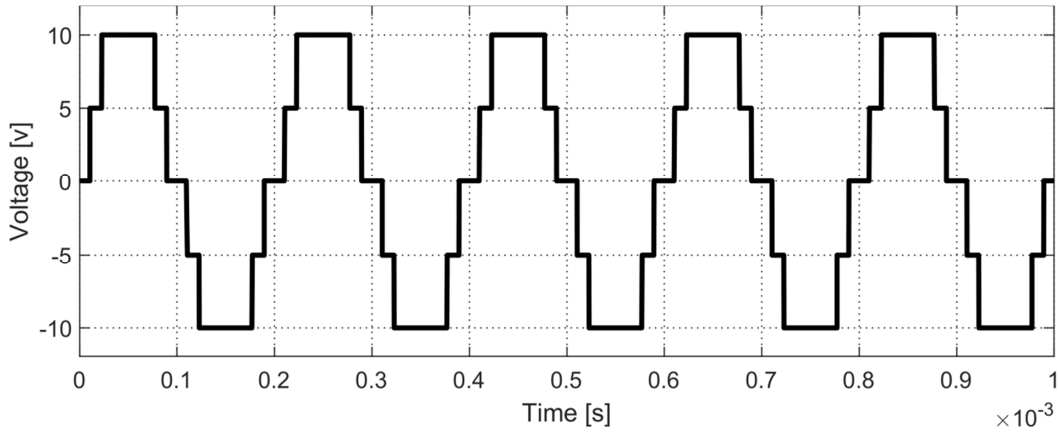

Figure 44: The output voltage waveform of the five-level inverter with ANN-SHE.

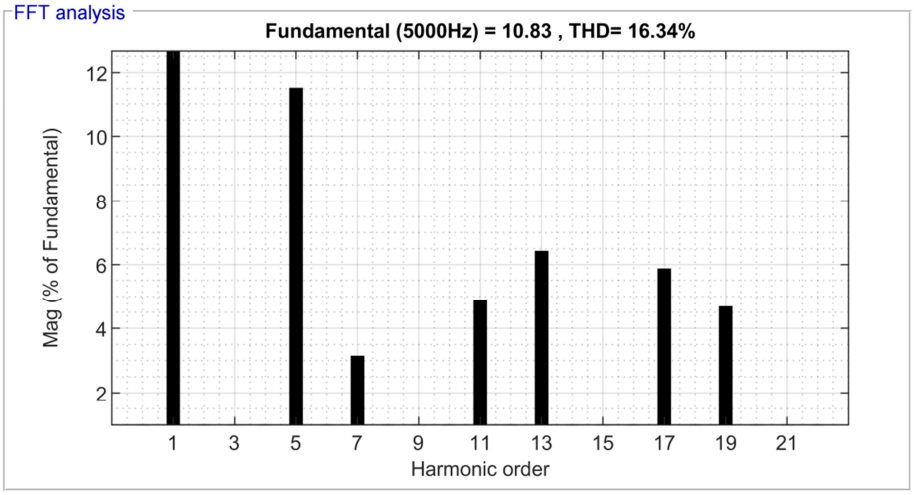

Figure 45: The associated harmonic spectrum of the five-level output voltage.

Figure 46 shows the simulation waveforms of the output inverter voltage $V_{inv}(t)$ and the output capacitor voltage $V_c(t)$ with frequency (f_s<f_0) equal to 2 kHz.

Figure 47 shows the simulation waveforms of the output inverter voltage $V_{inv}(t)$ and the output capacitor voltage $V_c(t)$ with frequency (f_s=f_0) equal to 5.3 kHz.

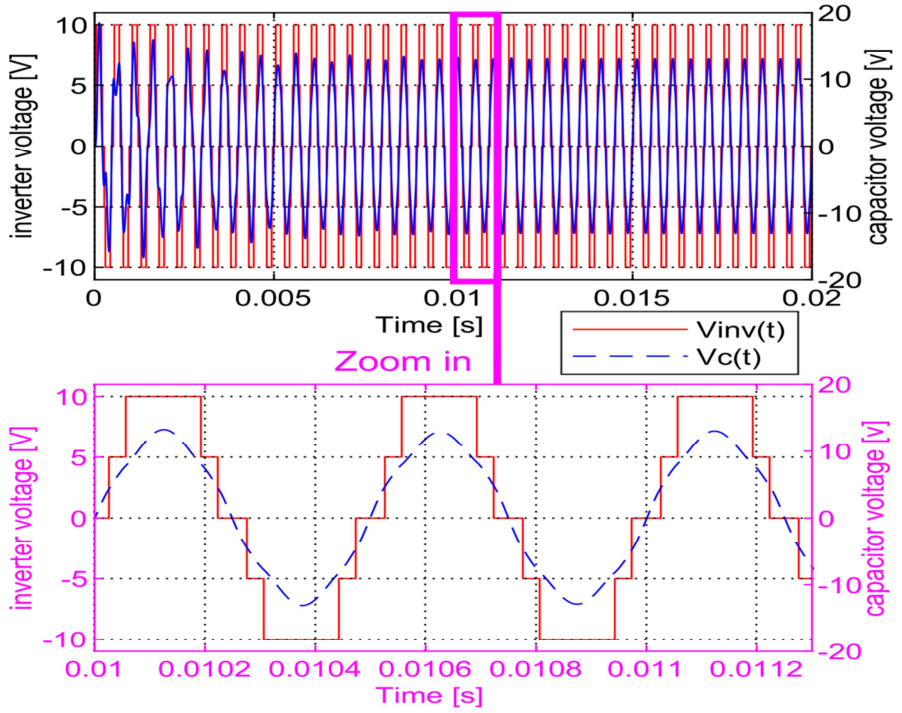

Figure 46: Simulation waveforms of output inverter and output capacitor voltages with f_s =2 kHz.

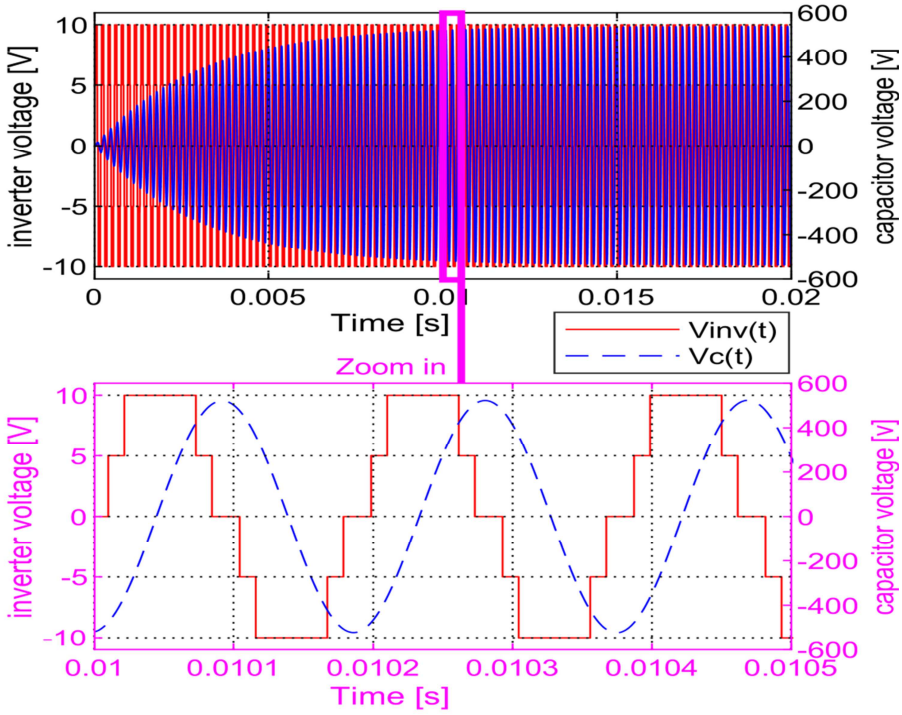

Figure 47: Simulation waveforms of output inverter and output capacitor voltages with f_s =5.3 kHz.

Figure 48 shows the simulation waveforms of the output inverter voltage $V_{inv}(t)$ and the output capacitor voltage $V_c(t)$ with frequency (f_s>f_0) equal to 8 kHz.

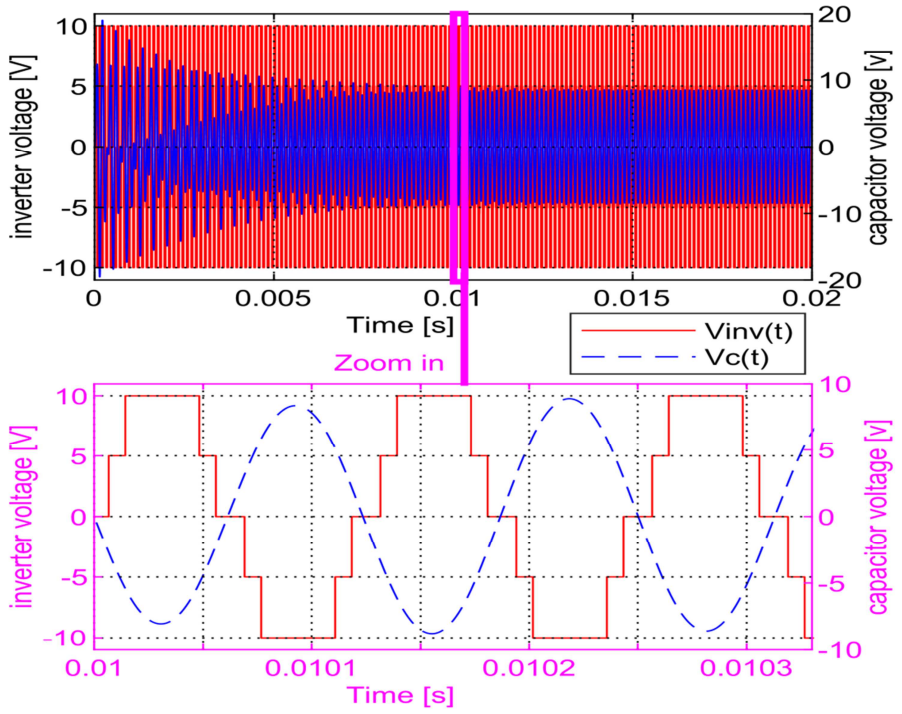

Figure 48: Simulation waveforms of output inverter and output capacitor voltages with f_s =8 kHz.

As displays in Figure 46, there are two regimes, permanent and transient regimes. The transient regime is imposed by the nonlinearity saturation and hysteresis of electronic components. Inductances and capacitors components are sources of transient voltages. As noticed from the zoom-in from 10 ms to 12 ms, the output inverter voltage $V_{inv}(t)$ and the output capacitor voltage $V_c(t)$ are in the same phase. As observed, the output capacitor voltage $V_c(t)$ is sinusoidal, with a maximum value of 13 V.

As displays in Figure 47, there are two regimes, permanent and transient regimes. We can notice that the waveform is quite particular, where the wavelength is regularly growing from zero to a permanent regime. As seen from the zoom-in from 10 ms to 10.5 ms, the output capacitor voltage $V_c(t)$ lags 90 degrees from the output inverter voltage $V_{inv}(t)$ compared with the previous case. As observed, the output capacitor voltage $Vc(t)$ is sinusoidal, with a maximum value of 538 V.

As displays in Figure 48, there are two regimes, permanent and transient regimes. As noticed from the zoom-in from 10 ms to 10.33 ms, the output capacitor voltage $V_c(t)$ lags 90 degrees from the output inverter voltage $V_{inv}(t)$ compared with the previous case. As observed, the output capacitor voltage $V_c(t)$ is sinusoidal, with a maximum value of 8 V.

4.4.2 Experimental results

A laboratory prototype of the five-level series resonant inverter is realized, as shown in Figure 49. (1): Pc + Matlab software. (2): C2000 Delfino DSP320F28379D Board. (3): Gate Driver circuits. (4): Inverter (MOSFET switches). (5): Current and voltage sensors. (6): series RLC (Resistor, Inductor, Capacitor) circuit. (7): Power supplies (Vdc). (8): Digital oscilloscope. The control signals are implemented in real-time using an embedded board C2000 Delfino DSP320F28379D. GWINSTEK Digital oscilloscope is used to extract the voltage waveforms.

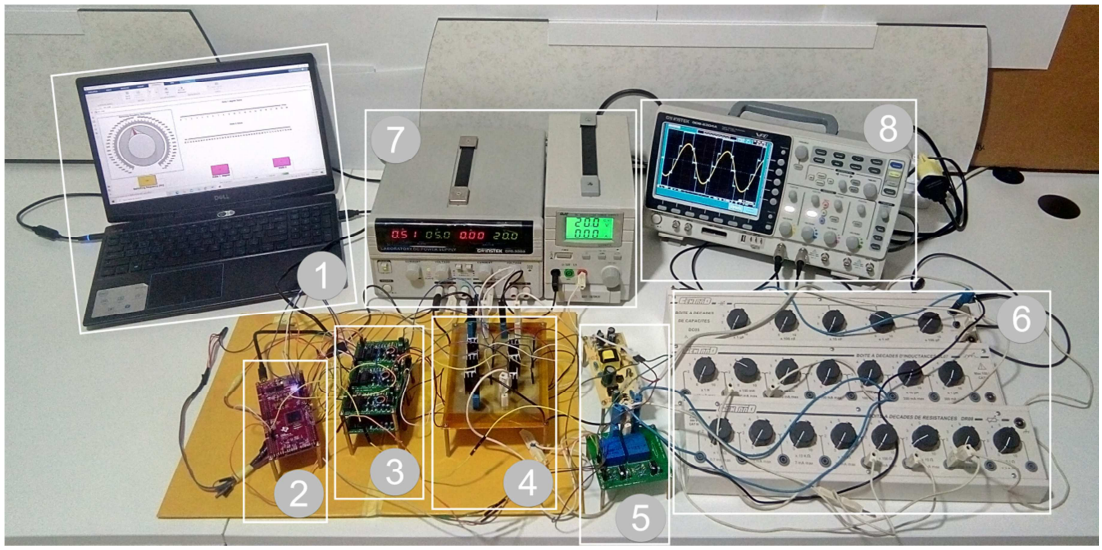

Figure 49: The Experimental Laboratory Prototype of a five-level series resonant inverter.

Figure 50 shows an example of the gating signals of switches S_1~S_3~S_5 with a frequency of 1 kHz, and Figure 51 illustrates the gating signals of switches S_2~S_4~S_6.

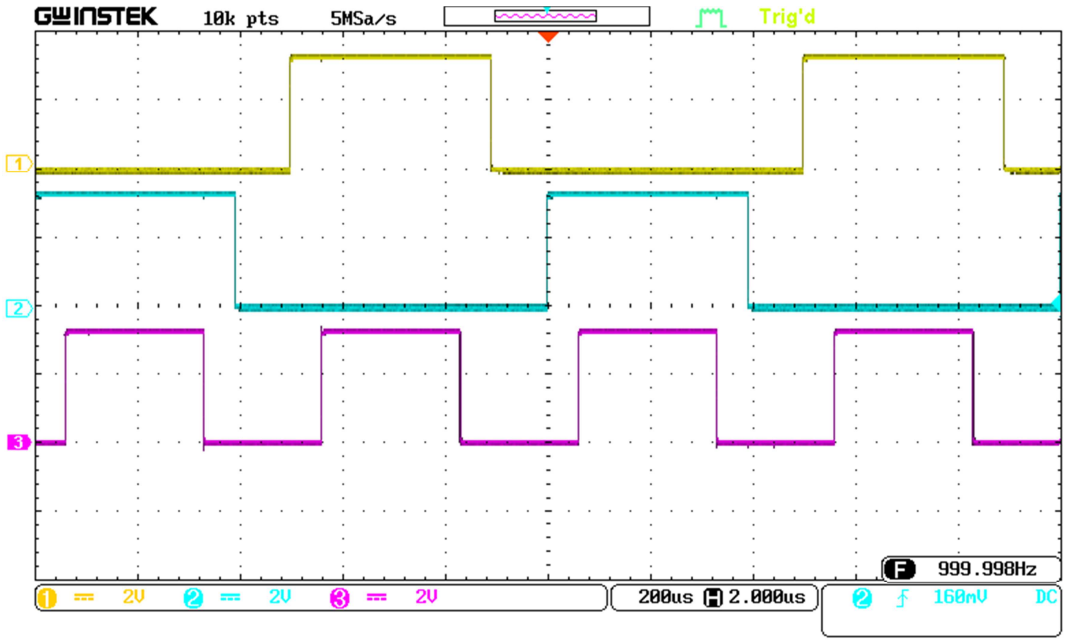

Figure 50: The gating signals of S_1~S_3~S_5 with frequency of 1 kHz

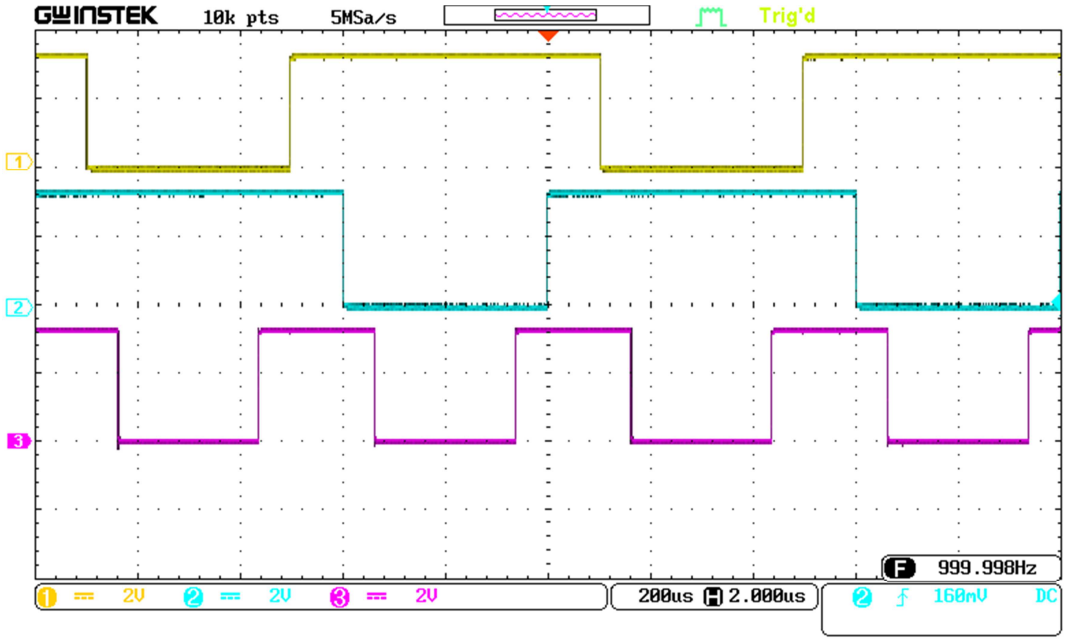

Figure 51: The gating signals of S_2~S_4~S_6 with frequency of 1 kHz

Figure 52 illustrates the experimental phase voltage of the five-level inverter with ANN-SHE modulation, modulation index M=0.85, and switching angles: θ_1=19°, θ_2=41°. f=1 [kHz], and V_{dc}=5 [V].

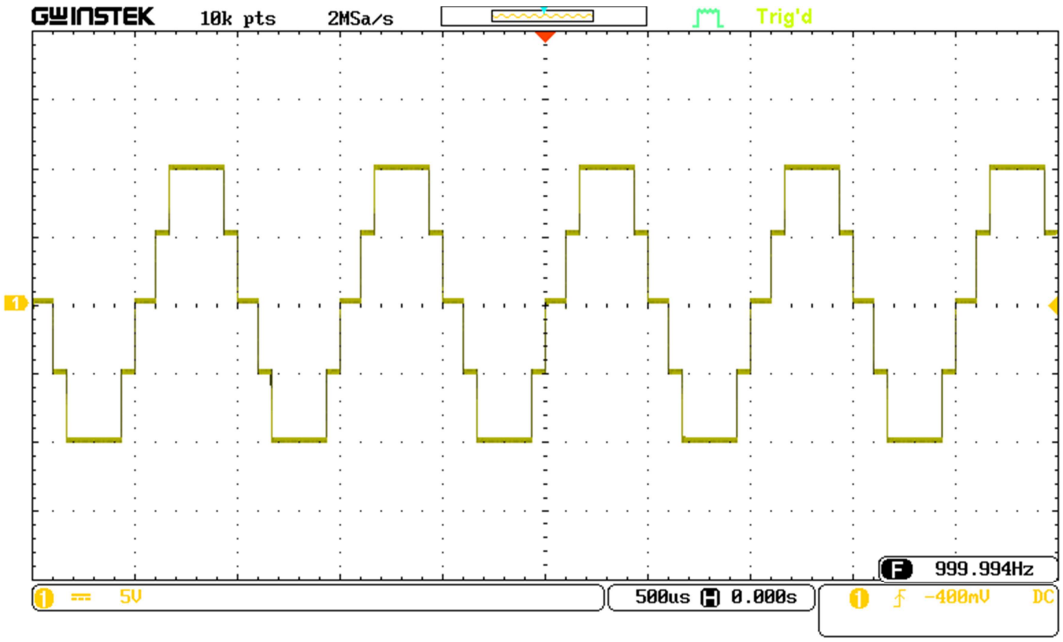

Figure 52: The experimental output voltage of the five-level inverter with ANN-SHE, and f=1 kHz

Figure 53 illustrates the experimental phase voltage of the five-level inverter with ANN-SHE modulation, modulation index M=0.85, and switching angles: θ_1=19°, θ_2=41°. f=5 [kHz], and V_{dc}=5 [V].

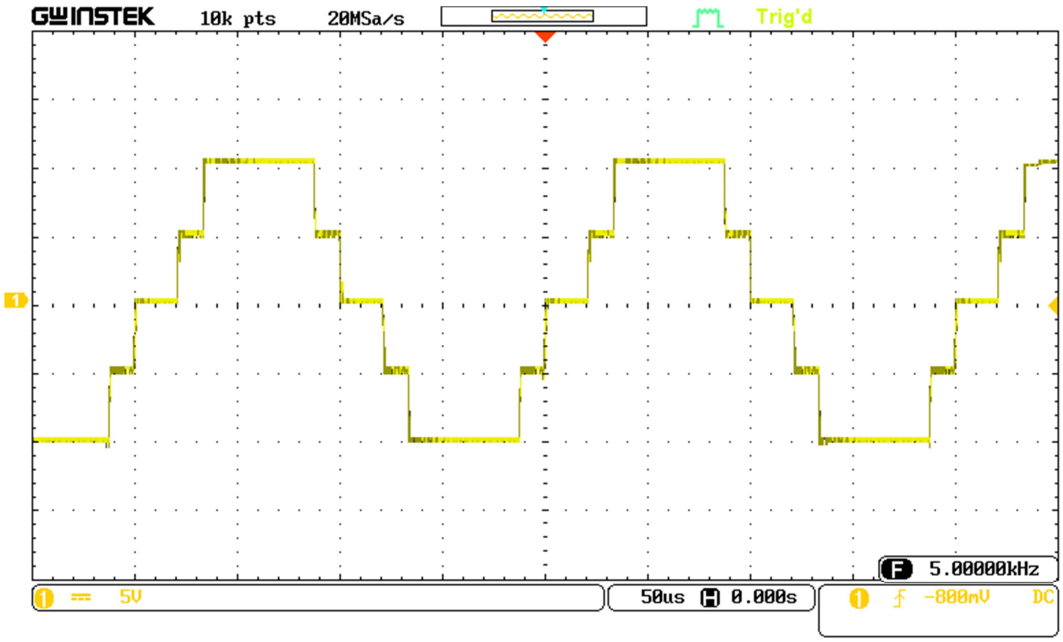

Figure 53: The experimental output voltage of the five-level inverter with ANN-SHE, and f=5 kHz

Figure 54 illustrates the experimental phase voltage of the five-level inverter with ANN-SHE modulation, modulation index M=0.85, and switching angles: θ_1=19°, θ_2=41°. f=10 [kHz], and V_{dc}=5 [V].

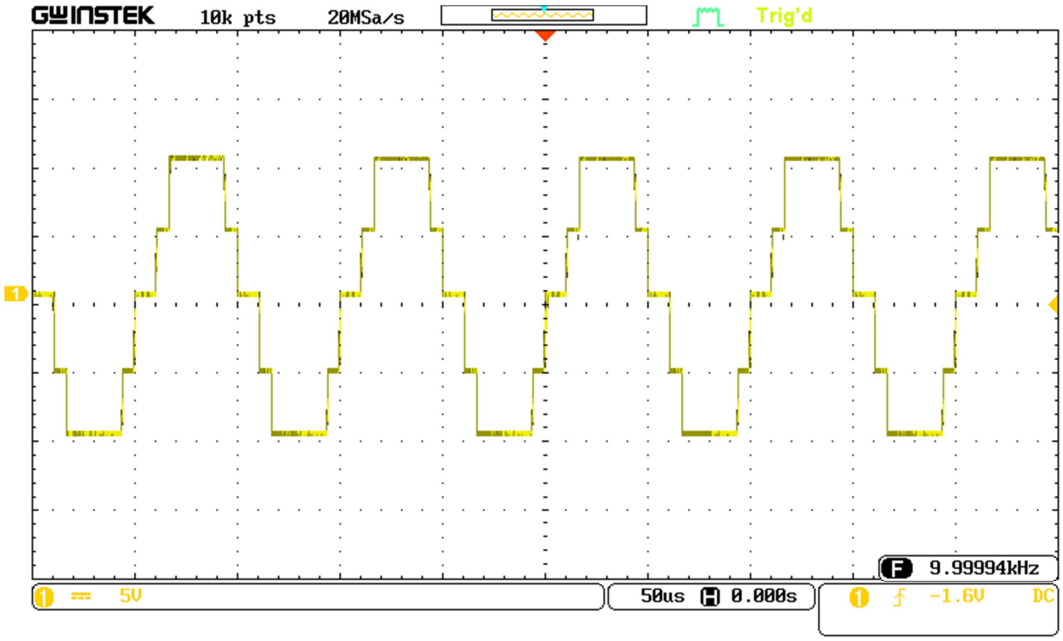

Figure 54: The experimental output voltage of the five-level inverter with ANN-SHE, and f=10 kHz

Figure 55 illustrates the experimental waveforms of the output inverter voltage $V_{inv}(t)$ and the output capacitor voltage $V_c(t)$ with switching frequency (f_s) equal to 2 kHz. A maximum voltage of 12 V in the capacitor is noted, and an RMS voltage equal to 8.23 V is measured.

Figure 56 illustrates the experimental waveforms of the output inverter voltage $V_{inv}(t)$ and the output capacitor voltage $V_c(t)$ with switching frequency (f_s) equal to 5.3 kHz. A maximum voltage of 520 V in the capacitor is noted, and an RMS voltage equal to 370.3 V is measured.

Figure 57 illustrates the experimental waveforms of the output inverter voltage $V_{inv}(t)$ and the output capacitor voltage $V_c(t)$ with switching frequency (f_s) equal to 8 kHz. A maximum voltage of 6 V in the capacitor is noted, and an RMS voltage equal to 4.37 V is measured.

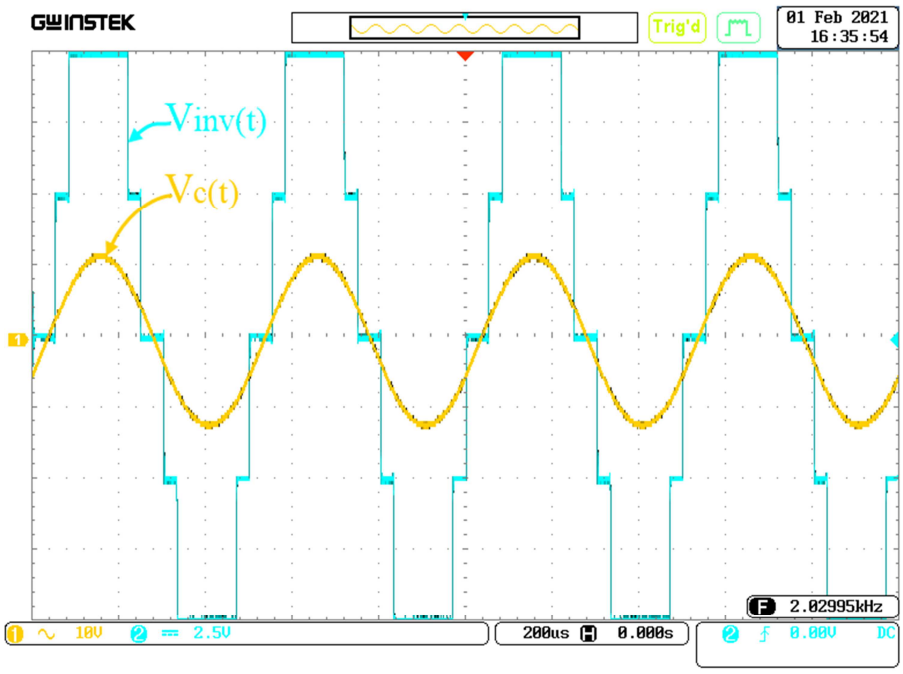

Figure 55: Experimental voltage waveforms of output inverter and output capacitor with f_s =2 kHz.

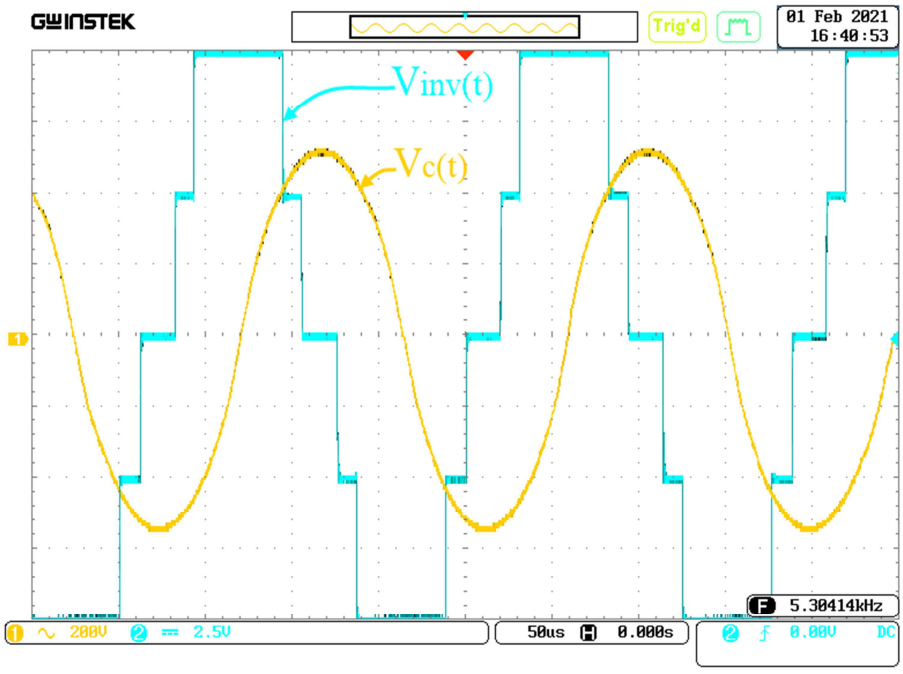

Figure 56: Experimental voltage waveforms of output inverter and output capacitor with f_s =5.3 kHz.

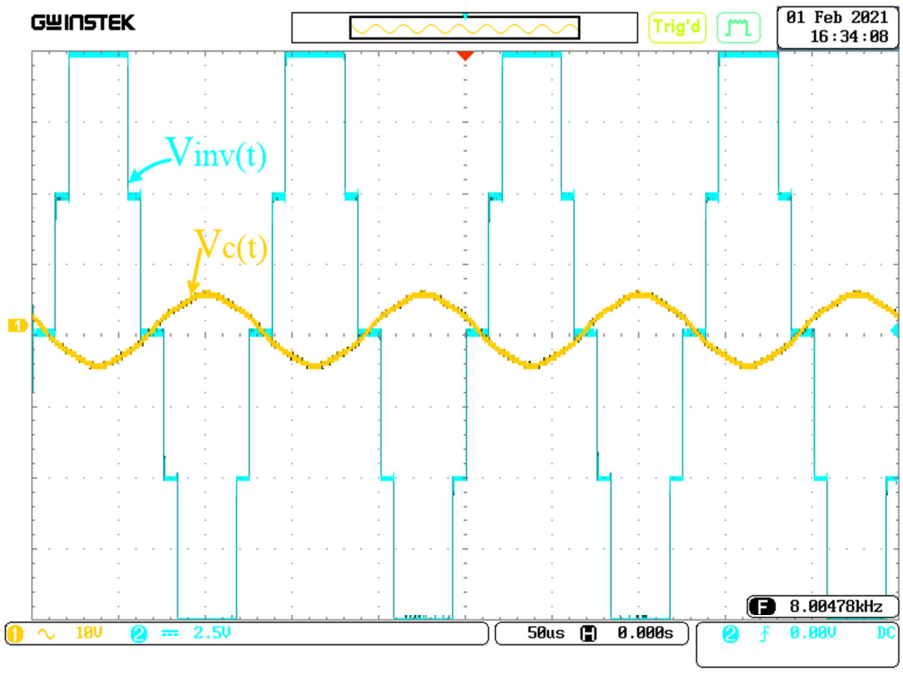

Figure 57: Experimental voltage waveforms of output inverter and output capacitor with f_s =8 kHz.

4.4.2 Comparison between the results of simulation and experimental

The experimental results match those observed in the simulation. We can show the similarity that exists between the simulation figures: Figs. 46, 47, and 48 and the experimental figures: Figs. 55, 56, and 57, respectively. Since we have an inductance L and a capacitor C in the series RLC circuit, we distinguish three operation cases depending upon the operating frequency: inductive circuit, capacitive circuit, a resonant circuit; this result is in accord with the conclusions given in [13].

Figure 58 shows the measured RMS output voltage in capacitor versus variable switching-frequency from 2 kHz to 8 kHz. As noticed from the waveforms, simulation and experimental data are closely matching. At 5.3 kHz, the output capacitor achieves a higher RMS voltage value, approximately equals to 370 V.

The obtained results with the proposed five-level series resonant inverter are in agreement with the findings of previous studies [14] with conventional Full-Bridge inverter; wherein at the resonance frequency: (1) the switching frequency of the inverter approaches the frequency of the series *RLC* circuit; (2) the inductive reactance equals the capacitive reactance (X_L=X_C); thus, the reactance's impact is canceled; and (3) the *RLC*

circuit becomes resistive circuit and the output capacitor achieves a higher *RMS* voltage value, and the current becomes maximal.

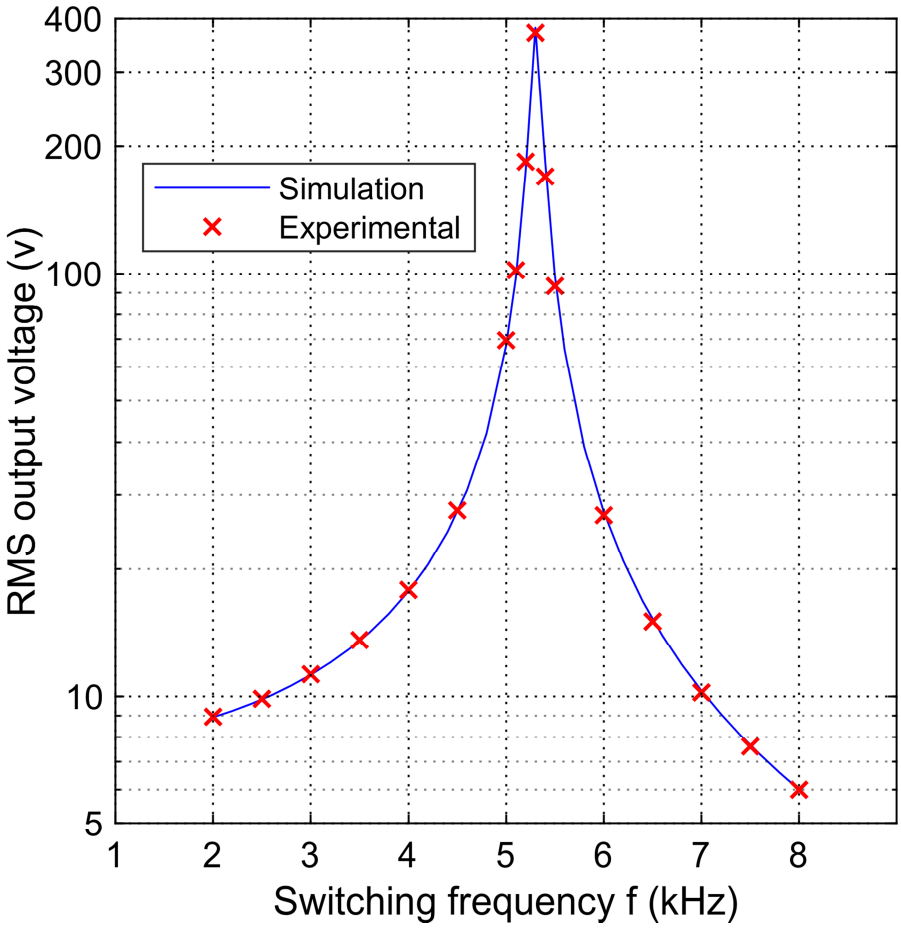

Figure 58: Comparison between results of simulation and experimental

4.5 Summary

The main goal of the current chapter was to develop and validate a small-signal model of a five-level series resonant inverter. The model analysis revealed that the developed Linear Time-Invariant LTI model of the five-level series resonant inverter could be used to design a closed-loop control system. In summary, the artificial neural network-based selective harmonic elimination SHE technique is used for the five-level inverter modulation. Also, the small-signal model is validated with frequency analysis. Furthermore, the proposed circuit of a five-level series resonant inverter is evaluated using simulation and experimental results.

Chapter 05:

CONTROL TECHNIQUES FOR A FIVE-LEVEL SERIES RESONANT INVERTER

CHAPTER 5 CONTROL TECHNIQUES FOR A FIVE-LEVEL SERIES RESONANT INVERTER

5.1 Introduction

This chapter is focused on the design and implementation of some control methods for controlling a five-level series resonant inverter; the purpose is to achieve a high performances control system. In process system control, high performances are achieved when the controlled variable of the system fellow the reference value with optimal values of system characteristics. The system responses characteristics are rise time, overshoot, settling time, and steady-state error. The conventional control techniques can be used to ensure the rise time, overshoot, and steady-state error criteria. However, a robustness criterion remains a challenge for the researchers; this criterion can be addressed using advanced control techniques.

This chapter is devised into three main parts, and each part is composed of sub-sections. The chapter organization aims to provide a comprehensive presentation of each control technique and discuss the obtained results. In the first part, a coefficient diagram method CDM is used to design the optimal parameters of the proportional-integral regulator. This part gives brief facts on the CDM and presents the general procedure for designing controller gains using CDM. Eventually, we discuss the CDM-based PI control for a five-level series resonant inverter

In the second part, the implementation of the adaptive control technique for a five-level series resonant inverter is presented. Also, the brief facts and classification of adaptive control techniques are discussed. The Model Reference Adaptive Control MRAC based MIT rule is used for controling the five-level series resonant inverter.

In the third part, another advanced technique is investigated for controling the five-level series resonant inverter, i.e., intelligence algorithm-based fractional proportional-integral regulator. A GA and PSO are the selected algorithms for determining the optimal parameters of the fractional PI regulator (PI^{λ}).

5.2 Part A: Implementation of the classical control technique: CDM-based PI control

5.2.1 Brief facts on the Coefficient Diagram Method (CDM)

Coefficient diagram method (CDM) is an algebraic approach, proposed by Prof. Shunji MANABE in 1991 to design the controller parameters [1].

The standard block scheme of CDM for a Single Input-to-Single Output (SISO) system is given in Figure 59. $R(s)$: Reference input signal. $D(s)$: The disturbance. $Y(s)$: The output signal. $N_p(s)$: The numerator polynomial of the plant. $D_p(s)$: The denominator polynomial of the plant. $N_c(s)$, $D_c(s)$, and $F(s)$ are the CDM controller polynomials.

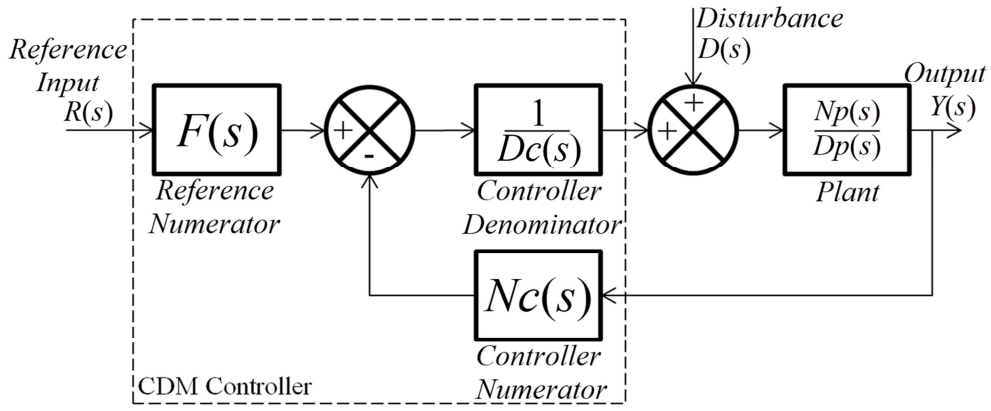

Figure 59: The block scheme of coefficient diagram method CDM

The coefficient diagram method CDM is a straightforward, simple, and effective technique to design a closed-loop controlled system. The most important advantage of CDM is the relationship between the desired performances of the system (the time response, stability, and robustness) and the coefficients of the controller polynomials, so adjusting the controller parameters is easy.

- Considering the disturbance equals zero ($D(s) = 0$), the new block scheme of CDM is given in Figure 60.

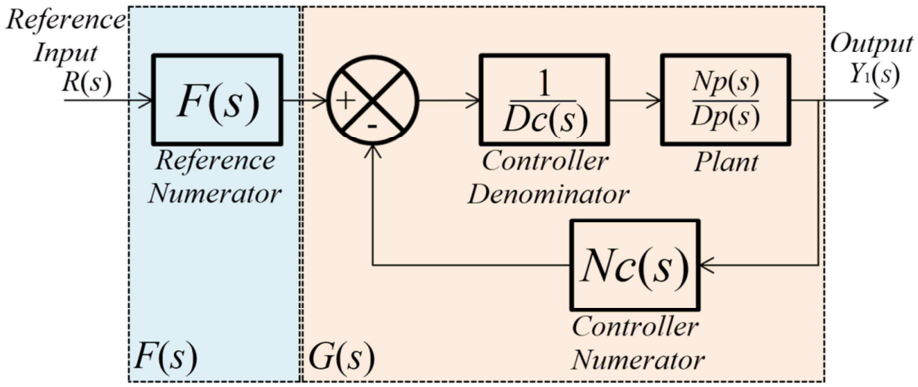

Figure 60: Equivalent CDM block scheme in case ($D(s) = 0$)

The transfer function of system in closed-loop form can be written as:

$$\frac{Y_1(s)}{R(s)} = F(s).G(s) = F(s).\frac{\dfrac{N_p(s)}{D_c(s).D_p(s)}}{1+\dfrac{N_p(s).N_c(s)}{D_c(s).D_p(s)}} \tag{51}$$

By applying some mathematical manipulations, the equations (51) can be expressed as:

$$\frac{Y_1(s)}{R(s)} = \frac{F(s).N_p(s)}{D_c(s).D_p(s)+N_p(s).N_c(s)} \tag{52}$$

In case of ($D(s) = 0$), the output of system is given as:

$$Y_1(s) = \frac{F(s).N_p(s)}{D_c(s).D_p(s)+N_p(s).N_c(s)}.R(s) \tag{53}$$

- Considering the reference equals zero ($R(s) = 0$), the new block scheme of CDM is given in Figure 61.

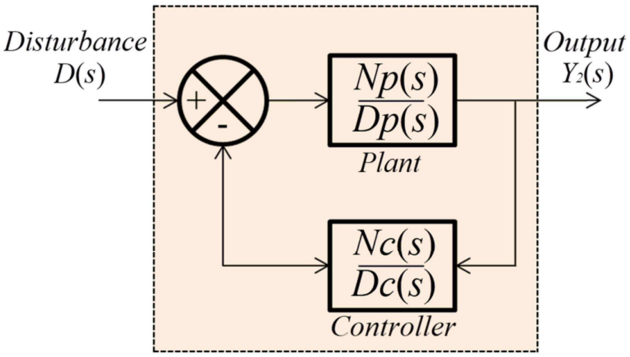

Figure 61: Equivalent CDM block scheme in case ($R(s) = 0$)

The transfer function of system in closed-loop form can be written as:

$$\frac{Y_2(s)}{D(s)} = \frac{\frac{N_p(s)}{D_p(s)}}{1 + \frac{N_p(s)}{D_p(s)} . \frac{N_c(s)}{D_c(s)}} \tag{54}$$

By applying some mathematical manipulations, the equations (54) can be expressed as:

$$\frac{Y_2(s)}{D(s)} = \frac{N_p(s).D_c(s)}{D_p(s).D_c(s) + N_p(s).N_c(s)} \tag{55}$$

In case of ($R(s) = 0$), the output of system is given as:

$$Y_2(s) = \frac{N_p(s).D_c(s)}{D_p(s).D_c(s) + N_p(s).N_c(s)} . D(s) \tag{56}$$

- Considering the total output response of the system to be controlled by CDM is $Y(s)$ equals ($Y_1(s) + Y_2(s)$), By adding the equation (53) and (56), $Y(s)$ can be written as:

$$Y(s) = \frac{N_p(s)F(s)}{D_c(s).D_p(s) + N_p(s).N_c(s)} R(s) + \frac{D_c(s).N_p(s)}{D_c(s).D_p(s) + N_p(s).N_c(s)} D(s) \tag{57}$$

The characteristic polynomial $P(s)$ of the closed-loop system presented as follows:

$$P(s) = D_c(s).D_p(s) + N_p(s).N_c(s) \tag{58}$$

5.2.2 Design procedure for the controller gains using CDM

The CDM technique is an algebraic approach that uses the polynomial representation. Design procedures for the controller gains using the CDM technique are:

1. Mathematical representation of the plant *G*(*s*) in polynomial form.

$$\begin{cases} N_p(s) = n_a s^a + n_{a-1} s^{a-1} + ... + n_1 s + n_0 \\ D_p(s) = d_b s^b + d_{b-1} s^{b-1} + ... + d_1 s + d_0 \end{cases} \tag{59}$$

where: $N_p(s)$: The Numerator polynomial of the plant with degree (a). $D_p(s)$: The Denominator polynomial of the plant with degree (b).

2. Mathematical representation of the controller *C*(*s*) in polynomial form.

$$N_c(s) = \sum_{i=0}^{x} l_i s^i \,,\; D_c(s) = \sum_{i=0}^{y} k_i s^i \tag{60}$$

Where: x and y: are the degrees of controller. $N_c(s)$: The Numerator polynomial of the controller. $D_c(s)$: The Denominator polynomial of the controller.

3. Calculation of the characteristic polynomial *P*(*s*) of the closed-loop system using the polynomial form of the plant and the polynomial form of the controller.

$$P(s) = D_c(s).D_p(s) + N_p(s).N_c(s) \tag{61}$$

3. Calculation of the target characteristic polynomial $P_t(s)$.

$$P_t(s) = a_0 \left[\left\{ \sum_{i=2}^{n} \left(\prod_{j=1}^{i-1} \frac{1}{\gamma_{i-j}^{j}} \right) (\tau s)^i \right\} + \tau s + 1 \right] \tag{62}$$

Where, n: is the order of the characteristic polynomial *P(s)*. τ: The equivalent time constant. γ_i: The stability indices.

In design of CDM controller, the most important point is setting of key parameters (γ_i and τ), because the key parameters come into closely relation with the dynamic system performances (rapidity, robustness, stability). Value of equivalent time constant (τ) has relation with the system rapidity, because it has an impact on the rise time and settling

time. Values of stability parameter (γ_i) have relation with the system stability and robustness, because have impact on the steady state error. According to S. Manabe's, (γ_i and τ) values can be selected as follows: γ_i values can be written as: {2.5, 2, 2 . . . 2}. Usually (γ_i) is selecting from the range of (1.5 to 4) to have a good stability performance based on Routh-Hurwitz stability criterion and Lipatov's stability criterion. In other hand, the key parameters (γ_i and τ) can be adjusted to have good desired performances [1]-[5].

5. Determination of the PI controller gains.

Putting $P(s) = P_t(s)$, then presenting the equations system in matrix form ($Ax=B$). Note that $x= [k_1; k_0; l_1]$ is the state vector of the gains for estimating the PI controller parameters. K_p: The proportional gain of PI controller. K_i: The integral gain of PI controller.

$$k_p = \frac{k_1}{l_1},\ k_i = \frac{k_0}{l_1}$$

5.2.3 CDM-based PI control for a five-level series resonant inverter

This subsection aims to design a PI controller utilizing the coefficient diagram method (CDM) for a five-level series resonant inverter. The technique is used to implement a closed-loop system for controlling the output capacitor voltage of the system. The controller synthesis is done using the small-signal model of the five-level series resonant inverter (CHAPTER 4). Firstly, we synthesize the control scheme and adjust the CDM for our system. The second step is a numerical application to test the synthesized control scheme and the designed controller. The results are obtained using the Matlab/Simulink environment.

5.2.3.1 Structure of the CDM-based PI control

1. Mathematical representation of the plant $G(s)$ in polynomial form, where the plant $G(s)$ is the small-signal model of a five-level series resonant inverter.

$$\begin{cases} N_p(s) = n_3 s^3 + n_2 s^2 + n_1 s^1 + n_0 \\ D_p(s) = d_4 s^4 + d_3 s^3 + d_2 s^2 + d_1 s^1 + d_0 \end{cases} \tag{63}$$

$N_p(s)$: The Numerator polynomial of degree (3). $D_p(s)$: The Denominator

polynomial of degree (4).

2. The polynomials $N_c(s)$ and $D_c(s)$ of the Controller $C(s)$ are:

$$\begin{cases} N_c(s) = k_3 s^3 + k_2 s^2 + k_1 s^1 + k_0 \\ D_c(s) = l_3 s^3 + l_2 s^2 + l_1 s^1 + l_0 \end{cases} \quad (64)$$

$N_c(s)$: The Numerator polynomial of degree (3). $D_c(s)$: The Denominator polynomial of degree (3).

The standard block of *PI* controller is given in Figure 55, the characteristic expression of the *PI* controller can be written as:

$$G_{PI}(s) = k_p + \frac{k_i}{S} \quad (65)$$

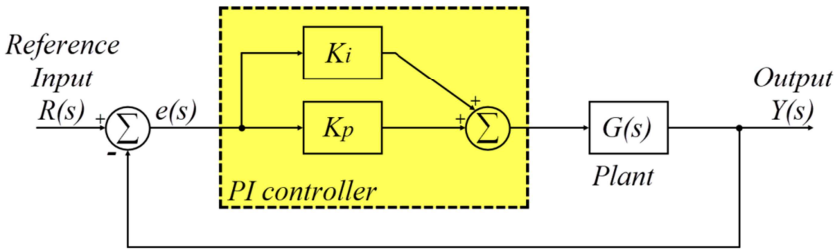

Figure 62: The standard block of PI controller for a five-level series resonant inverter

Putting ($F(s)$=$N_c(s)$ and $D(s)$ = 0), the simplified form of the CDM block scheme is given in Figure 63, where the characteristic expression of the controller can be written as:

$$\frac{N_c(s)}{D_c(s)} = \frac{k_1}{l_1} + \frac{k_0}{l_1 S} \quad (66)$$

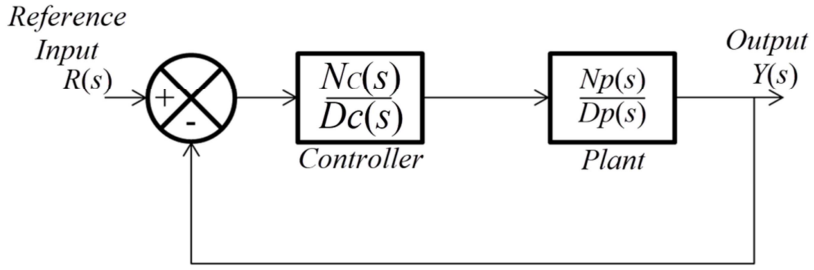

Figure 63: The simplified block scheme of CDM control.

By identification between the previous equation systems (65) and (66), the PI controller parameters can be estimated as:

$$\begin{cases} k_p = \dfrac{k_1}{l_1} \\ k_i = \dfrac{k_0}{l_1} \end{cases} \tag{67}$$

3. Calculation of the characteristic polynomial *P*(*s*) of the closed-loop system:

$$\begin{aligned} P(s) &= D_c(s).D_p(s) + N_p(s).N_c(s) \\ &= \begin{pmatrix} (l_1 s).(d_4 s^4 + d_3 s^3 + d_2 s^2 + d_1 s^1 + d_0) + \\ (k_1 s + k_0).(n_3 s^3 + n_2 s^2 + n_1 s^1 + n_0) \end{pmatrix} \\ &= \begin{pmatrix} l_1 d_4 s^5 + l_1 d_3 s^4 + l_1 d_2 s^3 + l_1 d_1 s^2 + l_1 d_0 s + \\ k_1 n_3 s^4 + k_1 n_2 s^3 + k_1 n_1 s^2 + k_1 n_0 s + \\ k_0 n_3 s^3 + k_0 n_2 s^2 + k_0 n_1 s + k_0 n_0 \end{pmatrix} \end{aligned} \tag{68}$$

The calculated characteristic polynomial *P*(*s*) can be simplified to the following form:

$$p(s) = \begin{pmatrix} (l_1 d_4) s^5 + (l_1 d_3 + k_1 n_3) s^4 + (l_1 d_2 + k_1 n_2 + k_0 n_3) s^3 + \\ (l_1 d_1 + k_1 n_1 + k_0 n_2) s^2 + (l_1 d_0 + k_1 n_0 + k_0 n_1) s + k_0 n_0 \end{pmatrix} \tag{69}$$

4. Calculation of the target characteristic polynomial $P_t(s)$.

$$P_t(s) = a_0 \left[\left\{ \sum_{i=2}^{n=5} \left(\prod_{j=1}^{i-1} \frac{1}{\gamma_{i-j}^{j}} \right) (\tau s)^i \right\} + \tau s + 1 \right] \tag{70}$$

Applying some mathematical manipulations, the target characteristic polynomial $P_t(s)$ can be calculated as:

$$P_t(s) = a_0 \left[\left\{ \frac{\tau^2 s^2}{\gamma_1^1} + \frac{\tau^3 s^3}{\gamma_2^1 \gamma_1^2} + \frac{\tau^4 s^4}{\gamma_3^1 \gamma_2^2 \gamma_1^3} + \frac{\tau^5 s^5}{\gamma_4^1 \gamma_3^2 \gamma_2^3 \gamma_1^4} \right\} + \tau s + 1 \right] \tag{71}$$

The calculated target characteristic polynomial $P_t(s)$ can be simplified to the following form:

$$P_t(s)=\left(\frac{a_0\tau^5}{\gamma_4^1\gamma_3^2\gamma_2^3\gamma_1^4}\right)s^5+\left(\frac{a_0\tau^4}{\gamma_3^1\gamma_2^2\gamma_1^3}\right)s^4+\left(\frac{a_0\tau^3}{\gamma_2^1\gamma_1^2}\right)s^3+\left(\frac{a_0\tau^2}{\gamma_1^1}\right)s^2+\left(a_0\tau\right)s+a_0 \quad (72)$$

5. Determination of the PI controller gains

Putting $P(s) = P_t(s)$, by identification between (69) and (72), the polynomials expressions can be written as:

$$\begin{cases} l_1d_4=\dfrac{a_0\tau^5}{\gamma_4^1\gamma_3^2\gamma_2^3\gamma_1^4} \\ l_1d_3+k_1n_3=\dfrac{a_0\tau^4}{\gamma_3^1\gamma_2^2\gamma_1^3} \\ l_1d_2+k_1n_2+k_0n_3=\dfrac{a_0\tau^3}{\gamma_2^1\gamma_1^2} \\ l_1d_1+k_1n_1+k_0n_2=\dfrac{a_0\tau^2}{\gamma_1^1} \\ l_1d_0+k_1n_0+k_0n_1=a_0\tau \\ k_0n_0=a_0 \end{cases} \quad (73)$$

In matrix form ($Ax=B$), the state equations of the polynomials expressions (73) are given as:

$$A=\begin{pmatrix} 0 & 0 & d_4 \\ n_3 & 0 & d_3 \\ n_2 & n_3 & d_2 \\ n_1 & n_2 & d_1 \\ n_0 & n_1 & d_0 \\ 0 & n_0 & 0 \end{pmatrix},\quad x=\begin{pmatrix} k_1 \\ k_0 \\ l_1 \end{pmatrix},\quad B=\begin{pmatrix} \dfrac{a_0\tau^5}{\gamma_4^1\gamma_3^2\gamma_2^3\gamma_1^4} \\ \dfrac{a_0\tau^4}{\gamma_3^1\gamma_2^2\gamma_1^3} \\ \dfrac{a_0\tau^3}{\gamma_2^1\gamma_1^2} \\ \dfrac{a_0\tau^2}{\gamma_1^1} \\ a_0\tau \\ a_0 \end{pmatrix}$$

x is the state vector of the gains for estimating the PI controller parameters.

5.2.3.2 Results & Discussions

The design procedure of the CDM controller is programmed in MATLAB editor. Then, the robustness tests of the technique under servo control and regulation control are presented using MATLAB Simscape and Simulink libraries. Regulatory control is more popular than servo control in industrial processes. If the reference input $R(s)$ is changed and the output $Y(s)$ moves to the value of $R(s)$, this is known as a servo control. A servo control loop reacts to changes in the set-point (reference input). If the control system ignores the disturbances $D(s)$, it is a regulatory control system.

The input-voltage-to-capacitor-output-voltage transfer function of the five-level series resonant inverter using small-signal modeling is found as follows:

$$G_{\tilde{v}}^{\tilde{V}_c}(s) = \frac{\tilde{V}_c(s)}{\tilde{v}(s)} = \frac{1.649e08\,S^2 + 1.129e14\,S + 3.794e16}{S^4 + 1333\,S^3 + 4.441e09\,S^2 + 2.96e12\,S + 4.975e14} \tag{74}$$

The polynomials form of the transfer function is given as:

$$\begin{cases} N_p(s) = 0s^3 + 1.649e8\,s^2 + 1.129e14\,s^1 + 3.794e16 \\ D_p(s) = 1s^4 + 1333\,s^3 + 4.441e9\,s^2 + 2.96e12\,s^1 + 4.975e14 \end{cases} \tag{75}$$

The stability of the system model is checked by using the MATLAB function (isstable(G)). If the system model is stable, then the **isstable** function gives a logical value of 1 (true), else the **isstable** function gives a logical value of 0 (false). The given system model is stable.

Table 9 illustrates the obtained PI controller parameters using the CDM technique, where the Manabe's parameter (τ) was varied to present their influence to PI parameters values. The PI parameters values are rounded to the nearest Ten-Thousandths (0.0001). Figure 64 illustrates the unit step response of the closed-loop system with the CDM.

Table 9: The PI controller parameters using coefficient diagram method CDM

Manabe's parameters		*PI controller parameters*	
		K_p	K_i
$\gamma_1 = 2.5$ $\gamma_2 = 2$ $\gamma_3 = 2$ $\gamma_4 = 2$	$\tau = 0.005$	0.0068	9.8181
	$\tau = 0.006$	0.0087	7.2268
	$\tau = 0.007$	0.0075	5.1174
	$\tau = 0.008$	0.0053	3.6635
	$\tau = 0.009$	0.0031	2.6952
	$\tau = 0.010$	0.0012	2.0425

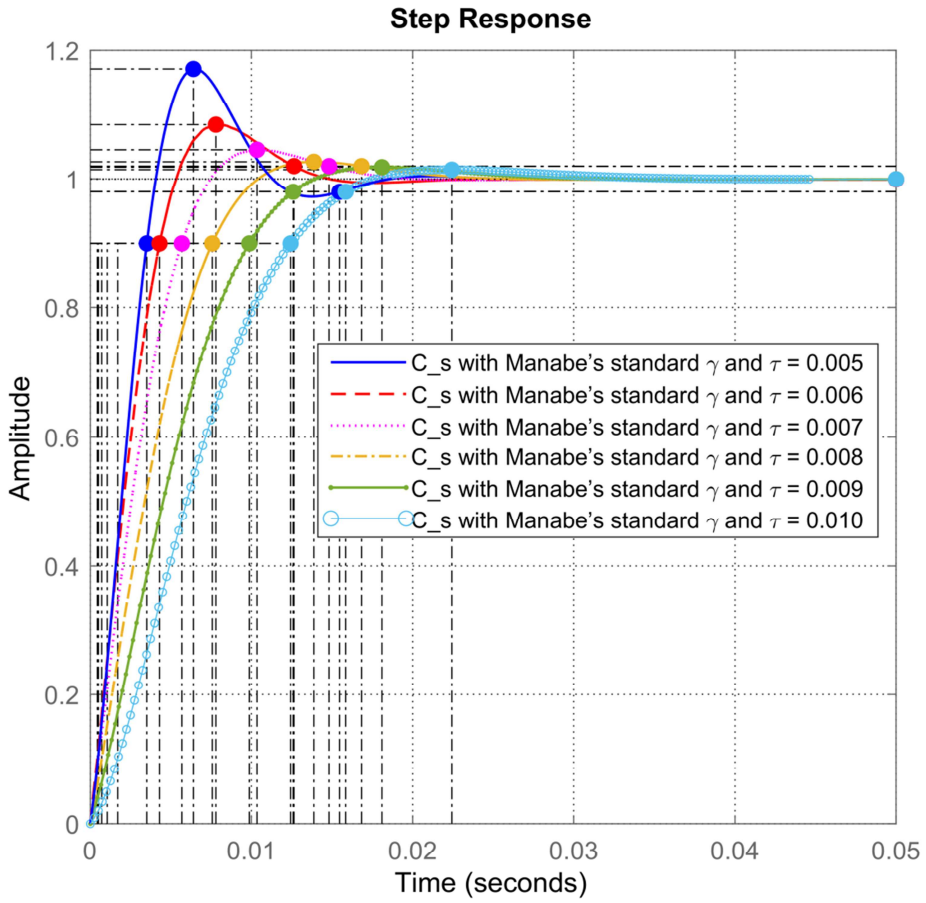

Figure 64: Unit step response of the closed-loop system with the CDM technique

To evaluate the controller performances, we define the following common characteristics from the systems control theory: peak response, settling time, rise time, and overshoot. Peak time is the time necessary for the response to attain its first peak, i.e., the maximum of the first oscillation cycle or the first overshoot. Settling time is the time taken

by the response to attain and keep within a specified range of its final value, where 2% or 5% are the common percentages of the final value. The rise time is the time needed for its transition from 10% to 90% of the final value. Overshoot is the maximum peak value of the response minus the step value, and the result is divided by the step value and multiplied by 100 because the overshoot is written as a percentage [6], [7]. According to the international standards IEC and IEEE concerning the overshoot tolerance limits, 10% is good, and the recommended overshoot during the impulse tests is 5% [8].

From Figure 64 of the unit step responses, we can note that Manabe's parameters influence the performances of the feedback control system. The performance characteristics of the feedback control system with the CDM under variable values of the equivalent-time constant (τ) and fixed values of the stability indices (γ_1=2.5, γ_2=2, γ_3=2, γ_4=2.5) according to Manabe's standard is summarized in Table 10.

Table 10: Performance characteristics of the feedback control system with the CDM.

Equivalent-time constant	*Peak response*	*Settling time (s)*	*Rise time (s)*	*Overshoot (%)*
$\tau = 0.005$	1.1710	0.0155	0.00303	17.10
$\tau = 0.006$	1.0843	0.0126	0.00386	08.43
$\tau = 0.007$	1.0453	0.0148	0.00518	04.53
$\tau = 0.008$	1.0267	0.0168	0.00686	02.67
$\tau = 0.009$	1.0183	0.0126	0.00882	01.83
$\tau = 0.010$	1.0145	0.0158	0.01070	01.45

Table 10 proves that the peak response and overshoot are decreased when increasing the value of the equivalent-time constant (τ), so there is an inverse correlation between the equivalent-time constant (τ) and the overshoot, and there is an inverse correlation between the equivalent-time constant (τ) and the peak response. Also, we can note the positive correlation between the equivalent-time constant (τ) and the rise time. A correlation between the equivalent-time constant (τ) and the settling time could not be determined.

During the design of the feedback control system, the designer must follow the specifications provided by the user in the specification sheet. Let's assume that our design criteria are: overshoot less than 5% and less value possible of settling time (2%). According to the assumptions, the best achieved parameters of the PI controller using CDM are given in Table 11.

Table 11: The best parameters of PI controller using CDM

PI controller parameters	*Value*
K_p	0.0031
K_i	2.6952

After achieving the best PI controller parameters using the coefficient diagram method and the small-signal model of the proposed five-level series resonant inverter, the next step is testing the system responses using MATLAB Simscape and Simulink libraries. Figure 65 illustrates the system's output with the PI-CDM controller in the case of the variable reference. The reference was changed from 100 Volts to 300 Volts, and then to 200 Volts.

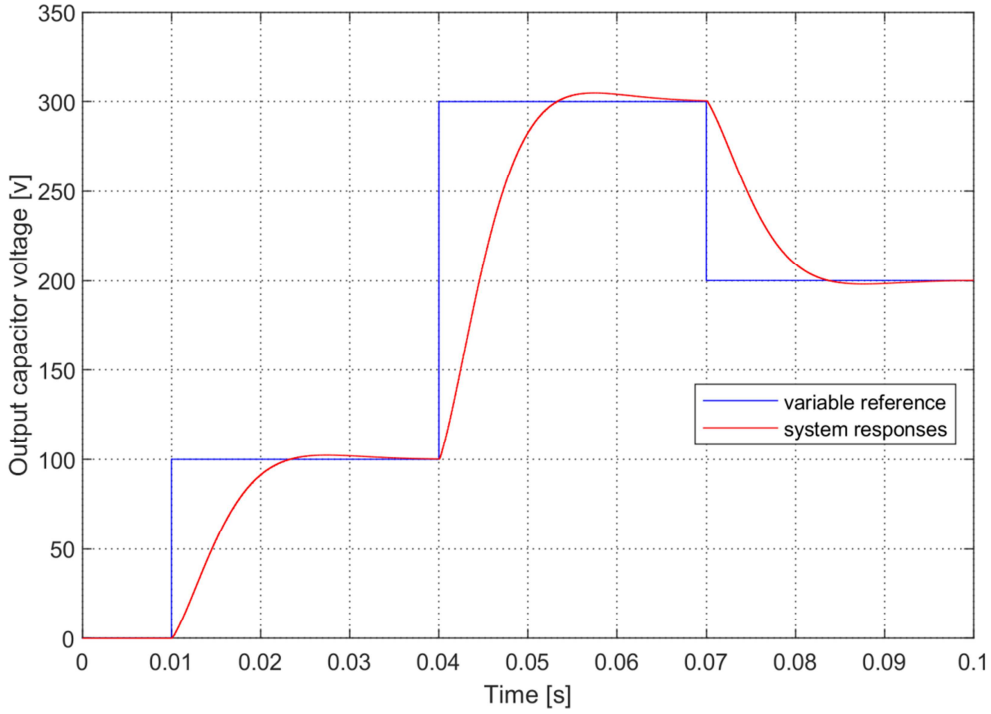

Figure 65: System responses with the PI based on CDM controller in the case of variable reference.

According to the obtained simulation results, it can be seen that the system output tracks the variable reference with a good accuracy and quickly, where the system output follows the reference path after 20 ms approximately of varying its value; therefore, the PI based on CDM controller provides a good dynamic response to the system.

For testing the robustness of the PI-CDM controller, the system parameters are varied, and the results of the responses are compared with the nominal case parameter.

Figure 66 (a) shows the responses of the system if the resistance value changes. Figure 66 (b) shows the responses of the system if the inductance value varies. Figure 66 (c) shows the responses of the system if the capacitance value changes.

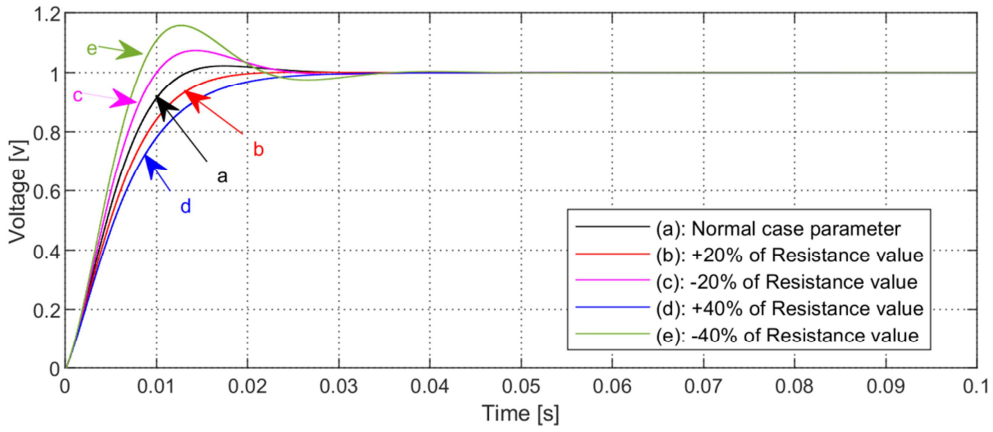

(a)

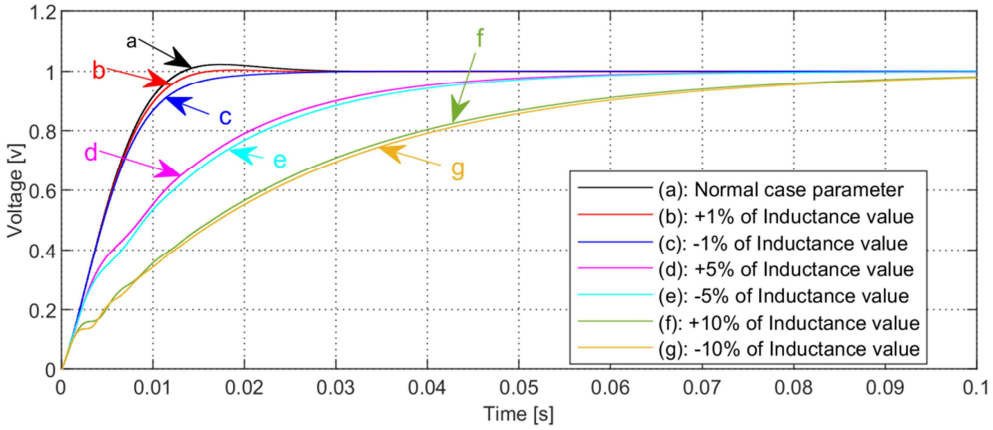

(b)

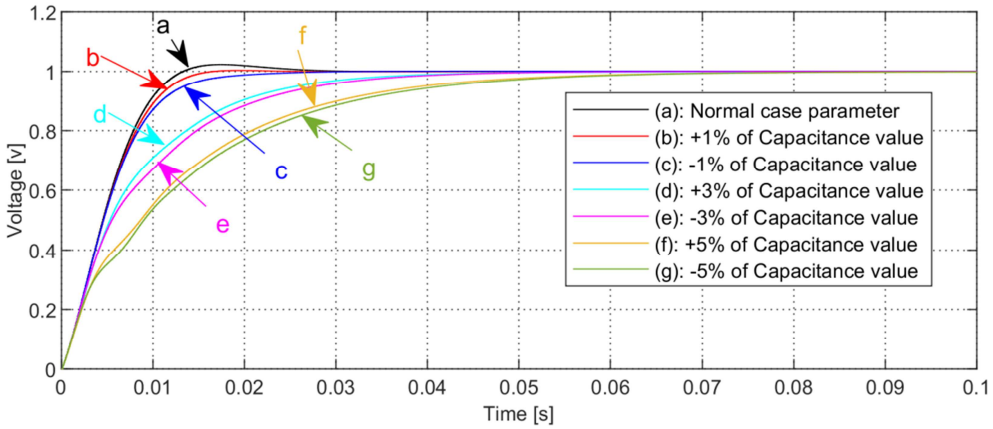

(c)

Figure 66: Unit step responses of the system with the PI based on CDM controller in case of: (a) resistance value changes, (b) inductance value changes, (c) capacitance value changes.

From the curves of Figure 66(a), it can be seen that the system output tracks the

unit step reference with good accuracy, good settling time, and good overshoot even though the resistance value is changed by +20% and +40%. Otherwise, the system output tracks the unit step reference with good accuracy but poor performance because of the high overshoot when the resistance value is changed by -20% and -40%. From the curves of Figure 66(b), it can be seen that the system output tracks the unit step reference with good accuracy, good settling time, and good overshoot even though the inductance value is changed by +1% and -1%. Otherwise, the system output tracks the unit step reference but with poor performances because of the high settling time when the inductance value is changed by +5%, -5%, +10%, and -10%. From the curves of Figure 66(c), it can be seen that the system output tracks the unit step reference with good accuracy, good settling time, and good overshoot even though the capacitance value is changed by +1% and -1%. Otherwise, the system output tracks the unit step reference but with poor performances because of the high settling time when the capacitance value is changed by +3%, -3%, +5%, and -5%. Generally, the decrease or increase of a system parameter value requires a new controller design to obtain high performance. Based on the achieved results, the acceptable ranges of varying the system parameters without designing new PI-CDM controller are [0; +40%] of resistance value, [-1%; +1%] of inductance value, [-1%; +1%] of capacitance value.

Also, in the robustness tests of the PI based on CDM controller, disturbances of 1%, 3%, 5% are injected in the closed-loop system. Figure 67 shows the block diagram of the closed-loop system when adding disturbance. The effects of the disturbances and their corresponding system responses are depicted in Figure 68.

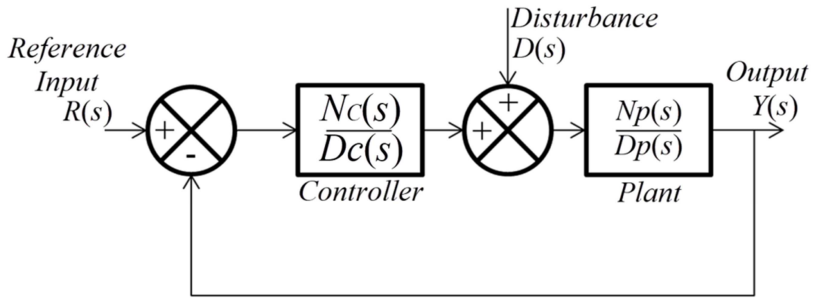

Figure 67: Block diagram of the closed-loop system when adding disturbance.

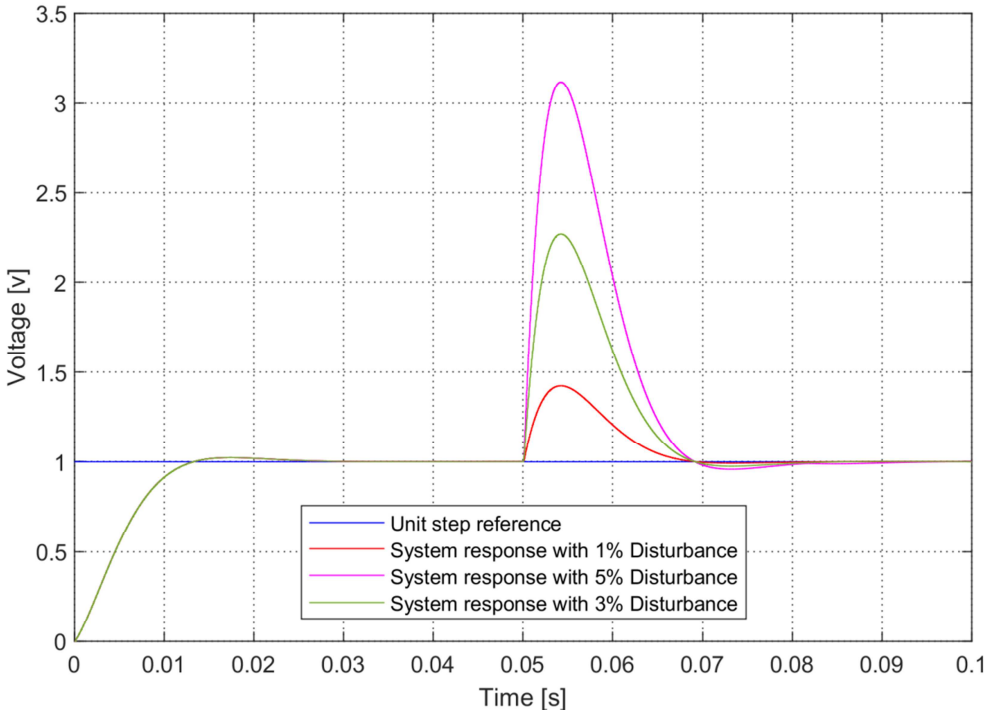

Figure 68: Unit step responses of the system with PI-CDM controller when adding disturbances.

The curves of Figure 68 demonstrate that the disturbances are rejected. The system responses return to the reference trajectory within 20 ms in the case of step disturbance.

According to the obtained simulation results, it can be seen that the PI-CDM controller provides good system responses and robust rejection of the disturbances.

5.3 Part B: Implementation of the advanced control technique: adaptive control

5.3.1 Brief facts on the adaptive control techniques

The high-quality techniques for designing control systems are based on a good analysis of the system under various step changes and disturbances of its environment. In the control theory area, adaptive is one of the advanced control techniques; adaptive controls denote the ensemble of methods allowing the real-time automatic adjustment of the controller parameters. There are several schemes for designing an adaptive control system, yet for the same aim, to achieve or maintain a desired level of performance by making the model output follow the desired trajectory. Adaptation occurs at the level of the controller parameters (adjustments of parameters) or directly at the level of the command signal to satisfy or enhance a predefined performance index through an adaptation mechanism [9]-[11].

Figure 69 shows a general scheme of the adaptive control. From the system inputs/outputs, the performance index is determined by a pre-selected criterion. Based on the measured performance index and with the recognition of the desired performance, an adaptation mechanism (algorithm, optimization technique, … or other method) is set up to adjust the controller parameters. The adjustable controller receives the error between the reference signal and the model output, and then produces the command signal. $R(s)$: Reference input signal. $U(s)$: The input signal. $Y(s)$: The output signal.

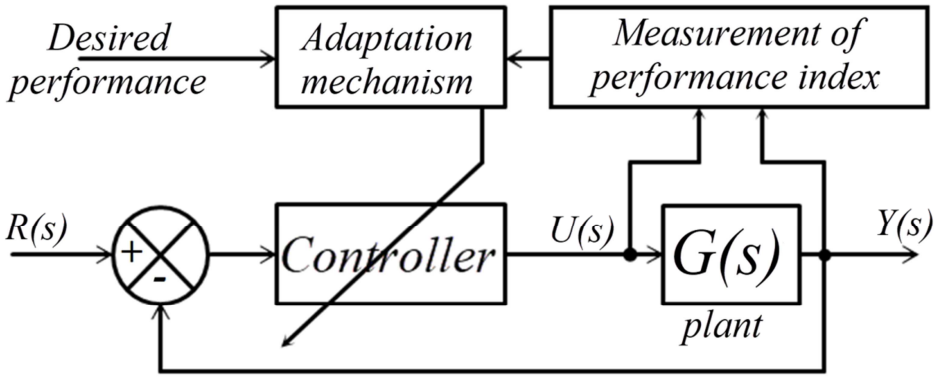

Figure 69: General scheme of the adaptive control.

5.3.2 Classification of adaptive control techniques

The adaptive controls strategies are based on error cancellation between the reference input and the output of the model, currently there are many scheme and algorithms for constructing an adaptive control. Basically, the adaptive controls strategies are classified into direct methods, and indirect methods. Also, the adaptive controls strategies are classified into feed-back methods and feed-forward methods, where the control parameter is computed based on the process measurements knowledge in feed-forward methods, on the other side, the control parameter is computed based on the error between outputs of the plant and the reference in feedback methods. Furthermore, the adaptive controls strategies are classified into model-based methods and model-independent methods [12], [13].

5.3.2.1 Classification based on scheme

Based on adaptation scheme, there are two scheme of the adaptive control: (1) Direct Adaptive Control; (2) Indirect Adaptive Control [12].

5.3.2.1.1 Direct adaptive control

The adaptive control direct methods denote the ensemble of methods allowing the direct adjustment of the controller parameters using an on-line estimation mechanism. Figure 70 illustrates an example of the direct adaptive control.

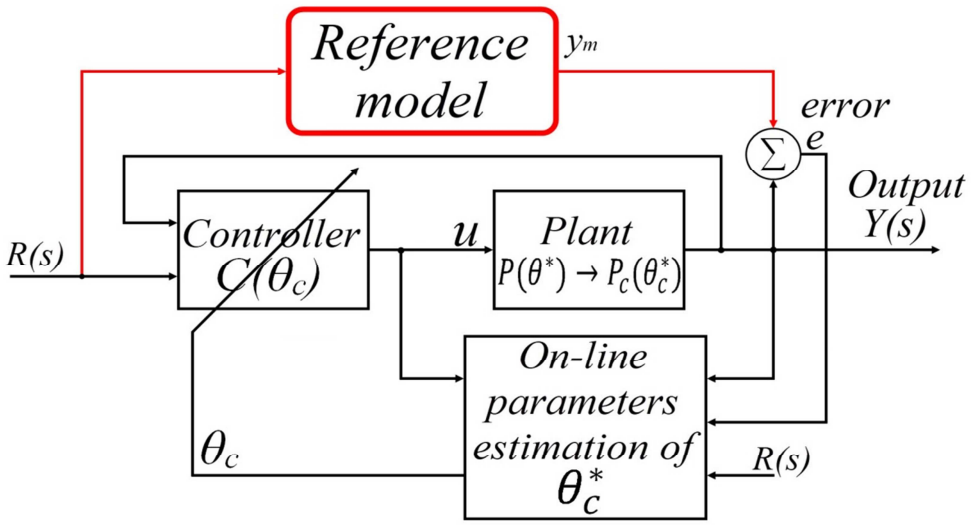

Figure 70: Scheme of direct adaptive control technique.

5.3.2.1.2 Indirect adaptive control

The adaptive control indirect methods denote the ensemble of methods allowing the indirect adjustment of the controller parameters using an on-line estimation mechanism through a parameters calculation block. Figure 71 illustrates an example of the indirect adaptive control.

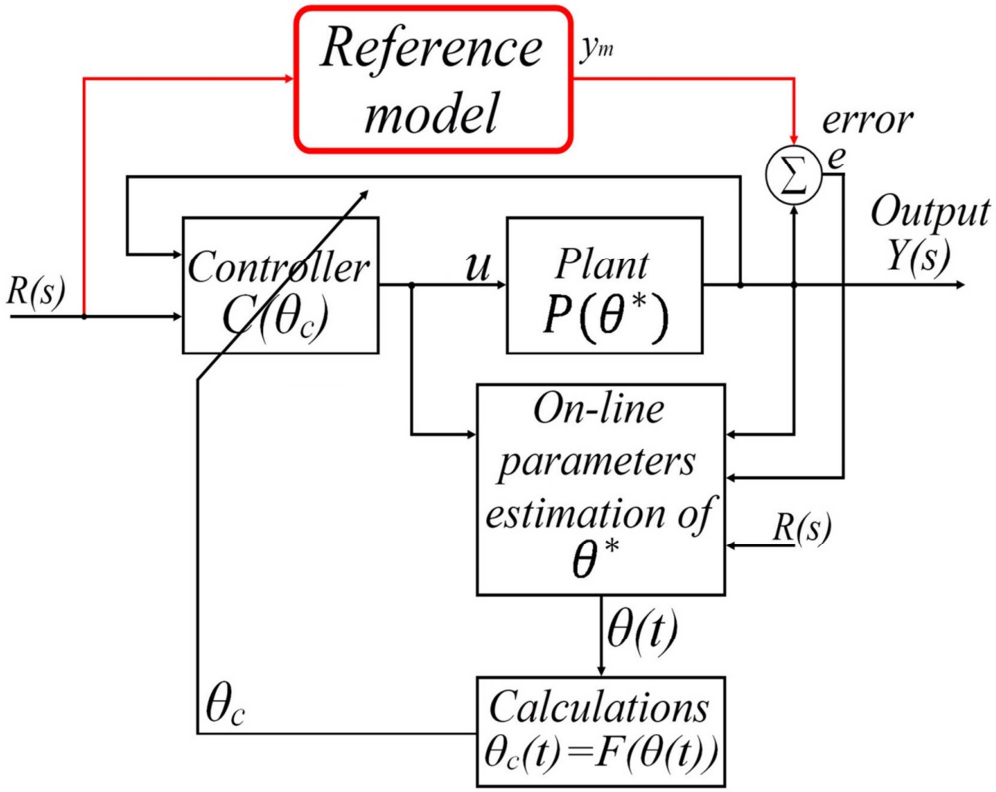

Figure 71: Scheme of indirect adaptive control technique.

5.3.2.2 Model-based or model-independent classification

Based on model, there are two methods of adaptive control: (1) Model-based adaptive control; and (2) Model-independent adaptive control [13].

5.3.2.2.1 Model-based adaptive control

Model-based adaptive control techniques require the knowledge of the system model parameters, so this techniques type allows the interpretation of the system behavior results [13]. Currently, there are a lot of model-based adaptive control techniques

including:

- *Gain Scheduling Adaptive Control.*
- *Adaptive Pole Placement Control.*
- *Model Reference Adaptive Control.*
- *Time Delay Adaptive Control.*
- *Adaptive Sliding Mode Control.*
- *Adaptive Backstepping Control.*

5.3.2.2.2 Model-independent adaptive control

In recent years, model-independent adaptive control techniques have gained a large attention of researchers because they do not require the knowledge of the system model. The model-independent adaptive control techniques offer many advantages and benefits as they can handle nonlinearity of system, and tolerate uncertainty. Furthermore, they are more versatile and flexible compared to model-based control algorithms, but sometimes they do not provide optimal control [13]. There are a lot of model-independent adaptive control techniques including:

- *Adaptive Control Based on Fuzzy Logic.*
- *Adaptive Control Based on Artificial Neural Networks.*
- *Adaptive Neuro-Fuzzy Control.*
- *Adaptive Brain Emotional Learning Control.*

5.3.3 Analysis of the Model Reference Adaptive Control MRAC

In control theory, Model Reference Adaptive Control (MRAC) is a direct adaptive strategy, and one of the widely used control strategies to design advanced control systems for high-performance and high robustness characteristics.

5.3.3.1 Principle of Model Reference Adaptive Control

The principle of model reference adaptive control (MRAC) is based on the minimization of the error between the plant output and the reference model using an

adjustment mechanism. The adjustment mechanism adjusts controller parameters based on the received information (y, u, e) using an adaptive control rule [14], [15]. Figure 72 illustrates the basic structure of a model reference adaptive control (MRAC), where y_m: The output of reference model, y: The plant output, e: The difference between the outputs of plant and reference model.

The MRAC is composed of: (1): Process (plant): a model of the controlled system. (2): Reference model: a model that gives an idyllic output based on the reference input. (3): Controller: describes the adjustable parameters that used to define the control law. The adjustable parameters values are dependent on adaptation gain. (4): Adjustment mechanism: this block is used for adapting the controller parameters, so for forcing the actual plant track the reference model. MIT rule, Lyapunov rule and Normalized Algorithm are the widely used Mathematical approaches to develop the adjustment mechanism [15]-[17].

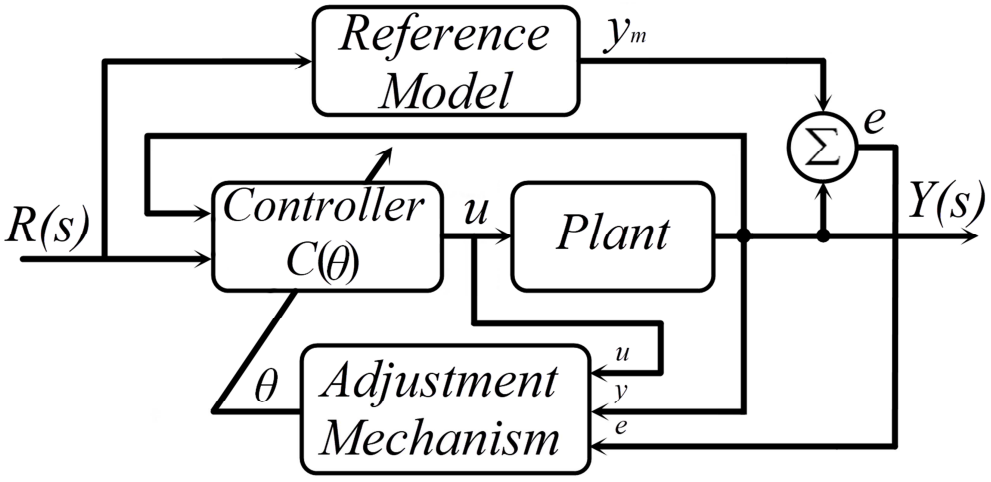

Figure 72: General scheme of the Model Reference Adaptive Control.

5.3.3.2 Basic rules to design the adaptation mechanism

Based on the literature overviews, we noted that MIT rule and Lyapunov rule are the basic methods used to design the adjustment mechanism. In this subsection the principle of the two rules is discussed.

5.3.3.2.1 Adaptation mechanism based on MIT rule

MIT rule was first developed in Massachusetts Institute of Technology (MIT), in

1961s. MIT rule was originally proposed to design the autopilot system for aircrafts based on MRAC scheme, and then it is generalized to design a controller for any practical system [18]. MIT provides a very simple solution to the MRAC problem based on scalar parameter adjustment law; their principle is adjusting the controller's parameters θ by the minimization of a parametric error function (cost function or loss function) using a gradient descent adaptation law [18], [19].

Figure 73 illustrates the block diagram of MRAC using MIT rule. The plant model output (y) is compared with that of reference model (y_m); next, the error (e) is feeding the adjustment mechanism through the sensitivity derivative, where the adjustment mechanism calculates the controller's parameters θ using the error (e), the transfer function of reference model, the reference input (R), and the plant model output (y) [20].

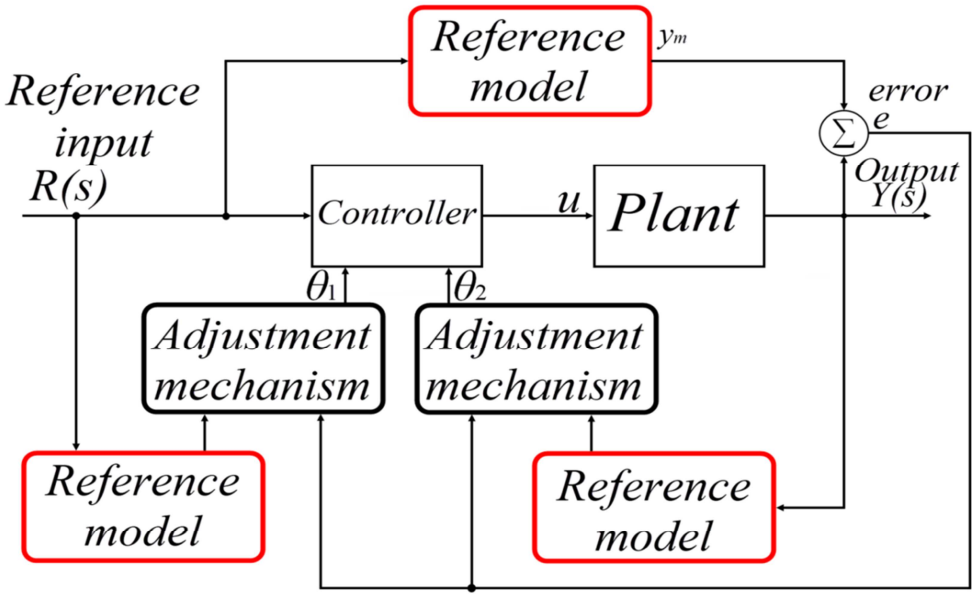

Figure 73: Block diagram of MRAC using MIT rule for two adjustable parameters.

For two adjustable parameters (θ) the control law u can be defined as follow:

$$u = R\theta_1 - y\theta_2 \tag{76}$$

The transfer functions of plant $G(s)$ and reference model $G_m(s)$ are:

$$G(s) = \frac{y(s)}{u(s)}; \quad G_m(s) = \frac{y_m(s)}{R(s)}$$

The parametric error function or cost function $J(\theta)$ is usually written as:

$$J(\theta)=\frac{1}{2}e(\theta)^2 \tag{77}$$

Where, θ are the adjustable parameters, $e(\theta)$ represents the output error, defined as the difference between the reference model output and the actual model output, $e(\theta)$ is written as:

$$e(\theta)=y(\theta)-y_m \tag{78}$$

In MIT rule, the adaptation law is obtained based on the gradient-descent optimization algorithm, where the adaptation law is obtained by setting the time-derivative of the adjustable parameters (θ) to be proportional to the negative gradient of the error function $J(\theta)$.

$$\frac{d\theta}{dt}=-\gamma\frac{\partial J}{\partial\theta} \tag{79}$$

The derivative of the parametric error function $J(\theta)$ is emplaced in the previous formula to obtain:

$$\frac{d\theta}{dt}=-\gamma\left(\frac{\partial J}{\partial e}\frac{\partial e}{\partial\theta}\right) \tag{80}$$

The update rule for the adjustable parameters (θ) using MIT rule is described as:

$$\frac{d\theta}{dt}=-\gamma e\frac{\partial e}{\partial\theta} \tag{81}$$

$\partial e/\partial\theta$: The sensitivity derivative of the system, it is the partial derivative term of the error and the adjustable parameters (θ). γ: is a design parameter that defines the adaptive gain. Note that the cost function J and the adjustable parameters (θ) are alternatives, so can be adapted for different applications.

Another alternative for J based on sign algorithm is written as:

$$J(\theta)=|e| \tag{82}$$

This gives the following expression:

$$\frac{d\theta}{dt} = -\gamma\left(\frac{\partial e}{\partial \theta}\right) sign\, e \;; \qquad where: \begin{cases} sign\, e = 1 \;\; for \;\; e > 0 \\ sign\, e = 0 \;\; for \;\; e = 0 \\ sign\, e = -1 \;\; for \;\; e < 0 \end{cases} \tag{83}$$

5.3.3.2.2 Adaptation mechanism based on Lyapunov rule

Lyapunov rule is one of the basic methods used to design the adjustment mechanism in Model Reference Adaptive Control (MRAC) system. The adaptation mechanism based on the Lyapunov rule exploits the system error to form the appropriate Lyapunov function for adjusting parameters. Figure 74 illustrates the block diagram of MRAC using Lyapunov rule. The plant model output (y) is compared with that of reference model (y_m); next, the error (e) is feeding the adjustment mechanism; next, the adjustment mechanism calculates the controller's parameters θ using the error (e), the reference input (R), and the plant model output (y) [20].

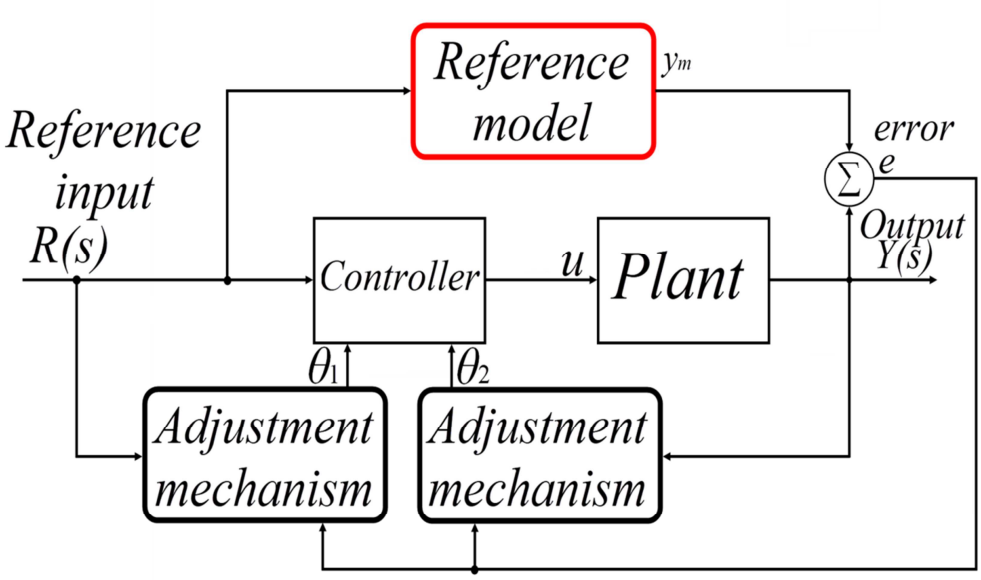

Figure 74: Block diagram of MRAC using Lyapunov rule for two adjustable parameters.

MIT and Lyapunov rules are basic methods for adapting the controller parameters in the model reference adaptive control system. The MIT rule operates by assuming that the control parameters θ change more slowly than the other variables in the system. The computational complexity is reduced in the MRAC scheme with the Lyapunov rule when

compared to the MIT rule, thus the implementation of the system is more feasible with the Lyapunov rule. But the mathematical modeling and design of the controller is simpler with the MIT rule.

In this current study Model Reference Adaptive Control (MRAC) Scheme is applied to a small-signal model of a five-level series resonant inverter using MIT rule.

5.3.4 Adaptive controller design for a five-level series resonant inverter

The simulation model of the MRAC using MIT rule for a small-signal model of a five-level series resonant inverter is built under a Matlab/Simulink environment. The structure of MRAC based MIT controller and results are discussed in this subsection.

5.3.4.1 Structure of the MRAC based on MIT controller

1. Mathematical representation of the plant $G(s)$ in polynomial form, where the plant $G(s)$ is the small-signal model of a five-level series resonant inverter.

$$G(s)=\frac{y(s)}{u(s)}=\frac{1.649e08\,s^2+1.129e14\,s+3.794e16}{s^4+1333\,s^3+4.441e09\,s^2+2.96e12\,s+4.975e14} \tag{84}$$

Where: $u(s)$ is the plant input and $y(s)$ is the plant output.

2. Mathematical representation of the reference model system $G_m(s)$ in transfer function form:

$$G_m(s)=\frac{y_m(s)}{R(s)}=\frac{\omega_n^2}{s^2+2\xi\,\omega_n\,s+\omega_n^2} \tag{85}$$

Where, $G_m(s)$ the reference model is a second-order system with known natural frequency (ω_n) and damping ratio (ξ). We want to force the system output to tracks the second-order reference model because a typical series *RLC* circuit is a second order system, if putting ($j^2 = -1$ and $s = j\omega$) the equation (17) can be written as:

$$H(s)=\frac{1}{1+RC\,s+j^2LC\omega^2}=\frac{1}{1+RC\,s+LC\,s^2} \tag{86}$$

3. The parametric error function $J(\theta)$, and the output error $e(\theta)$ are written as:

$$\begin{cases} J(\theta) = \dfrac{1}{2} e(\theta)^2 \\ e(\theta) = y(\theta) - y_m \end{cases} \tag{87}$$

4. The Model Reference Adaptive Control (MRAC) scheme is defined as:

a) The control law $u(t)$ is defined as follow:

$$u(t) = R(t)\theta_1 - y(t)\theta_2 \tag{88}$$

b) The adjustable parameters (θ) are chosen as:

$$\theta = \{\theta_1, \theta_2\} = \{K_p, K_i\} \tag{89}$$

c) The output error $e(s)$ is written as:

$$e(s) = y(s) - y_m(s) \tag{90}$$

Using the mathematical representations of the plant $G(s)$ and the reference model system $G_m(s)$, the output error $e(s)$ is written as:

$$e(s) = u(s)G(s) - R(s)G_m(s) \tag{91}$$

Replacing the control law $u(t)$ with its expression, the output error $e(s)$ can be presented as:

$$e(s) = \left(R(s)\theta_1 - y(s)\theta_2\right)G(s) - R(s)G_m(s) \tag{92}$$

d) The partial derivatives of the output error $e(s)$ are described as:

$$\begin{cases} \dfrac{\partial e}{\partial \theta_1} = R(s)G(s) = \dfrac{y_m(s)}{G_m(s)}G(s) \\ \dfrac{\partial e}{\partial \theta_2} = -y(s)G(s) \end{cases} \tag{93}$$

e) The adaptation law for the adjustable parameters (θ) using MIT rule is described as:

$$\begin{cases} \dfrac{d\theta_1}{dt} = -\gamma_1 e \dfrac{\partial e}{\partial \theta_1} = -\gamma_1 e \dfrac{y_m(s)}{G_m(s)} G(s) \\ \dfrac{d\theta_2}{dt} = -\gamma_2 e \dfrac{\partial e}{\partial \theta_2} = +\gamma_2 e\, y(s) G(s) \end{cases} \tag{94}$$

Assuming that the reference model transfer function $G_m(s)$ equal to the plant model $G(s)$ approximately ($G_m(s) \approx G(s)$), so the adaptation law for the adjustable parameters (θ) using MIT rule is written as:

$$\begin{cases} \dfrac{d\theta_1}{dt} = -\gamma_1 e \dfrac{\partial e}{\partial \theta_1} = -\gamma_1 e\, y_m(s) \\ \dfrac{d\theta_2}{dt} = -\gamma_2 e \dfrac{\partial e}{\partial \theta_2} = +\gamma_2 e\, y(s) G_m(s) \end{cases} \tag{95}$$

Where, γ_1 and γ_2: defines the adaptive gains.

5.3.4.2 Results & Discussions

In this subsection, the robustness tests of the adaptive technique with servo control, regulation control, and under disturbances are given. Figure 75 illustrates the MATLAB model of the MRAC using the MIT rule for a five-level series resonant inverter.

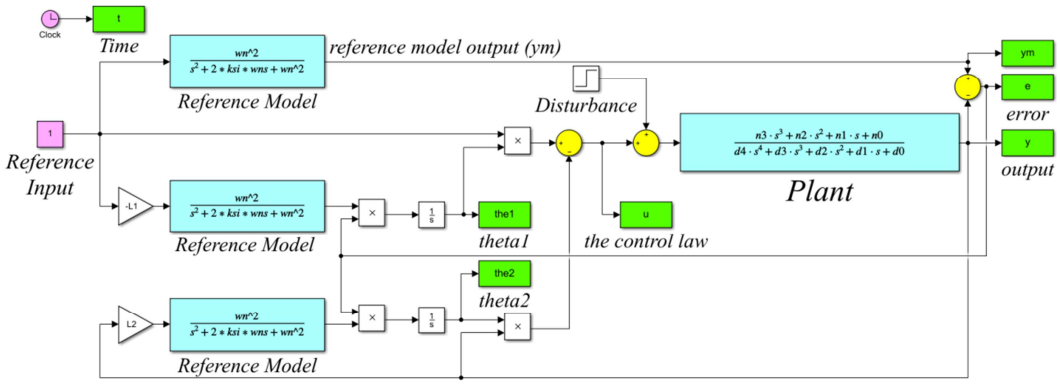

Figure 75: MATLAB model of the MRAC using MIT rule for a five-level series resonant inverter.

Table 12 shows the performance characteristics of the reference model with step response; after several tests, the system parameters are selected based on the step response performance (peak response, settling time, and overshoot).

Table 12: Performances characteristics of the reference model with step response

		Peak response	*Settling time (s)*	*Rise time (s)*	*Overshoot (s)*
Test$_1$	ω_n=1 ξ=0.7	1.05	02.13	05.98	04.60
Test$_2$	ω_n=1 ξ=0.8	1.02	03.76	02.47	01.52
Test$_3$	ω_n=1 ξ=0.9	1.00	04.70	02.88	00.15
Test$_4$	ω_n=1 ξ=1	1.00	05.83	03.36	00.00
Test$_5$	ω_n=100 ξ=0.7	1.05	00.06	00.02	04.60
**Test*$_6$	ω_n=100 ξ=0.8	1.02	00.04	00.02	01.52
**Test*$_7$	ω_n=100 ξ=0.9	1.00	00.05	00.03	00.15

Let's assume that our design criteria in order are: peak response equal or less than (1), overshoot less than 5%, and less value possible of settling time (2%). According to the assumptions, the best reference model $G_m(s)$ parameters are highlighted with color and mark (*).

Table 13 presents the adaptive control parameters for evaluating the system performances. Figure 76 shows the curves of the real system and reference model responses under step reference. The error between the real system and reference model responses is given in Figure 77. After that, Figure 78 illustrates the control law $u(t)$.

Table 13: The adaptive control parameters

Parameter	*Ref.*	*Value*
Natural frequency	ω_n	100
Damping ratio	ξ	0.9
Adaptive gain	γ_1	-20.65
Adaptive gain	γ_2	6.1797

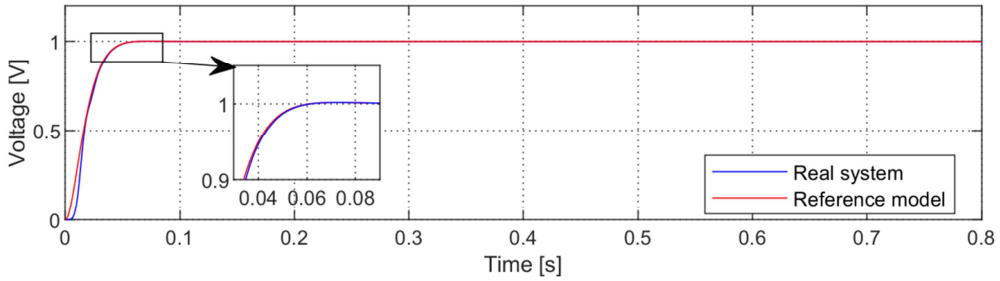

Figure 76: Curves of the real system and reference model responses

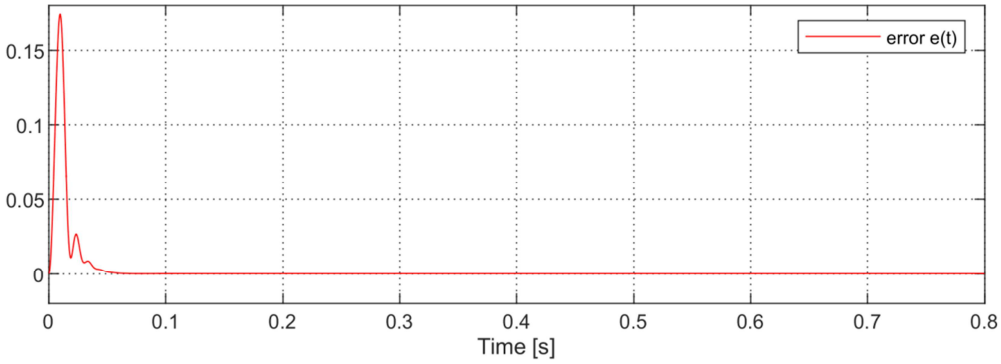

Figure 77: Error between the real system and reference model responses.

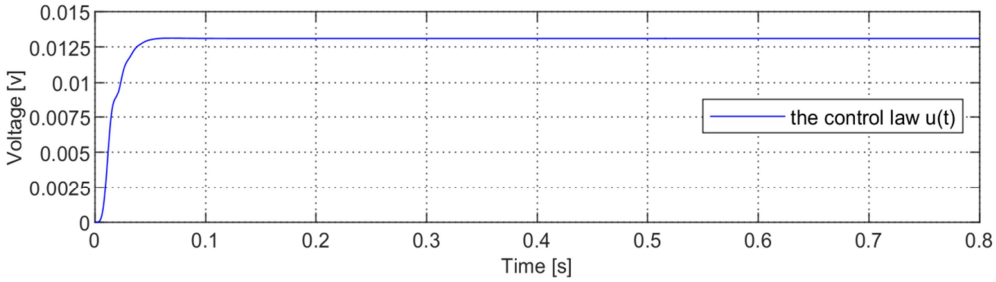

Figure 78: The control law u(t) under step reference.

According to Figures 76 and 77, it can be seen that the responses of the real system and the reference model are convergent, and the difference is evident only at the start of the runtime. There are two regimes: the transient and permanent; approximately, the system attains the permanent regime after a settling time of 50 ms.

Figure 79 illustrates the real system's output and reference model output with the adaptive control in the case of the variable reference. The reference was changed from 10 Volts to 30 Volts, and then to 20 Volts. The error between the real system and reference model responses under variable reference is given in Figure 80. After that, Figure 81 illustrates the control law $u(t)$ under the variable reference.

According to the obtained simulation results shown in Figures 79, 80, and 81, it can be seen that the system output tracks the variable reference with a good accuracy and quickly, where the system output follows the reference path after 50 ms approximately of varying its value; therefore, the adaptive controller provides a good dynamic response to the system.

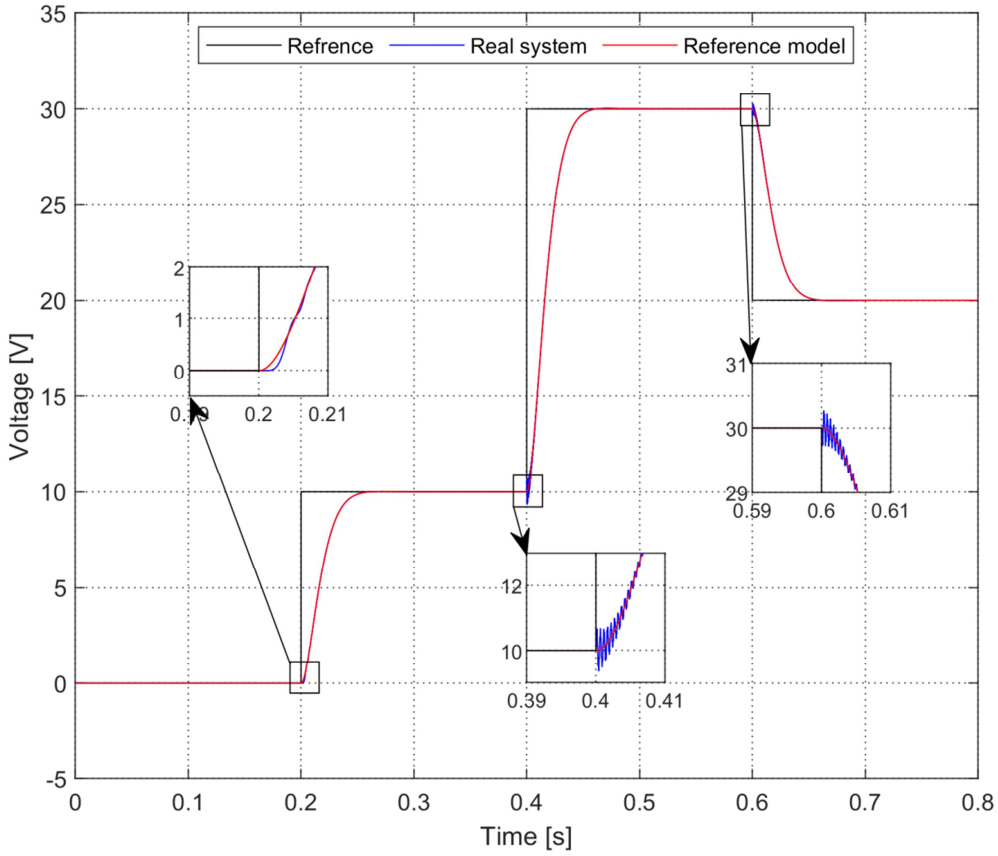

Figure 79: Real system and reference model responses under variable reference.

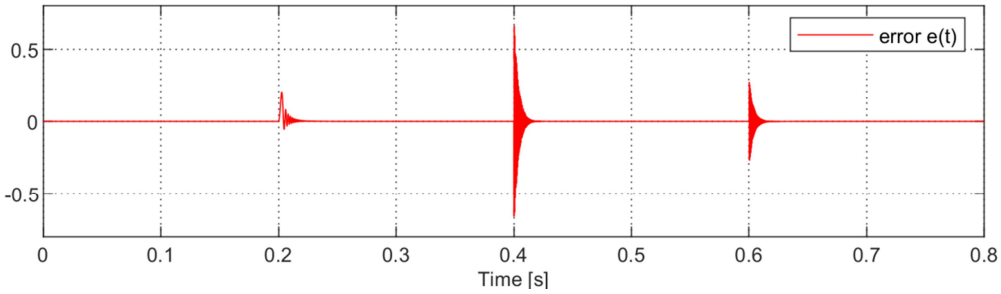

Figure 80: Error between the real system and reference model responses under variable reference.

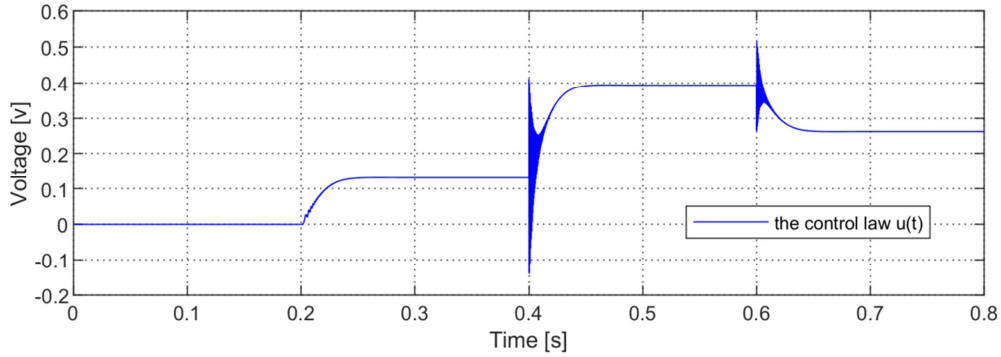

Figure 81: The control law u(t) under variable reference.

In the robustness tests of the adaptive controller, disturbances of 1%, 3% are injected in the closed-loop system. The effects of the disturbances and their corresponding system responses are depicted in Figures 82 and 83.

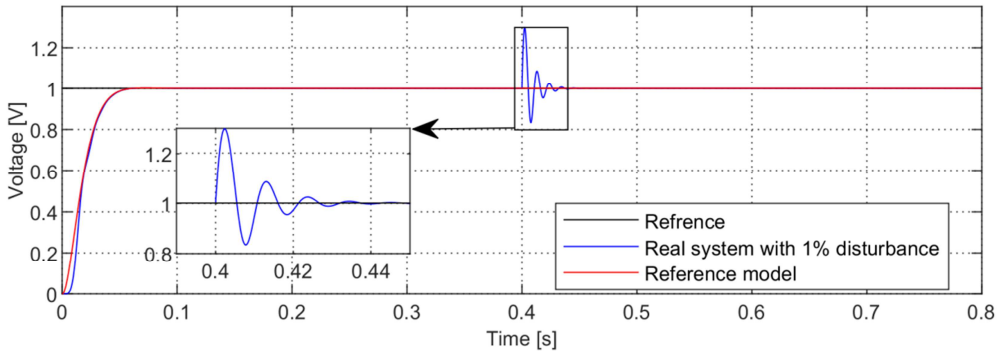

Figure 82: Unit step responses of the system and the reference model with adaptive control when adding 1% disturbance.

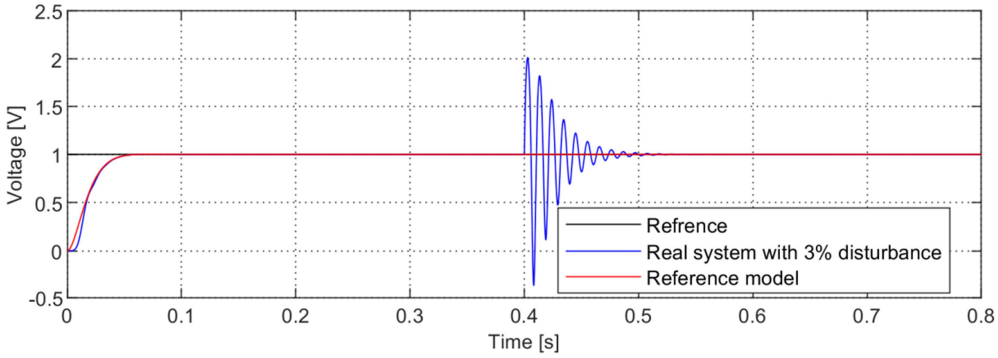

Figure 83: Unit step responses of the system and the reference model with adaptive control when adding 3% disturbance.

The curves of Figure 82 demonstrate that the 1% disturbance is rejected. The Zoom in demonstrates that the system responses return to the reference trajectory within 30 ms in the case of step disturbance. The curves of Figure 83 demonstrate that the 3% disturbance is rejected. The Zoom in demonstrates that the system responses return to the reference trajectory within 100 ms in the case of step disturbance.

According to the obtained simulation results, it can be seen that the adaptive controller provides good system responses and robust rejection of the disturbances.

5.4 Part C: Implementation of the advanced control technique: GA based PI$^{\lambda}$ and PSO based PI$^{\lambda}$

In this part, the intelligence algorithm-based fractional proportional-integral regulator is investigated for controlling the five-level series resonant inverter. First, brief facts on the fractional-order controllers, brief facts on the genetic algorithm GA, and brief facts on the particle swarm optimization PSO are discussed. Next, we design the fractional PI$^{\lambda}$ based on GA and the fractional PI$^{\lambda}$ based on PSO controllers for the five-level series resonant inverter. A GA and PSO are the selected algorithms for determining the optimal parameters of the fractional PI regulator (PI$^{\lambda}$).

5.4.1 Brief facts on the fractional-order controllers

Fractional calculus is a purely mathematical problem that deals with integrals and derivatives of non-integer orders. Modeling natural physical systems by differential equations based on fractional derivatives is becoming the focus of numerous studies. Developing efficient methods to solve these equations numerically has been getting more and more attention during recent years. Various methods have been suggested and investigated based on Grünwald-Letnikov, Caputo, or Riemann-Liouville definitions [21], [22]. The simulation and the implementation of a fractional-order physical system require its approximation by a transfer function of integer-order finite-dimension. In recent years, several approximation methods have been developed using continuous rational models, including Carlson's method, Oustaloup's method, Matsuda's method, Charef's method [22], [23].

Proportional **I**ntegral **D**erivative **PID** controller is one the most used in the industrial area. Eq. (96) shows the **PID** controller expression [24].

$$C_{PID}(s) = k_p + \frac{k_i}{S} + k_d S \tag{96}$$

In 1999, Podlubny proposed a **F**ractional **O**rder **P**roportional **I**ntegral **D**erivative **FOPID** to improve the control performance by adding two extra real parameters, λ and μ. The FOPID controller is defined by the following mathematical expression [25]:

$$C_{FOPID}(s) = k_p + \frac{k_i}{S^{\lambda}} + k_d S^{\mu}, \quad (\lambda, \mu > 0) \tag{97}$$

Figure 84 illustrates the scheme of a closed-loop system with fractional controller $PI^{\lambda}D^{\delta}$.

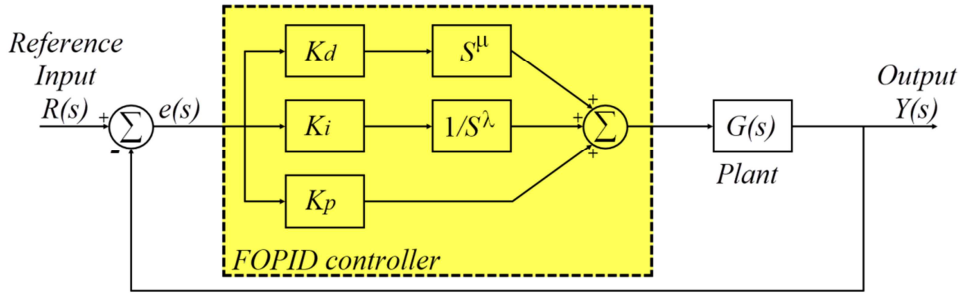

Figure 84: Scheme of a closed-loop system with fractional controller $PI^{\lambda}D^{\delta}$.

The fractional PI^{λ} controller is presented by Eq. (98), where (k_p, $k_i \in \Re$) are the proportional and integral parameters to design the controller, and ($\lambda \in \Re+$) is the order of the S operator to design the controller ($0< \lambda <1$). In dynamic system control, the challenge is determining the FOPI parameters in such a specific way that a pre-determined set of control objectives is attained.

$$C_{FOPI}(s) = k_p + \frac{k_i}{S^{\lambda}}, \quad (\lambda > 0) \tag{98}$$

Figure 85 illustrates the scheme of a closed-loop system with fractional controller PI^{λ}.

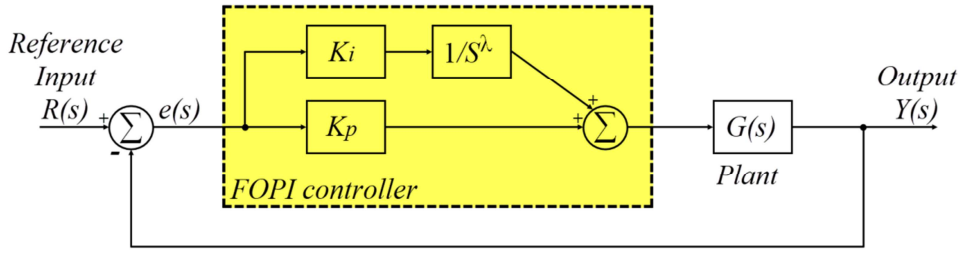

Figure 85: Scheme of a closed-loop system with fractional controller PI^{λ}.

As mentioned above in this section, there are several methods for approximating the fractional order controller. In this work, we used the FOMCON Toolbox based on the

method of Oustaloup's recursive approximation, where the method is based on the approximation of S^{λ} in desired frequency band $\omega \in [\omega_b; \omega_h]$ by the following rational function [26].

$$S^{\lambda} = C \prod_{i=-N}^{N} \frac{S + \omega_i'}{S + \omega_i} \tag{99}$$

ω'_i, ω_i, and C: are the zeros, poles, and gain of the rational function, respectively. N: the approximation order. C: a gain. The following formulas can calculate the parameters of S^{λ}:

$$\begin{cases} C = \omega_h^{\lambda} \\ \omega_i' = \omega_b \left(\dfrac{\omega_h}{\omega_b} \right)^{\frac{i+N+\frac{1}{2}(1-\lambda)}{2N+1}} \\ \omega_i = \omega_b \left(\dfrac{\omega_h}{\omega_b} \right)^{\frac{i+N+\frac{1}{2}(1+\lambda)}{2N+1}} \end{cases} \tag{100}$$

5.4.2 Brief facts on the Genetic Algorithm GA

John Holland and his partners introduced the Genetic Algorithms in 1975. A Genetic Algorithm (GA) is a model of biological evolution and is one of the first evolutionary algorithms. This algorithm can be an excellent method for solving optimization problems if well configured in a data space [22]. The optimization aims to find a better solution to a specific problem considering one or several criteria concerning the system's characteristics and the imposed constraints. The best solution is found from a set of solutions through randomized processes based on producing a new generation of solutions. The method of finding the best solution applies three leading operators in succession: selection, crossover, and mutation, to the current population. These operations are repeated until a stopping criterion is satisfied [27]-[29].

Figure 86 illustrates the procedure of a genetic algorithm. There are five main phases in the genetic algorithm. (1): Initial population, (2): Fitness function, (3): Selection,

(4): Crossover, and (5): Mutation.

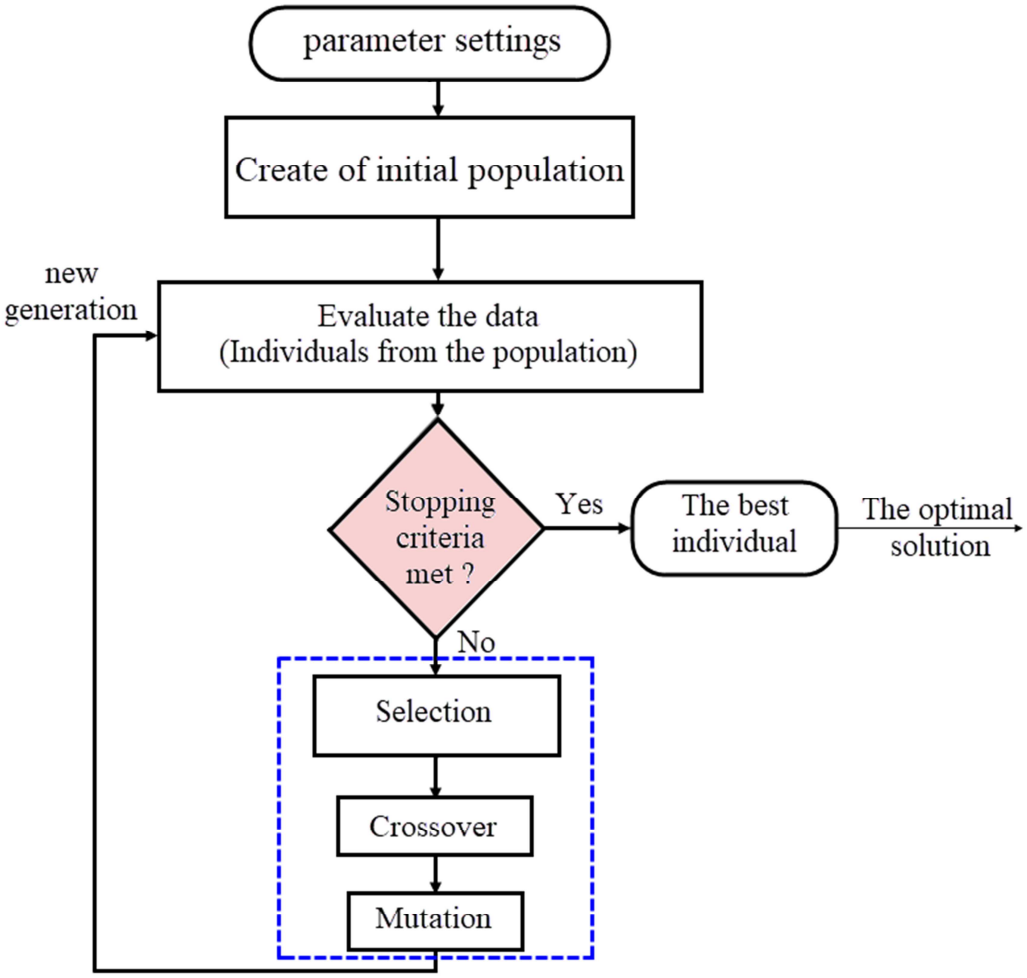

Figure 86: Flowchart of a Genetic Algorithm.

Based on the article [30] and the papers [31], [32], we can describe the basic steps of the Genetic Algorithm as:

(1): Initial Population: At first, the initial population is created randomly. The procedure starts with a set of initial individuals that we call a population. Where each individual is a solution to the problem, we want to solve. An individual is identified by a set of variables (parameters) called genes. The genes are combined into a string to form a chromosome (solution). In the genetic algorithm, the set of the individual's genes is described by a string in an alphabet. Usually, binary code values (a string of 1 and 0) are chosen. It is said that the genes are coded in a chromosome. Figure 87 illustrates an example of population, chromosomes and genes.

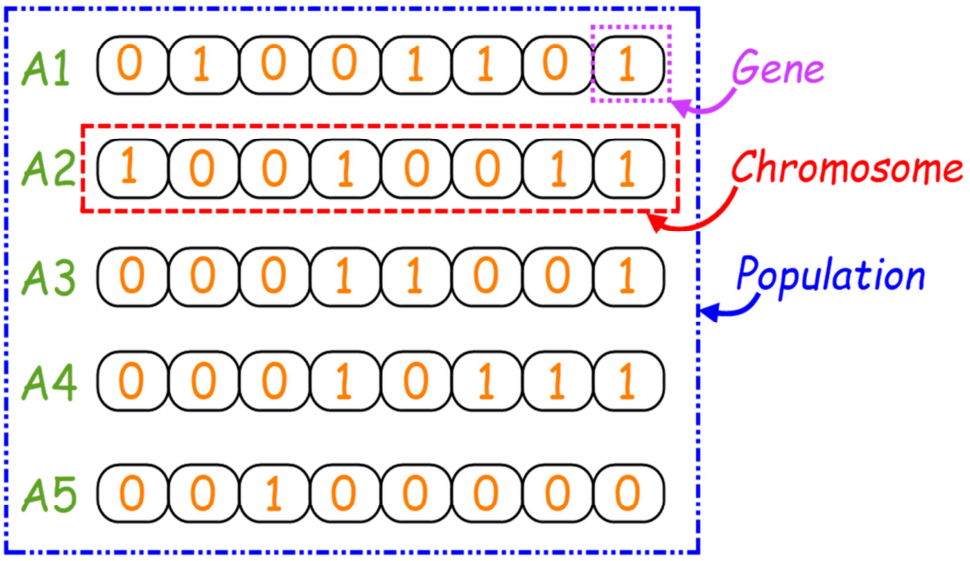

Figure 87: An example of Population, Chromosomes and Genes in genetic algorithm.

(2): Fitness Function: The second step of GA is to evaluate the data using the fitness function and check the met of stopping criteria. The fitness function determines the ability of an individual (his capacity to compete with other individuals) and provides a fitness score for each individual. The probability that an individual will be chosen for selection (reproduction) is related to its fitness score.

(3): Stopping criteria: The stopping criteria are essential property for GAs. The yes answer terminates the iteration and displays the result. The no answer allows the possibility of a selection of parents. Among the criteria proposed in the literature, we can cite the maximum number of generations, the elapsed time.

(4): Selection: Selection is an operation that allows selecting the fittest individuals of a population and eliminating the bad ones. Two pairs of individuals (parents) are chosen from the individuals that have high fitness scores. The aim is to pass the genes of the fittest individuals to the next generation. There are many selection methods in the literature: selecting individuals by the artificial roulette system, selection by rank.

(5): Crossover is an essential mechanism of the genetic algorithm that allows the production of chromosomes that partially inherit the parents' characteristics. In this phase, each pair of parents to be mated has a cross point that is randomly selected from the genes. Offspring are formed through the exchange of genes between the parents until the met of

the crossover point. Crossover aims to allow the recombination of the information present in the genetic heritage of the population. We distinguish many crossover point methods, including One-point crossover and Two-point crossover, as shown in Figures 88 and 89, respectively. Through crossover alone, the next generation will only know what the previous generation knows, which is the drawback of crossover alone.

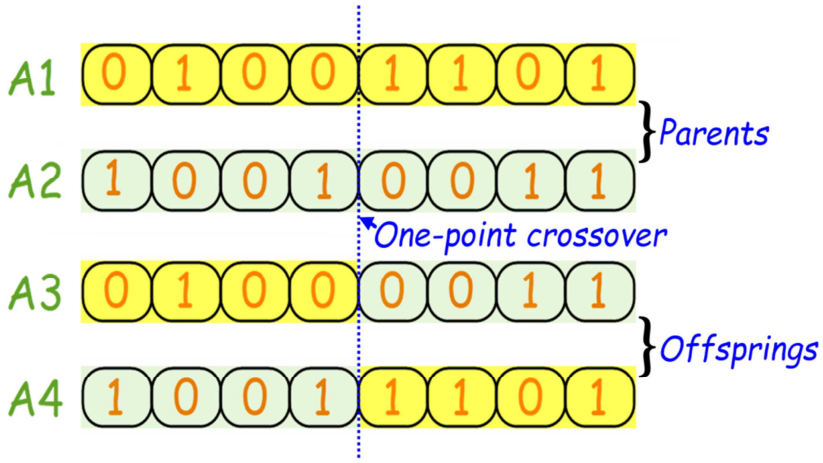

Figure 88: An example of One-point crossover in genetic algorithm.

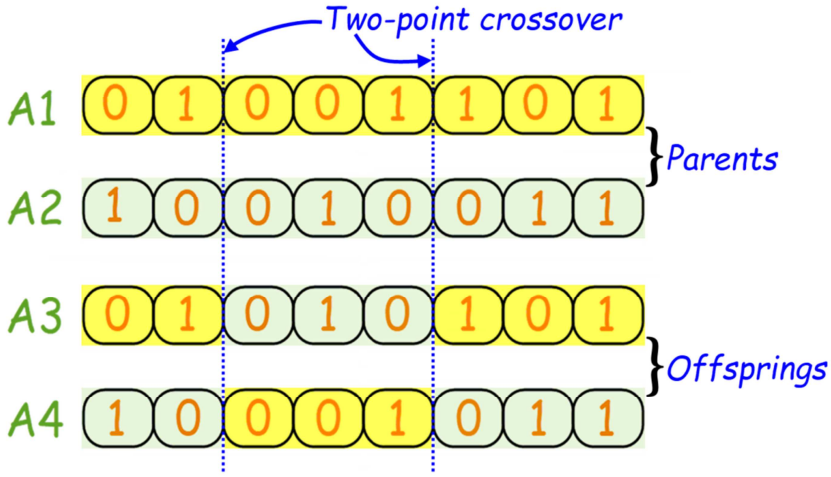

Figure 89: An example of Two-point crossover in genetic algorithm.

(6): Mutation: is a simple concept that plays a disruptive role: introducing noise into the population. It randomly modifies the characteristics of a solution. The mutation is a significant step in the genetic algorithm because it allows us to introduce and maintain diversity within our population of solutions. Therefore, a mutation covers the crossover drawback. Figure 90 illustrates examples of a mutation in a chromosome.

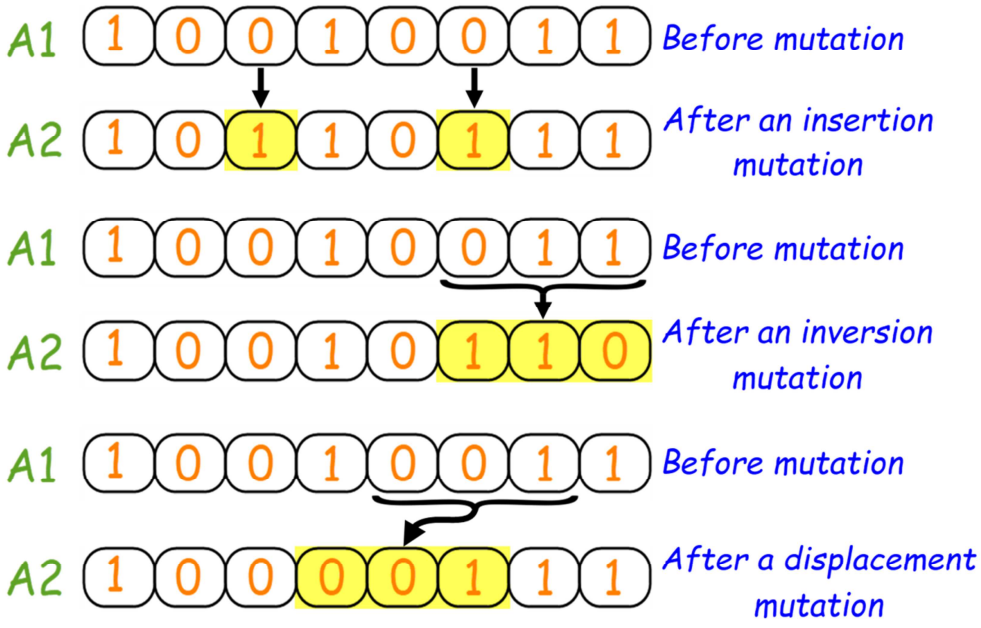

Figure 90: Examples of mutation process in the genetic algorithm.

There are many advantages of genetic algorithms compared to the traditional optimization algorithms, such as the ability to deal with several complex problems (stationary (time-invariant), non-stationary (time-variant), linear, nonlinear, continuous, discontinuous, noisy system). The concept of GA is easy to understand. GA supports multi-objective optimization. GA requires less information about the problem. The genetic algorithm searches for solutions to the problem in parallel since the multiple offspring of a population act as independent agents, the population (or any subgroup) can explore the search space in many directions simultaneously. On the other part, genetic algorithms also have some disadvantages, such as GA is a slow process, thus computationally expensive, i.e., time-consuming. The major obstacle of genetic algorithms is the presentation of the objective function. There isn't a method or expression to set the parameters of the genetic algorithms (number of population, size, and choice of the suitable method in crossover and promising method in mutation for a specific problem). Notwithstanding these shortcomings, genetic algorithms remain popular optimization algorithms used for advanced control of engineering systems [33]-[35].

5.4.3 Brief facts on the Particle Swarm Optimization PSO

In the 1990s, many researchers have proposed studies of the social behavior of

animal groups. These studies showed that some animals livening in swarms could share information among their group as the birds and fishes, and such capability for searching any target or food. According to the study's results of the animal social behavior, Eberhart and Kennedy (1995) are proposed the Particle Swarm Optimization (PSO). PSO is a stochastic diffusion algorithm and part of the family of swarm intelligence (SI). The swarm's intelligence family is a cooperation between agents. The PSO algorithm is inspired by the social behavior (cooperation) of flocks, birds, and fishes. Currently, SI algorithms are adapted to solve various discrete or continuous problems; also, the algorithms have been used in several research areas [36], [37].

In the PSO model, a swarm consists of several members. Each swarm member is a particle associated with a vector of parameters and solves the problem. In the beginning, the particle's velocity and position are defined as (V_i) and (X_i), respectively, where its initial position is treated as its best position (P_{best}). The particles are initialized with a random position and velocity. Then, the fitness of each particle is evaluated using the fitness function. The global best particle (G_{best}) is selected according to the minimum fitness value. The particles move in a D-dimension search space using three factors. (1): The past behavior of (G_{best}); (2): The past behavior of (P_{best}); and (3): The inertia weight (w). The new velocity (V_{i+1}) and position (X_{i+1}) of each particle is calculated using the formulas (101) and (102) respectively [38]-[40]. c_1, c_2: are acceleration coefficients, where c_1 is the cognitive constant and c_2 is the social constant. r_1, r_2: are random numbers of the cognitive and social terms. w_{min}, w_{max}: are the minimum and the maximum limits of the inertia weight. N_{Iter}, k: are the iterations number and the current iteration.

$$V_{i+1} = \left[V_i \times w\right] + \left[c_1 \times r_1 \left(P_{best} - X_i\right)\right] + \left[c_2 \times r_2 \left(G_{best} - X_i\right)\right] \tag{101}$$

$$X_{i+1} = X_i + V_{i+1} \tag{102}$$

$$w = w_{\max} - \left(\frac{w_{\max} - w_{\min}}{N_{Iter}}\right) \times k \tag{103}$$

Figure 91 illustrates the flowchart of the particle swarm optimization. There are three main phases in the PSO algorithm. (1): Initial population, (2): Fitness function, (3): Particles' movement (Update the velocity and the position of particles).

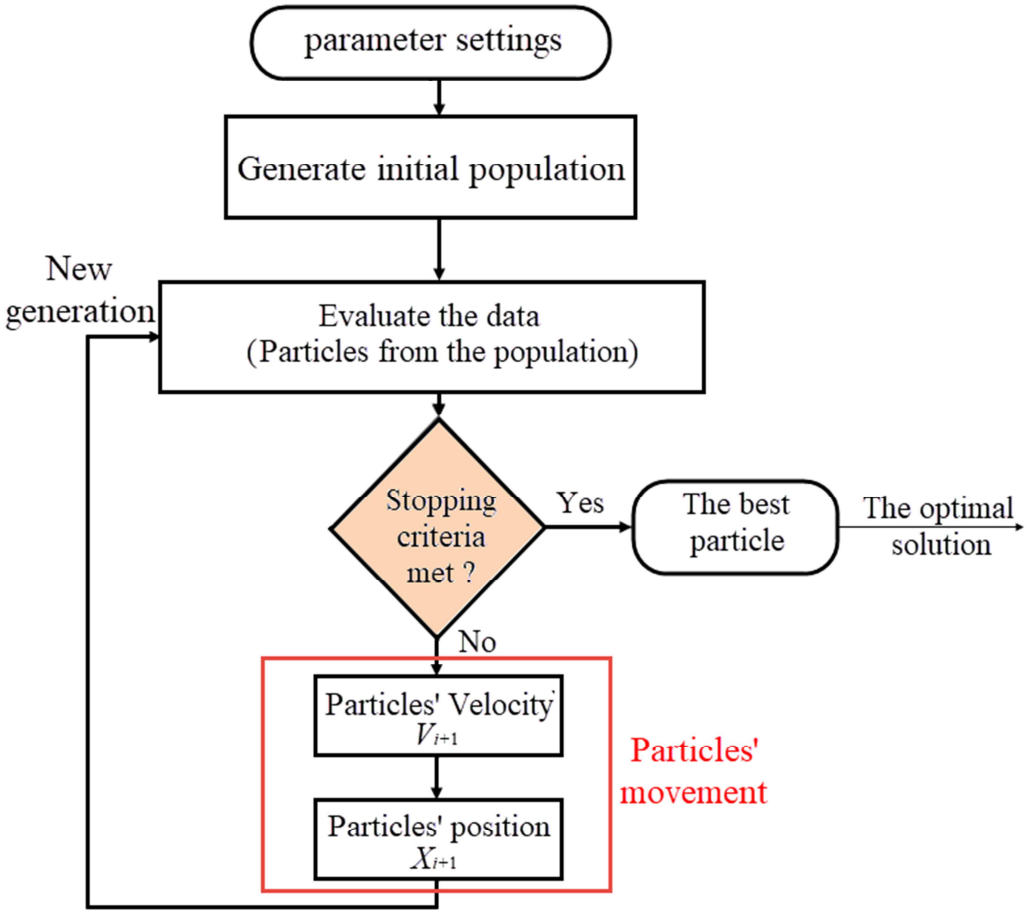

Figure 91: Flowchart of a Particle Swarm Optimization Algorithm.

Like the other intelligent algorithms, also PSO has advantages and disadvantages. It is easy to understand the working principle of PSO and then modify and implement it. The PSO doesn't use selection, which means all population members survive from the beginning to the end of the algorithm. PSO has fewer parameters for tuning. PSO doesn't need the calculation of the error function gradient. PSO doesn't need good beginning points or detailed knowledge about the most promising zones of the search space. PSO is efficient in finding the optimal solution in global optimization. PSO techniques can give a high-quality solution with rapid convergence and shorter calculation time compared to the genetic algorithm.

On the other hand, the well-known disadvantages of PSO are: PSO is weak for finding the optimal solution in the local optimization. PSO method requires a longer computation time than the mathematical approaches. To PSO programming, there is the

problem of finding the optimal design and the initial setting of the parameters [41]-[43].

NOTE: The Particle Swarm Optimization (PSO) and the Genetic Algorithm (GA) can be applied to similar types of problems. PSO and GA are algorithms of iterative type, and they are used as cost functions. The difference between the PSO and the GA is that GA doesn't traverse the search space like birds in flight, covering the intervening areas. PSO algorithm needs normalization of the input vectors to achieve faster convergence. GA operates more like Monte Carlo, where the candidate solutions are random, and the best solutions are chosen to compete with a new set of random solutions.

5.4.4 Design of the GA-based PI$^{\lambda}$ for the five-level series resonant inverter

This subsection aims to design a fractional controller (PI$^{\lambda}$) utilizing the genetic algorithm (GA) for a five-level series resonant inverter. The GA-based PI$^{\lambda}$ is used to implement a closed-loop system for controlling the output capacitor voltage of the system. The controller synthesis is done using the small-signal model of the five-level series resonant inverter (CHAPTER 4). Firstly, we synthesize the control scheme. The next step is a numerical application to test the synthesized control scheme and the designed controller. The results are obtained using the Matlab/Simulink environment. The scheme of GA-based PI$^{\lambda}$ controller is given in Figure 92.

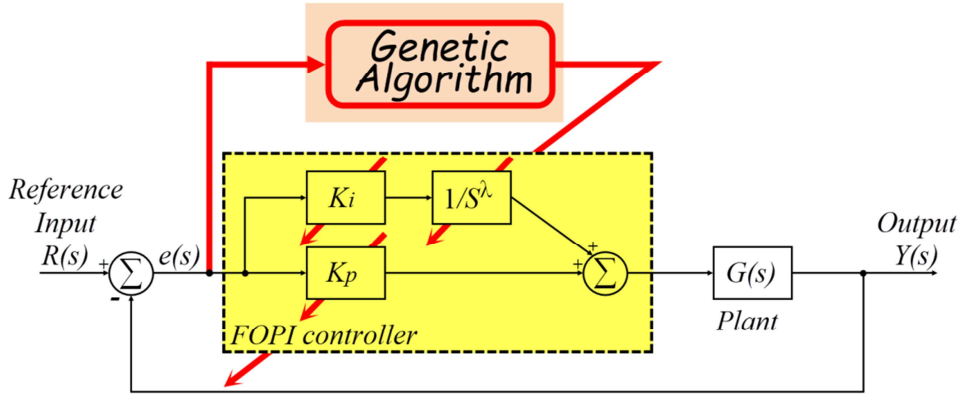

Figure 92: Scheme of the GA-based PI$^{\lambda}$ controller.

The expressions of the common criteria to evaluate a closed-loop controller performance are given in Eq. 104, where: ISE: Integral of Square Error, IAE: Integral of Absolute Error, ITAE: Integral of Time-weighted Absolute Error, and ITSE: Integral Time-weighted Square Error. ISE is used to be optimized in our study.

$$\begin{cases} ISE = \int_0^t e^2(t)dt \\ IAE = \int_0^t |e(t)|dt \\ ITAE = \int_0^t t|e(t)|dt \\ ITSE = \int_0^t te^2(t)dt \end{cases} \quad (104)$$

The genetic algorithm is programmed in MATLAB editor, and the system model is built using MATLAB Simscape and Simulink libraries. The challenge is to find the optimal parameters so that the response of the closed-loop system is stable and robust; this requires a good choice of the genetic algorithm parameters concerning the population size, generations, crossover and mutation probabilities, etc. The available method for choosing the controller's best parameters is to experiment with several genetic algorithm parameters and then test the system's performance. Eight scenarios are selected for setting the genetic algorithm parameters.

In the first scenario, the settings of the Genetic Algorithm (GA) parameters are given in Table 14.

In the second scenario, we increase the number of generations to 50 and leave all other parameters as they are in the first scenario. In the third scenario, we increase the population size to 50 and leave all other parameters as they are in the first scenario. In the fourth scenario, we increase the population size to 50, the number of generations to 50, and leave all other parameters as they are in the first scenario.

In the fifth scenario, we update the limit interval of K_p to [0, 5], the limit interval of K_i to [0, 10], and leave all other parameters of the first scenario. In the sixth scenario, we increase the number of generations to 50 and leave all other parameters as they are in the fifth scenario. In the seventh scenario, we increase the population size to 50 and leave all other parameters as they are in the fifth scenario. In the eighth scenario, we increase the population size to 50, the number of generations to 50, and leave all other parameters like the fifth scenario.

Table 14: Setting of the genetic algorithm parameters

Parameter	*Value*
Population size	20
Number of Generations	20
Number of variables	3 (k_p, k_i, λ)
Limit interval	$k_p \in [0, 1]$
	$k_i \in [0, 1]$
	$\lambda \in [0, 1]$
length of binary number	10
Selection type	*Roulette*
Crossover type	*Random*
Mutation type	*Random*
Mutation probability	5 %
Crossover probability	100 %
Fitness function	*Integral of Square Error*
Stooping condition	*Number of generations*

Figure 93 illustrates the unit step response of the closed-loop system with the GA-based PI$^{\lambda}$ controller.

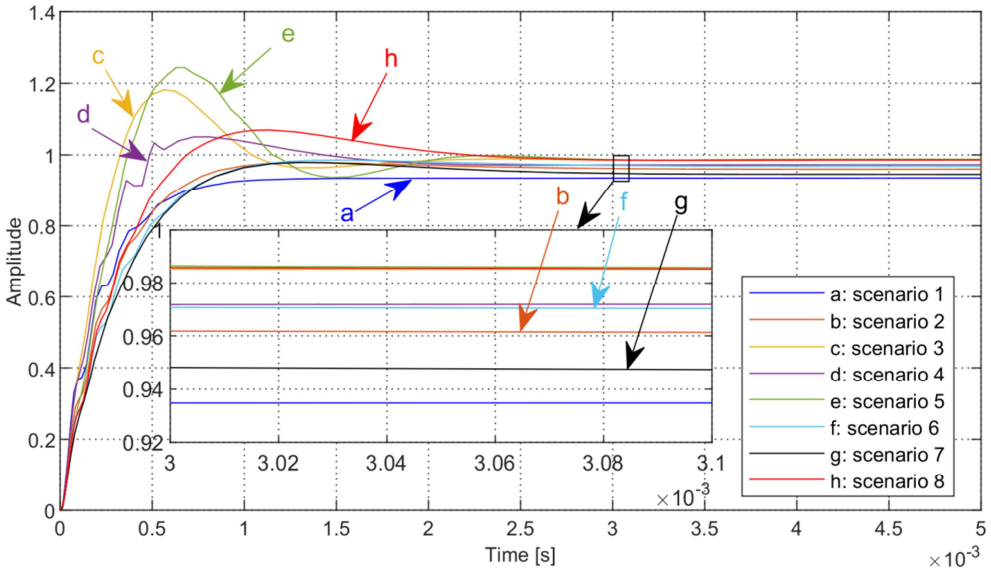

Figure 93: Unit step response of the closed-loop system with the GA based PI$^{\lambda}$ technique

From Figure 93 of the unit step responses, we can note that GA parameters influence the performances of the feedback control system. The performance characteristics of the feedback control system with the eight scenarios are summarized in Table 15. Overshoot values are rounded to the nearest Hundredths (0.01). PI$^{\lambda}$ parameters, settling time, rise time, and peak response values are rounded to the nearest Ten

Thousandths (0.0001).

Table 15: PI$^{\lambda}$ parameters and performances characteristics of the feedback control system with GA

Scenario	*Elapsed runtime (s)*	*PI$^{\lambda}$ parameters*	*Overshoot (%)*	*Settling time (s)*	*Rise time (s)*	*Peak response*
Scenario 1	0372	$K_p = 0.1711$ $K_i = 0.2258$ $\lambda = 0.5503$	00.00	0.0009	0.0005	0.9369
Scenario 2	0590	$K_p = 0.1378$ $K_i = 0.7478$ $\lambda = 0.3529$	01.58	0.0008	0.0005	0.9780
Scenario 3	0606	$K_p = 0.1515$ $K_i = 0.7537$ $\lambda = 0.0029$	19.88	0.0015	0.0002	1.1816
Scenario 4	1559	$K_p = 0.1681$ $K_i = 0.3118$ $\lambda = 0.0166$	08.02	0.0016	0.0003	1.0503
Scenario 5	0273	$K_p = 0.1026$ $K_i = 1.7107$ $\lambda = 0.1496$	25.83	0.0018	0.0003	1.2436
Scenario 6	0672	$K_p = 0.1222$ $K_i = 2.0137$ $\lambda = 0.5093$	01.40	0.0009	0.0006	0.9851
Scenario 7	0963	$K_p = 0.1124$ $K_i = 0.2121$ $\lambda = 0.1496$	03.20	0.0020	0.0006	0.9770
Scenario 8	2115	$K_p = 0.1173$ $K_i = 5.2590$ $\lambda = 0.5112$	08.11	0.0021	0.0005	1.0682

To evaluate the performances characteristics of the GA-based PI$^{\lambda}$ controller, we define the following design criteria: overshoot less than 5% and less value possible of settling time (2%). According to the design criteria, the best-achieved parameters of the PI$^{\lambda}$ controller using GA are given in Table 16.

Table 16: The best-achieved parameters of PI$^{\lambda}$ controller using genetic algorithm

PI$^{\lambda}$ controller parameters	*Value*
K_p	0.1378
K_i	0.7478
λ	0.3529

NOTE: The best parameters of the PI$^{\lambda}$ controller using the genetic algorithm given in table 16 are valid in the case of the unit step reference. For example, if the target value (set-point) is set to 10, the MATLAB model possibly not be executed and will display an

error. Testing the system's performance under a variable reference or disturbances requires searching for other genetic algorithm parameters then a new execution of the GA pseudo-code taking into account the variable reference and the disturbances to ensure the controller works. This problem is one of the drawbacks of the GA-based PI^{λ} technique. Furthermore, the selected limit intervals in the GA parameters setting can give singularity problems and stop the simulation. The singularity might be solved by resetting the upper or lower bound of the limit intervals.

5.4.5 Design of the PSO-based PI^{λ} for the five-level series resonant inverter

In this subsection, the design of the PSO-based PI^{λ} controller for the five-level series resonant inverter is discussed. The technique is used to implement a closed-loop system for controlling the output capacitor voltage of the system. The control synthesis is done using the small-signal model of the five-level series resonant inverter (CHAPTER 4). Firstly, we present the control scheme and the pseudo-code of the particle swarm optimization. Then, a numerical application is made for testing the control scheme and the designed controller. The simulation model and results are given using a Matlab/Simulink environment. Scheme of the PSO-based PI^{λ} controller is given in Figure 94.

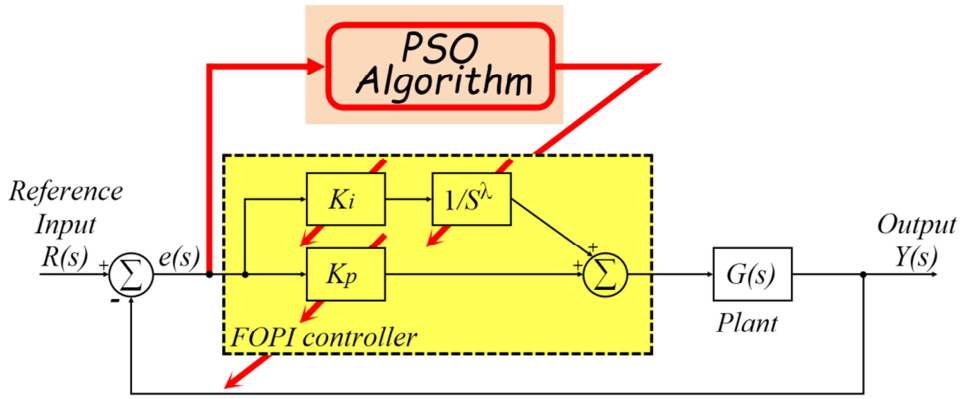

Figure 94: Scheme of the PSO-based PI^{λ} controller.

The fitness function is the ISE criteria. The PSO algorithm is programmed in MATLAB editor, and the system model is built using MATLAB Simscape and Simulink libraries. We select eight scenarios to test the system's performance and then find the best parameters of the PSO. In the first scenario, the settings of the PSO algorithm parameters are given in Table 17.

In the second scenario, we increase the iterations number to 60 and leave all other parameters like the first scenario. In the third scenario, we increase the population size to 30 and leave all other parameters like the first scenario. In the fourth scenario, we increase the population size to 30, the iterations number to 60, and leave all other parameters like the first scenario. In the fifth scenario, we increase the population size to 30, the iterations number to 100, and leave all other parameters like the first scenario. In the sixth scenario, we increase the population size to 60, decrease the iterations number to 10, and leave all other parameters like the first scenario. In the seventh scenario, we increase the population size to 60, and leave all other parameters like the first scenario. In the eighth scenario, we increase the population size to 60, the iterations number to 60, and leave all other parameters like the first scenario.

Table 17: Setting of the particle swarm optimization parameters

Parameter	*Value*
Population size	10
Iterations number, N_{Iter}	30
Number of variables	3 (k_p, k_i, λ)
Limit interval	$k_p \in [0, 5]$
	$k_i \in [0, 10]$
	$\lambda \in [0, 1]$
Cognitive constant, c_1	2.05
Social constant, c_2	2.05
Minimum inertia weight, w_{min}	0.4
Maximum inertia weight, w_{max}	0.9
Fitness function	*Integral of Square Error*
Stooping condition	*Number of iterations*

Figure 95 illustrates the unit step response of the closed-loop system with the PSO-based PI^{λ} controller.

From Figure 95 of the unit step responses, we can note that PSO parameters influence the performances of the feedback control system. Also, finding a direct or indirect correlation between PSO parameters (*Population size*, *Iterations number*) and system performance is complex and requires several tests using a high-performance computer. The performance characteristics of the feedback control system with the eight scenarios are summarized in Table 18. Overshoot values are rounded to the nearest Hundredths (0.01). Settling time, rise time, and peak response values are rounded to the nearest Ten-Thousandths (0.0001).

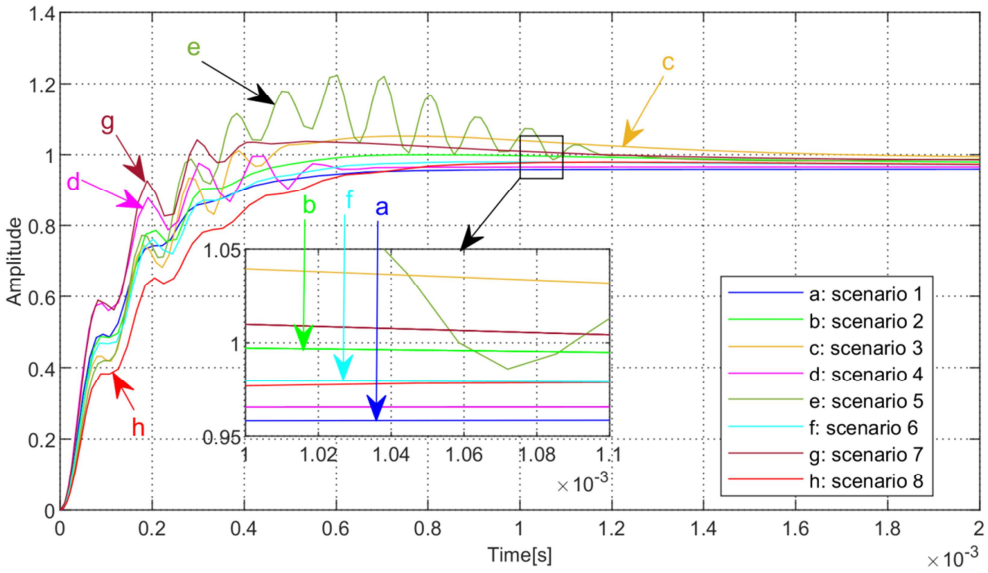

Figure 95: Unit step response of the closed-loop system with the PSO-based PI$^{\lambda}$ technique

Table 18: PI$^{\lambda}$ parameters and performances characteristics of the feedback control system with PSO

Scenario	*Elapsed runtime (s)*	*PI$^{\lambda}$ parameters*	*Overshoot (%)*	*Settling time (s)*	*Rise time (s)*	*Peak response*
Scenario 1	032	$K_p = 0.2770$ $K_i = 3.9438$ $\lambda = 0.9310$	00.00	0.0006	0.0003	0.9644
Scenario 2	082	$K_p = 0.2533$ $K_i = 0.4969$ $\lambda = 0.1670$	00.00	0.0011	0.0003	0.9996
Scenario 3	121	$K_p = 0.2171$ $K_i = 4.9046$ $\lambda = 0.4152$	06.17	0.0014	0.0002	1.0518
Scenario 4	216	$K_p = 0.3545$ $K_i = 2.3064$ $\lambda = 0.9765$	02.89	0.0005	0.0002	0.9954
Scenario 5	184	$K_p = 0.1897$ $K_i = 2.6573$ $\lambda = 0.2160$	23.45	0.0012	0.0002	1.2232
Scenario 6	084	$K_p = 0.2452$ $K_i = 0.4486$ $\lambda = 0.2496$	01.05	0.0005	0.0003	0.9798
Scenario 7	250	$K_p = 0.3209$ $K_i = 0.5439$ $\lambda = 0.0338$	05.83	0.0011	0.0002	1.0412
Scenario 8	388	$K_p = 0.1843$ $K_i = 1.3594$ $\lambda = 0.4401$	00.78	0.0007	0.0004	0.9792

From Table 18, the elapsed runtime of the PSO algorithm proves the rapid convergence of PSO compared to the genetic algorithm. Also, finding results demonstrates the ability of the PSO algorithm.

The best controller parameters must be chosen for the good performance of the system, when selecting the parameters, the following criteria must be respected in order: overshoot less than 5% and less value possible of settling time (2%). According to the design criteria, the best-achieved parameters of the PI^{λ} controller using PSO are given in Table 19.

Table 19: The best-achieved parameters of PI^{λ} controller using particle swarm optimization

PI^{λ} controller parameters	*Value*
K_p	0.2452
K_i	0.4486
λ	0.2496

NOTE: As the genetic algorithm case, the best parameters of the PI^{λ} controller using the PSO algorithm given in Table 19 are valid only for the unit step reference. For example, if the target value (set-point) is set to 5, the MATLAB model possibly not be executed and will display an error. Also, testing the system's performance under a variable reference or disturbances requires searching for other PSO parameters. Then, a new execution of the PSO pseudo-code considers the variable reference and the disturbances to ensure the controller works. This problem is one of the drawbacks of the PSO-based PI^{λ} technique. Furthermore, the selected limit intervals or some values in the PSO parameters setting can give singularity problems and stop the simulation. The singularity might be solved by resetting the parameters.

5.5 Comparisons between the implemented control techniques

Table 20 presents a summary of the parameters and the performance comparison between the CDM-based PI, Adaptive, GA-based PI^{λ}, and PSO-based PI^{λ} control techniques. Figure 96 illustrates the closed-loop step responses of the system using the designed control techniques.

Table 20: Performance comparison of the designed control techniques

Method	*Elapsed runtime (s)*	*Controller parameters*	*Overshoot (%)*	*Settling time (s)*	*Rise time (s)*	*Peak response*
CDM-based PI	0.45	$K_p = 0.0031$ $K_i = 2.6952$	01.83	0.0126	0.0088	1.0183
Adaptive	4.29	$\omega_n = 100$ $\xi = 0.9$ $\gamma_1 = -20.65$ $\gamma_2 = 6.1797$	00.15	0.05	0.03	1
GA-based PI$^{\lambda}$	590	$K_p = 0.1378$ $K_i = 0.7478$ $\lambda = 0.3529$	00.13	0.0009	0.0005	0.9787
PSO-based PI$^{\lambda}$	084	$K_p = 0.2452$ $K_i = 0.4486$ $\lambda = 0.2496$	01.05	0.0005	0.0003	0.9798

From Table 20, the execution time (elapsed runtime) demonstrates the speed of the CDM technique compared to the Adaptive, PSO, GA techniques, respectively. The performance of the closed-loop system with the designed control techniques is well because each control technique provides an overshoot of less than 2%, max settling time of 50 ms, max rise time of 30 ms, peak response of 1 approximately.

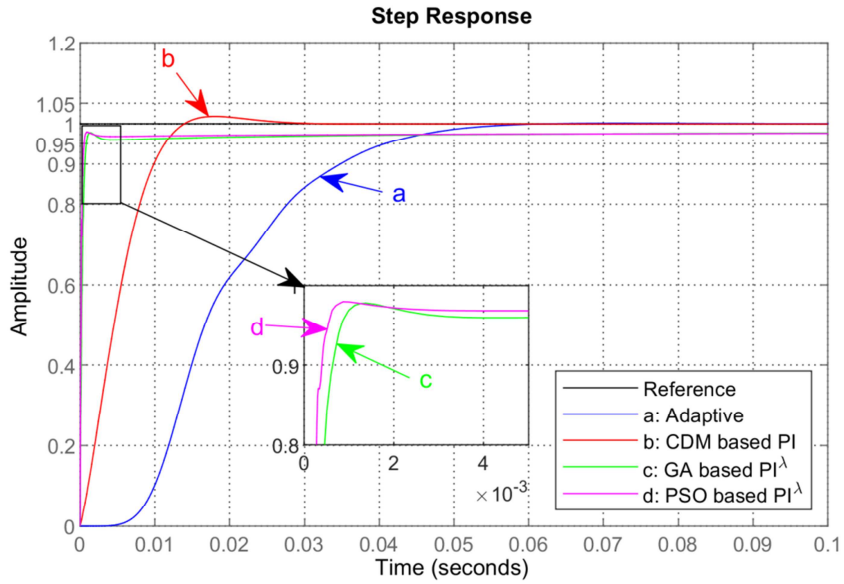

Figure 96: The closed-loop step response comparison of the system using the designed control techniques

Figure 96 of the unit step responses shows that the GA-based PI$^{\lambda}$ and PSO-based PI$^{\lambda}$ controllers are faster than the CDM-based PI and Adaptive controllers; also, the CDM-

based PI controller is faster than the Adaptive controller. Moreover, in the selected simulation time, the closed-loop step responses of the system achieve a zero value of steady-state error when using CDM-based PI or Adaptive controllers. There is acceptable steady-state error SSE of the system responses when using GA-based PI^{λ} or PSO-based PI^{λ} controllers, but this SSE value is due to step input. Maybe the SSE value will be higher than the desired value if the set-point (reference input) is changed to a higher value. However, the GA and PSO can achieve good results when updating the reference value or adding a new disturbance value with a new execution of the algorithms considering the modifications. On another part, the figure shows that adaptive control has a delay of 5ms approximately to start, and there aren't delays with the other control technique.

An example of the robustness test of the designed control techniques under 1% disturbance is carried out, Figure 97 presents the achieved results.

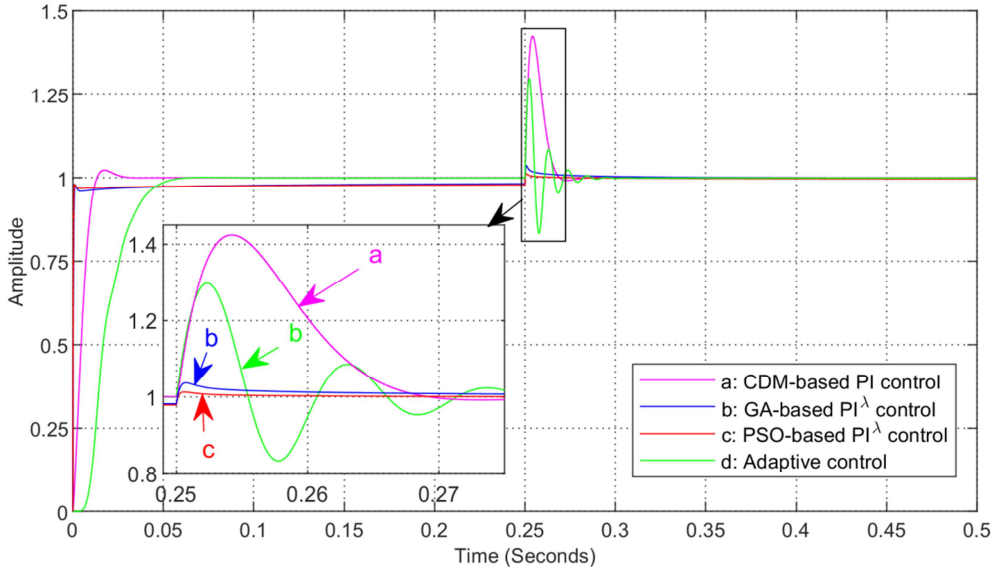

Figure 97: The closed-loop step response comparison of the system using the designed control techniques when adding 1% disturbance.

The curves of Figure 97 show that a perturbation of 1% is efficiently ignored using the four control techniques. The Zoom in demonstrates that the system responses return to the reference trajectory within 20 ms using the CDM-based PI control, within 30 ms using the adaptive control, and within 2 ms using the GA-based PI^{λ} or the PSO-based PI^{λ} control.

According to the obtained simulation results, it can be seen that the intelligent algorithms give us better results than the CDM and the adaptive methods, and PSO gives us better results than the GA. Based on the achieved results, we can't give a direct opinion and say that a specific method is better than the other methods because the parameters setting of methods plays a significant role in the quality of the results. Key remarks of the comparison are:

Remark 1: The coefficient diagram method (CDM) is a simple algebraic approach, which makes it the faster method for getting the results.

Remark 2: Adaptive is an online method for controlling the systems. CDM, GA, and PSO are offline techniques for tuning the controllers' parameters.

Remark 3: The advantage of intelligent algorithms is that the user does not need any knowledge about the system or much information; the user sets the parameters and leaves the algorithm search the solution in space. In intelligent algorithms, the fitness function plays an essential part in the quality of the results.

Remark 4: A feedback control system's task is to ensure that the system output has desired performances and characteristics.

Remark 5: Intelligent algorithms (PSO, GA) are considered the best techniques for rapid response and robustness. CDM is regarded as the best technique in terms of elapsed runtime. Adaptive is viewed as the best technique in terms of steady-state response.

Remark 6: Understanding the basics of the genetic algorithm allows you to develop new genetic algorithms because there aren't any precise criteria or methods to choose the good crossover point or the good mutation method; always tests and comparison are the existing methods for choosing the parameters.

Remark 7: In the systems control field, sometimes the user needs speed, other times he needs precision; As these factors guide the user to choose the best control method for the system. For example, in the induction heating process, there are heat efficiency and heating speed.

5.6 Summary

In this chapter, some control techniques have been introduced and designed for the proposed five-level series resonant inverter. A coefficient diagram method CDM has been investigated to find the optimal parameters of the proportional-integral controller. The MRAC based MIT rule has been designed for controlling the five-level series resonant inverter. The intelligent algorithms GA and PSO have been investigated to find the optimal parameters of the fractional proportional-integral controller. Moreover, a comparison between the designed control techniques has been given; the results show the efficiency and ability of intelligent algorithms. But, there are challenges when using intelligent algorithms like the parameters setting; there isn't a direct method to set the parameters of the algorithms; also, there isn't a single model that works best for all possible situations.

Chapter 06:
CONCLUSION

CHAPTER 6 CONCLUSION

In this chapter, a summary of the thesis' main points and recommended future works are presented.

6.1 Summary of key points

The thesis addresses the topic “Contribution to the modeling and advanced control of a multilevel resonant inverter”. After organizing the bibliographical research on the subject, we have proposed new circuits in the power electronics field: the improved asymmetrical Twenty-one level inverter and the five-level resonant inverter. The presented circuit of a five-level series resonant inverter combines the advantages of the multilevel inverter with reduced device count and the physical phenomenon “resonance” characteristics. Furthermore, a modeling of the proposed circuit was performed using the small-signal model technique. Eventually, four control techniques for the five-level series resonant inverter were discussed. The control techniques are PI-based on Coefficient Diagram Method (CDM), the Model Reference Adaptive Control (MRAC) using MIT rule, the fractional controller (PI^{λ}) design using the Genetic Algorithm (GA), the fractional controller (PI^{λ}) design using the Particle Swarm Optimization (PSO). The thesis consists of six chapters with a bibliography and appendices.

Chapter 1 focuses on introducing the research topic and its importance, presenting and discussing the study's problem based on the perspectives and shortcomings of similar previous works. Also, this chapter identifies the study approach adopted to investigate the topic: the analytical approach, the experimental approach, the comparative approach. In addition, the chapter presents the organization of the thesis.

Chapter 2 of this thesis deals with state of the art about inverters and electrical control systems; for a clear presentation of the information gathered from the bibliography references, the chapter was split into two parts. In the first part, the chapter presents a number of the latest valuable information that researchers have achieved; the information gives new concepts and knowledge to the reader about the topologies and modeling techniques of resonant inverters. Also, the chapter presents the multilevel inverters and

their modulation strategies, where an emerging topology with a reduced number of components is used in this study because of its many advantages. Part two focuses on the electrical control systems, where much information about the controller actions was presented; also, the classical and advanced control techniques were discussed. The second chapter was concluded with positioning our study based on the state of art. The choice of topology, a resonant circuit, the modulation technique, the small-signal model method, and the control techniques was justified. Generally, the chapter is very significant and can be cited to write scientific articles.

Chapter 03 presents the proposed circuit of the five-level series resonant inverter, in which the circuit analysis was carried, and the principle of its operation was presented. The circuit consists of 02 DC power supplies, 06 electronic switches, capacitance, resistance, and inductance. It was important to note that the resonant inverter is an interesting component in technological development in telecommunication, wireless energy transfer, induction heating processes. This chapter gives brief information about the physical phenomenon “resonance” and the mathematical expressions for understanding the proposed circuit.

Chapter 4 of this thesis provides the mathematical modeling of the five-level series resonant inverter using the small-signal method. The artificial neural network-based selective harmonic elimination technique SHE was employed for the modulation of the five-level inverter. The small-signal model of the proposed circuit was developed to aid in the control design. The transfer functions of the system were derived from the developed small-signal model, and the model was validated using frequency response (Bode diagram). To validate the proposed circuit and the small-signal model the MATLAB/SIMULINK software was used. The experimental results were obtained by using different tools of implementation, measurements, and tests like Electronic switches (MOSFET switches), digital oscilloscope (GWINSTEK), DC power supplies, electrical power components (Resistance, Inductance, Capacitor); the switching signals was implemented in real-time using an embedded board C2000 Delfino DSP320F28379D. This chapter presents clear and interesting results for researchers, where it gives useful

information to remove confusion about the modeling of converters by the small-signal model. A step-by-step tutorial for modeling the proposed five-level series resonant inverter using a small-signal method was presented. Also, this chapter reinforces the information contained in the previous works and gives a new perspective about the application of the small-signal method.

Chapter 5 describes four techniques for controlling the five-level series resonant inverter. The first part of chapter 05 presents the coefficient diagram method "CDM" for designing a high-performance PI controller, where the design and simulation of the CDM-based PI control for the five-level series resonant inverter was discussed. The second part of Chapter 05 introduces adaptive control for the controller design of a system. The third part of chapter 05 discusses the fractional controller and the intelligent algorithms for optimizing the controller parameters. The fractional PI^{λ} based on PSO, and the fractional PI^{λ} based on GA were explained. The four control techniques were designed for the five-level series resonant inverter. The system performances were tested in the closed-loop with unit step and variable step. Also, the robustness of the controller was evaluated by applying disturbances to the system parameters. Eventually, a comparison was done between the four control techniques. This chapter is very significant because it provides a number of brief facts about the advanced control techniques.

Circuit analysis, modeling, closed-loop control, and simulation were performed in the continuous conduction mode. Voltage control mode was employed for the five-level series resonant inverter.

Chapter 6 concludes the thesis. In this chapter, a summary of the thesis' main points and recommended future works were presented. In addition, the field was opened to researchers to address several topics based on the topic at hand using the given recommendations.

Generally, this research work has allowed us to enrich our knowledge in several areas, as the emerging power electronics, control theory, resonant inverters, multilevel inverters, programing of the embedded boards (Arduino, DSP) and the dSPACE DS1104, simulation with MATLAB/Simulink, Design and realization of the PCB boards, and

writing the scientific articles and reports.

Among the challenges of getting this research done was missing a powerful personnel PC to simulate the systems and control methods. In addition, the expensive cost of the electronic components and the difficulty to obtain them. However, the internship awarded from UHBC to conduct experiments at PEARL was the key to overcoming the challenges and accomplishing some scientific papers on the part of my thesis topic.

The next section of this thesis is dedicated to the future plans based on the current discussed work. Some of the proposed and recommended works could be a topic of a new research plan.

6.2 Future works

It will be interesting to implement other resonant inverters at high-frequency using SiC Mosfets, but experimental tests are dangerous at high-frequency because the voltage or current will be amplified as shown in the thesis results, and these requires many safety precautions, the availability of special measuring and analysis equipment and money for funding the research.

The experimental implementation for the proposed control techniques and publishing the results of controllers design are our future purpose. The digital controller design and the modeling of the system in discrete-domain will be attractive because the digital control has many advantages like the low cost of implementation compared to analog one; also, the manipulation and adaptation of parameters in the digital control is easy and accurate.

To address new research subjects, we opened the way to study other configurations of resonant inverters like the Five-level parallel resonant inverter as presented in Figure 98 and The Five-level LLC resonant inverter as shown in Figure 99.

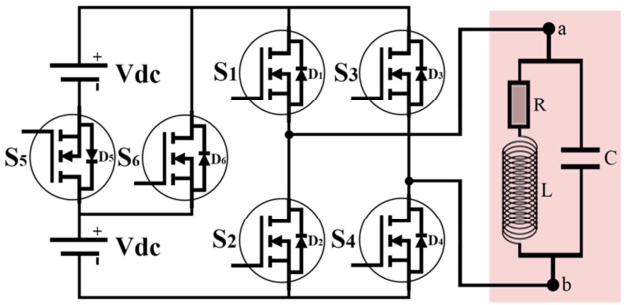

Figure 98: Topology of the Five-level parallel resonant inverter.

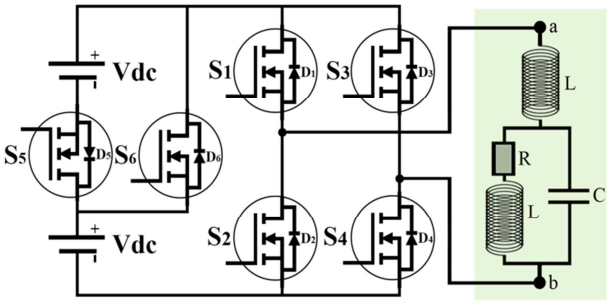

Figure 99: Topology of the Five-level LLC resonant inverter.

Also, as a recommendation, it would be beneficial to feed the inverter by a renewable energy system as PV solar or Wind or a hybrid system as PV-Wind, where these sustainable energies have attracted the attention of the human. Figure 100 illustrates the five-level series resonant inverter supplied by renewable sources. Sustainable energies have many benefits: environmental and economic. The most advantages of sustainable energies are reducing air pollution, reducing global warming, and lowering electricity production prices.

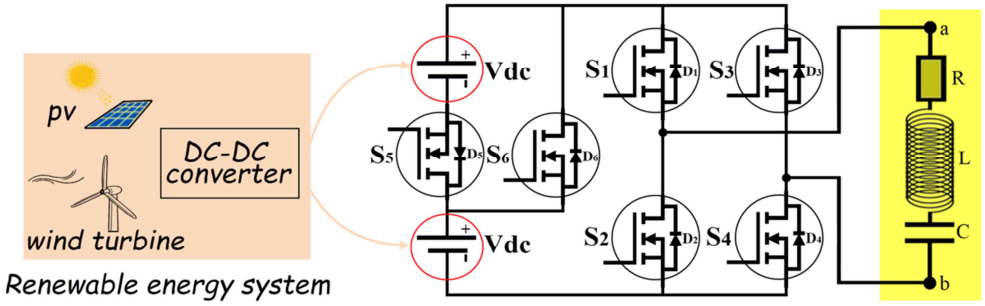

Figure 100: Block diagram of the five-level series resonant inverter supplied by renewable sources.

In the industrial trend, it would be beneficial to use the five-level LLC resonant inverter for the induction heating process, as shown in Figure 101. The power of the induction heating system can be increased, and the control is convenient, especially with the development of high-speed mini processors with high performances, and the huge development of power semiconductors that support high frequency with good power, such as SiC Mosfet and GaN.

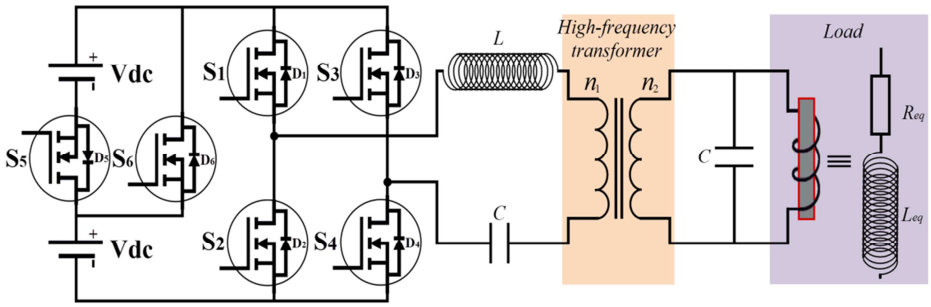

Figure 101: Five-level LLC resonant inverter for induction heating process

Finally, to achieve a more satisfactory performance, we opened the way to address the following points: (1): Use a neural network-based control technique. (2): Analysis and design of Internal Model Control (IMC). (3): Use the recent Model Predictive Control (MPC) techniques for controlling the system. (4): Implementation of other improved Intelligent Algorithms.

REFERENCES

REFERENCES

CHAPTER-1 REFRENCES

[1] Savekar A, Patil A, Kumar V. Power Electronics Market: Report A01456. https://www.alliedmarketresearch.com/power-electronics-market. Published June 2020. Accessed July 15, 2021.

[2] Energy consumption worldwide from 2000 to 2018, with a forecast until 2050, https://www.statista.com/statistics/222066/projected-global-energy-consumption-by-source/ [online web site] last access 31/10/2021.

[3] Han Y, Yang M, Li H, et al. Modeling and Stability Analysis of LCL -Type Grid-Connected Inverters: A Comprehensive Overview. *IEEE Access*. 2019; 7:114975-115001. doi:10.1109/access.2019.2935806

[4] Erickson RW, Maksimović D. Introduction. In: Fundamentals of Power Electronics. Springer US; 2001:1-10. doi:10.1007/0-306-48048-4_1

[5] Bana PR, Panda KP, Naayagi RT, Siano P, Panda G. Recently Developed Reduced Switch Multilevel Inverter for Renewable Energy Integration and Drives Application: Topologies, Comprehensive Analysis and Comparative Evaluation. *IEEE Access*. 2019; 7: 54888-54909. doi:10.1109/access.2019.2913447

[6] Prabaharan N, Palanisamy K. A comprehensive review on reduced switch multilevel inverter topologies, modulation techniques and applications. *Renewable and Sustainable Energy Reviews*. 2017;76:1248-1282. doi:10.1016/j.rser.2017.03.121

[7] Omer P, Kumar J, Surjan BS. A Review on Reduced Switch Count Multilevel Inverter Topologies. *IEEE Access*. 2020;8:22281-22302. doi:10.1109/access.2020.2969551

[8] Maamar AET, Kermadi M, Helaimi M, Taleb R, Mekhilef S. An Improved Single-Phase Asymmetrical Multilevel Inverter Structure With Reduced Number of Switches and Higher Power Quality. *in IEEE Transactions on Circuits and Systems II: Express Briefs*. 2021;68(6):2092-2096. doi:10.1109/tcsii.2020.3046186

[9] Vemuganti HP, Sreenivasarao D, Ganjikunta SK, Suryawanshi HM, Abu-Rub H. A Survey on Reduced Switch Count Multilevel Inverters. *IEEE Open Journal of the Industrial Electronics Society*. 2021;2:80-111. doi:10.1109/ojies.2021.3050214

[10] Sheng-Yang Yu, Runruo Chen and Ananthakrishnan Viswanathan. Survey of

Resonant Converter Topologies. 2018 Texas Instruments Power Supply Design Seminar, pp.1-23. TI Number: SLUP376. https://www.ti.com/seclit/ml/slup376/slup376.pdf

[11] Yang EX, Lee FC, Jovanovic MM. Small-signal modeling of series and parallel resonant converters. *In: [Proceedings] APEC '92 Seventh Annual Applied Power Electronics Conference and Exposition*. IEEE. 1992: 785-792.

doi:10.1109/apec.1992.228333

[12] Helaimi M, Bettayeb M, Benghanem M and Belmadani B. Control system design and small signal analysis of APWM resonant inverter for induction heating. *International Conference on Electric Power and Energy Conversion Systems (EPECS)*. 2009: 1-6.

[13] Memon MA, Mekhilef S, Mubin M, Aamir M. Selective harmonic elimination in inverters using bio-inspired intelligent algorithms for renewable energy conversion applications: A review. *Renewable and Sustainable Energy Reviews*. 2018;82:2235-2253. doi:10.1016/j.rser.2017.08.068

[14] Vemuganti HP, Sreenivasarao D, Siva Kumar G, Sai Spandana A. Reduced carrier PWM scheme with unified logical expressions for reduced switch count multilevel inverters. *IET Power Electronics*. 2018;11(5):912-921. doi:10.1049/iet-pel.2017.0586

[15] Prabaharan N, Palanisamy K. A comprehensive review on reduced switch multilevel inverter topologies, modulation techniques and applications. *Renewable and Sustainable Energy Reviews*. 2017;76:1248-1282. doi:10.1016/j.rser.2017.03.121

[16] Yue X, Wang X, Blaabjerg F. Review of Small-Signal Modeling Methods Including Frequency-Coupling Dynamics of Power Converters. *IEEE Transactions on Power Electronics*. 2019;34(4):3313-3328. doi:10.1109/tpel.2018.2848980

[17] Ayachit A, Kazimierczuk MK. Averaged Small-Signal Model of PWM DC-DC Converters in CCM Including Switching Power Loss. *IEEE Transactions on Circuits and Systems II: Express Briefs*. 2019;66(2):262-266. doi:10.1109/tcsii.2018.2848623

[18] Schmitz L, Martins DC, Coelho RF. A Simple, Accurate Small-Signal Model of a Coupled-Inductor-Based DC-DC Converter Including the Leakage Inductance Effect. *IEEE Transactions on Circuits and Systems II: Express Briefs*. 2021;68(7):2533-2537. doi:10.1109/tcsii.2021.3061942

[19] Yan D, Yang C, Hang L, et al. Review of general modeling approaches of power converters. *Chin J Electr Eng*. 2021;7(1):27-36. doi:10.23919/cjee.2021.000002

[20] Freitas CM, Watanabe EH, Monteiro LFC. A linearized small-signal Thévenin-equivalent model of a voltage-controlled modular multilevel converter. *Electric Power Systems Research*. 2020;182:106231. doi:10.1016/j.epsr.2020.106231

[21] Asa E, Yamamoto Y. Aircraft Flight Stabilizer System by CDM Designed Servo State-Feedback Controller. *Aerospace*. 2021;8(2):45. doi:10.3390/aerospace8020045

[22] Meenakshipriya B, Kalpana K. Modelling and Control of Ball and Beam System using Coefficient Diagram Method (CDM) based PID controller. *IFAC Proceedings Volumes*. 2014;47(1):620-626. doi:10.3182/20140313-3-in-3024.00079

[23] Gopi RS, Srinivasan S, Panneerselvam K, Teekaraman Y, Kuppusamy R, Urooj S. Enhanced Model Reference Adaptive Control Scheme for Tracking Control of Magnetic Levitation System. *Energies*. 2021;14(5):1455. doi:10.3390/en14051455

[24] Airikka P. Advanced control methods for industrial process control. *Computing and Control Engineering*. 2004;15(3):18-23. doi:10.1049/cce:20040303

[25] Momani S, El-Khazali R, Batiha IM. Tuning PID and $PI^{\lambda}D^{\delta}$ controllers using particle swarm optimization algorithm via El-Khazali's approach. *In: PROCEEDINGS OF THE 45TH INTERNATIONAL CONFERENCE ON APPLICATION OF MATHEMATICS IN ENGINEERING AND ECONOMICS (AMEE'19). AIP Publishing*; 2019. doi:10.1063/1.5133522

[26] Tenreiro Machado JA. Optimal tuning of fractional controllers using genetic algorithms. *Nonlinear Dyn*. 2010;62(1-2):447-452. doi:10.1007/s11071-010-9731-5

[27] Jaiswal S, Suresh Kumar C, Seepana MM, Babu GUB. Design of Fractional Order PID Controller Using Genetic Algorithm Optimization Technique for Nonlinear System. *Chemical Product and Process Modeling*. 2020;15(2). doi:10.1515/cppm-2019-0072

CHAPTER-2 REFRENCES

[1] Lucia O, Maussion P, Dede EJ, Burdio JM. Induction heating technology and its applications: Past developments, current technology, and future challenges. *IEEE Trans Ind Electron*. 2014;61(5):2509-2520. doi:10.1109/tie.2013.2281162

[2] MUĆKO J. Parallel resonant inverter with non dissipative snubber used for induction heating. *in PRZEGLĄD ELEKTROTECHNICZNY*, No.01a/2012, pp. 61-64, 2012.

[3] Mollov SV, Theodoridis M, Forsyth AJ. High frequency voltage-fed inverter with phase-shift control for induction heating. *IEE Proc-Electr Power Appl*. 2004;151(1):12. doi:10.1049/ip-epa:20031058

[4] Tu Z, Zhou Y, Zhang N. Study of control for induction heating power supply with LLC resonant load based on DSP. In: *2012 2nd International Conference on Consumer Electronics, Communications and Networks (CECNet)*. IEEE, Yichang, 2012, pp. 1313-1316, doi: 10.1109/CECNet.2012.6202075.

[5] Yue X, Wang X, Blaabjerg F. Review of small-signal modeling methods including frequency-coupling dynamics of power converters. *IEEE Trans Power Electron.* 2019;34(4):3313-3328. doi:10.1109/tpel.2018.2848980

[6] Belhadj-Youssef N. Modélisation et commande des redresseurs triphasés fonctionnnant à haut rendement et à faible taux de distorsion harmonique : application au redresseur triphasé de Vienne. *PhD-Thesis in Electronics*, École de technologie supérieure, Montréal, Canada, 2007.

[7] Merdassi A. Outil d'aide à la modélisation moyenne de convertisseurs statiques pour la simulation de systèmes mécatroniques. *PhD-Thesis in Engineering Sciences [physics]*. Institut National Polytechnique de Grenoble - INPG, 2009. Français. tel-00434953f.

[8] Helaimi M. Contribution a la commande d'un onduleur a resonance destine au chauffage par induction. *PhD-Thesis in Electrical control*, Universite des sciences et de la technologie d'oran mohamed boudiaf, Oran, Algeria, 2014.

[9] Merdassi A, Gerbaud L, Bacha S. General Average Modelling for Power Electronics Systems: Automatic Building Approach. *In Proceedings of the Conference Electrimacs* 2008, Quebec,Canada.

[10] Sanders SR, Noworolski JM, Liu XZ, Verghese GC. Generalized averaging method for power conversion circuits. In: *21st Annual IEEE Conference on Power Electronics Specialists*. IEEE; San Antonio, TX, USA, 1990, pp. 333-340, doi: 10.1109/PESC.1990.131207.

[11] Vorperian V. Simplified analysis of PWM converters using model of PWM switch. Continuous conduction mode. *IEEE Trans Aerosp Electron Syst*. 1990;26(3):490-496. doi:10.1109/7.106126

[12] Vorperian V. Simplified analysis of PWM converters using model of PWM switch. II. Discontinuous conduction mode. *IEEE Trans Aerosp Electron Syst*. 1990;26(3):497-505. doi:10.1109/7.106127

[13] Kanaan HY. Contribution à la modélisation et au réglage des redresseurs triphasés non polluants unidirectionnels de type élévateur et à fréquence de commutation fixe. *PhD-Thesis in Engineering*, Ecole de Technologie Supérieur, Université du Québec, Montréal, Canada, Mars 2002

[14] Merdassi A, Gerbaud L, Bacha S. Automatic generation of average models for power electronics systems in VHDL-AMS and Modelica modelling languages. *Journal of Modelling and Simulation of Systems*. 2010; 1 (3): 176-186. ⟨hal-00539558⟩

[15] Grajales L, Lee FC. Control system design and small-signal analysis of a phase-shift-controlled series-resonant inverter for induction heating. *Power Electronics Specialists Conference PESC'95, Record, 26th Annual IEEE*, Vol. 01, pp. 450-456, Juin 1995

[16] Ahmed S, Shen Z, Mattavelli P, Boroyevich D, Karimi KJ. Small-signal model of voltage source inverter (VSI) and voltage source converter (VSC) considering the Dead Time effect and space vector modulation types. *IEEE Trans Power Electron*. 2017;32(6):4145-4156. doi:10.1109/tpel.2016.2595568

[17] Tian S, Lee FC, Mattavelli P, Yan Y. Small-Signal Analysis and Optimal Design of Constant Frequency V^2 Control. *IEEE Trans Power Electron*. 2015;30(3):1724-1733. doi:10.1109/tpel.2014.2320980

[18] Maamar AET, Kermadi M, Helaimi M, Taleb R, Mekhilef S. An improved single-phase asymmetrical multilevel inverter structure with reduced number of switches and higher power quality. *IEEE Trans Circuits Syst II Express Briefs*. 2021;68(6):2092-2096. doi:10.1109/tcsii.2020.3046186

[19] Akagi H. Multilevel converters: Fundamental circuits and systems. *Proc IEEE Inst Electr Electron Eng*. 2017;105(11):2048-2065. doi:10.1109/jproc.2017.2682105

[20] Akagi H. Classification, terminology, and application of the modular multilevel cascade converter (MMCC). *IEEE Trans Power Electron*. 2011;26(11):3119-3130. doi:10.1109/tpel.2011.2143431

[21] Akagi H. A review of developments in the family of modular multilevel cascade converters. *IEEJ trans electr electron eng*. 2018;13(9):1222-1235. doi:10.1002/tee.22731

[22] Omer P, Kumar J, Surjan BS. A review on reduced switch count multilevel inverter topologies. *IEEE Access*. 2020;8:22281-22302. doi:10.1109/access.2020.2969551

[23] Trabelsi M, Vahedi H, Abu-Rub H. Review on single-DC-source multilevel inverters: Topologies, challenges, industrial applications, and recommendations. *IEEE Open J Ind Electron Soc*. 2021;2:112-127. doi:10.1109/ojies.2021.3054666

[24] Saeedian M, Adabi ME, Hosseini SM, Adabi J, Pouresmaeil E. A novel step-up single source multilevel inverter: Topology, operating principle, and modulation. *IEEE Trans Power Electron*. 2019;34(4):3269-3282. doi:10.1109/tpel.2018.2848359

[25] Vivert ME, Patino D, Diez R. Modulation strategy and controller for grid-tied trinary hybrid multilevel inverter. *IEEE J Emerg Sel Top Power Electron*. 2021;9(1):539-548. doi:10.1109/jestpe.2019.2942325

[26] Chen T, Narimani M. Soft-Switching T-Type Multilevel Inverter. *Journal of Power Electronics*. 2019;19(5):1182-1192. doi:10.6113/JPE.2019.19.5.1182

[27] Chen T, Narimani M. A new ZVZCS three-level inverter. In: *IECON 2017 - 43rd Annual Conference of the IEEE Industrial Electronics Society*. IEEE; 2017:601-606. doi: 10.1109/IECON.2017.8216105.

[28] Sahin Y, Ting NS, Akboy E, Aksoy I. A new soft switching three level T-type inverter. In: *2016 10th International Conference on Compatibility, Power Electronics and Power Engineering (CPE-POWERENG)*. IEEE; 2016:314-318. doi: 10.1109/CPE.2016.7544206.

[29] Anand V, Singh V. Compact symmetrical and asymmetrical multilevel inverter with reduced switches. *Int trans electr energy syst*. 2020;30(8). doi:10.1002/2050-7038.12458

[30] Prabaharan N, Palanisamy K. A comprehensive review on reduced switch multilevel inverter topologies, modulation techniques and applications. *Renew Sustain Energy Rev*. 2017;76:1248-1282. doi:10.1016/j.rser.2017.03.121

[31] Siddique MD, Mekhilef S, Shah NM, et al. Low switching frequency based asymmetrical multilevel inverter topology with reduced switch count. *IEEE Access*. 2019;7:86374-86383. doi:10.1109/access.2019.2925277

[32] Sakthisudhursun B, Arockiaraj S, Muralidharan S. Implementation of Nearest Level Control Modulation Technique for Multilevel Inverter using Arduino. *International Journal of Advanced Science and Technology*. 2020; 29(7s): 1096 - 1102.

[33] Toubal Maamar AE, Helaimi M, Taleb R, Mouloudj H, Elamri O, Gadoum A. Mathematical analysis of N-R algorithm for experimental implementation of SHEPWM control on single-phase inverter. *Int j eng trends technol*. 2020;68(2):9-16. doi:10.14445/22315381/ijett-v68i2p202

[34] Marín-Reyes M, Aguayo-Alquicira J, De León-Aldaco SE. Calculation of optimal switching angles for a multilevel inverter using NR, PSO, and GA- a comparison. *Eur J Electr Eng*. 2020;22(4-5):349-355. doi:10.18280/ejee.224-506

[35] Rodriguez J, Franquelo LG, Kouro S, et al. Multilevel converters: An enabling technology for high-power applications. *Proc IEEE Inst Electr Electron Eng*. 2009;97(11):1786-1817. doi:10.1109/jproc.2009.2030235

[36] Yaramasu V, Dekka A, Kouro S. Multilevel converters for renewable energy systems. In: *Multilevel Inverters*. Elsevier; 2021:155-184. Doi: 10.1016/B978-0-323-90217-5.00007-1.

[37] Pereda J, Dixon J. 23-level inverter for electric vehicles using a single battery pack and series active filters. *IEEE Trans Veh Technol*. 2012;61(3):1043-1051. doi:10.1109/tvt.2012.2186599

[38] Han Y, Yang M, Li H, et al. Modeling and stability analysis of LCL -type grid-connected inverters: A comprehensive overview. *IEEE Access*. 2019;7:114975-115001. doi:10.1109/access.2019.2935806

[39] Toubal Maamar AE, Helaimi M, Taleb R. Analysis and experimental validation of single phase series resonance inverter: A 3-7 KHz full-bridge inverter. In: *Lecture Notes in Electrical Engineering*. Singapore: Springer Singapore; 2021:203-216. Doi: 10.1007/978-981-15-6403-1_14

[40] Cheng L, Zhu L, Hu Y. Operation analysis of a new II-type 5-level inverter for robot motor drive. In: *Proceedings of the 2019 International Conference on Robotics, Intelligent Control and Artificial Intelligence - RICAI 2019*. New York, New York, USA: ACM Press; 2019. doi:10.1145/3366194.3366329

[41] Kouro S, Malinowski M, Gopakumar K, et al. Recent advances and industrial applications of multilevel converters. *IEEE Trans Ind Electron*. 2010;57(8):2553-2580. doi:10.1109/tie.2010.2049719

[42] Gray D. The principles of automatic control. In: *Centralized and Automatic Controls in Ships*. Elsevier; 1966:94-119. doi:10.1016/b978-1-4832-1355-2.50014-5

[43] Berk Z. Elements of process control. In: *Food Process Engineering and Technology*. Elsevier; 2009:129-151. doi:10.1016/b978-0-12-373660-4.00005-3

[44] Kerlin TW, Upadhyaya BR. Reactor control. In: *Dynamics and Control of Nuclear Reactors*. Elsevier; 2019:89-104. doi:10.1016/b978-0-12-815261-4.00008-1

[45] Lobontiu N. Time- and frequency-domain controls of feedback systems. In: *System Dynamics for Engineering Students*. Elsevier; 2018:647-708. doi:10.1016/b978-0-12-804559-6.00013-0

[46] Gray D. The basic principles of automatic controllers. In: *Centralized and Automatic Controls in Ships*. Elsevier; 1966:120-144. doi:10.1016/b978-1-4832-1355-2.50015-7

[47] Kim SH. Control of direct current motors. In: *Electric Motor Control*. Elsevier; 2017:39-93. doi:10.1016/b978-0-12-812138-2.00002-7

[48] Lloyds Raja G, Ali A. New PI-PD controller design strategy for industrial unstable and integrating processes with dead time and inverse response. *J Control Autom Electr Syst*. 2021. doi:10.1007/s40313-020-00679-5

[49] Podlubny I. Fractional-order systems and $PI^{\alpha}D^{\beta}$ controllers. *IEEE Trans Automat Contr*. 1999;44(1):208-214. doi:10.1109/9.739144

[50] Djari A, Bouden T, and Boulkroune A. Design of a fractional order PID controller, (FOPID) for a class of fractional order MIMO system. *Journal of Automation and Systems Engineering*. 2014;8(1): 25–39.

[51] Xia F, Yang C, Wang Y, and Youcef-Toumi K. Model and Controller Design for High-speed Atomic Force Microscope Imaging and Auto-tuning. *ASPE Spring Topical Meeting on Design and Control of Precision Mechatronic Systems*. 2020: 99-104.

[52] Xue D, Chen WQ, and Derek P. Atherton. PID Controller Design. In: Linear

Feedback Control. Society for Industrial and Applied Mathematics; 2007:181-233. doi:10.1137/1.9780898718621.ch6

[53] Borase RP, Maghade DK, Sondkar SY, Pawar SN. A review of PID control, tuning methods and applications. Int J Dynam Control. 2020;9(2):818-827. doi:10.1007/s40435-020-00665-4

[54] García CE, Prett DM, Morari M. Model predictive control: Theory and practice—A survey. Automatica. 1989;25(3):335-348. doi:10.1016/0005-1098(89)90002-2

[55] Rivera DE, Morari M, Skogestad S. Internal model control: PID controller design. Ind Eng Chem Proc Des Dev. 1986;25(1):252-265. doi: 10.1021/i200032a041

[56] Manabe S. Coefficient Diagram Method. IFAC Proceedings Volumes. 1998;31(21):211-222. doi:10.1016/s1474-6670(17)41080-9

[57] Airikka P. Advanced control methods for industrial process control. Computing and Control Engineering. 2004;15(3):18-23. doi:10.1049/cce:20040303

[58] Belgaid Y, Helaimi M, Taleb R, Benali Youcef M. Optimal tuning of PI controller using genetic algorithm for wind turbine application. *Indones j electr eng comput sci*. 2020;18(1):167. doi:10.11591/ijeecs.v18.i1.pp167-178

[59] Ladjouzi S, Grouni S. PID controller parameters adjustment using a single memory neuron. *J Franklin Inst*. 2020;357(9):5143-5172. doi:10.1016/j.jfranklin.2020.02.027

[60] Lei W, Li C, Chen MZQ. Robust adaptive tracking control for quadrotors by combining PI and self-tuning regulator. *IEEE Trans Control Syst Technol*. 2019;27(6):2663-2671. doi:10.1109/tcst.2018.2872462

[61] Damasceno NC, Filho OG. PI controller optimization for a heat exchanger through metaheuristic Bat Algorithm, Particle Swarm Optimization, Flower Pollination Algorithm and Cuckoo Search Algorithm. *IEEE Lat Am Trans*. 2017;15(9):1801-1807. doi:10.1109/tla.2017.8015088

[62] Thirumeni M, Thangavelusamy D. Design and analysis of hybrid PSO–GSA tuned PI and SMC controller for DC–DC Cuk converter. *IET Circuits Devices Syst*. 2019;13(3):374-384. doi:10.1049/iet-cds.2018.5164

[63] Bhatti OS, Shami UT, Mahmood-ul-Hasan K, Abbas F, Mahmood S. Robust-Optimal Output-Voltage Control of Buck Converter using Fuzzy Adaptive Weighted Combination of Linear Feedback Controllers. *J. Control Eng. Appl. Inform.* 2019; 21(2):43–53.

[64] Huang L, Yu L, Quan S, et al. Design of voltage loop for three-phase PWM rectifier based on single neuron adaptive PID control. In: *2017 32nd Youth Academic Annual Conference of Chinese Association of Automation (YAC)*. IEEE; 2017:171-175. doi:10.1109/YAC.2017.7967399

[65] Vazquez S, Rodriguez J, Rivera M, Franquelo LG, Norambuena M. Model predictive control for power converters and drives: Advances and trends. *IEEE Trans Ind Electron*. 2017;64(2):935-947. doi:10.1109/tie.2016.2625238

[66] Borase RP, Maghade DK, Sondkar SY, Pawar SN. A review of PID control, tuning methods and applications. *Int J Dyn Contr*. 2021;9(2):818-827. doi:10.1007/s40435-020-00665-4

[67] Andújar JM, Irigoyen E, Becerra VM. Intelligent Control Approaches for Modeling and Control of Complex Systems. *Complexity*. 2018;2018:1-2. doi:10.1155/2018/2090715

[68] Passino K. Intelligent Control: An Overview of Techniques. 2000.

[69] Biswas A, Biswas B. Swarm Intelligence Techniques and Their Adaptive Nature with Applications. *In: Complex System Modelling and Control Through Intelligent Soft Computations. Springer International Publishing*;. 2014:253-273. doi:10.1007/978-3-319-12883-2_9

[70] Adam slowik. Swarm Intelligence Algorithms. CRC Press, 1st Edition. ISBN-10: 0367023458. pp.768. 2020.

[71] Prathibanandhi K, Ramesh R. Hybrid control technique for minimizing the torque ripple of brushless direct current motor. *Measurement and Control*. 2018;51(7-8):321-335. doi:10.1177/0020294018786753

[72] Qian F, Mahmoudi MR, Parvïn H, Pho K-H, Tuan BA. An Adaptive Particle Swarm Optimization Algorithm for Unconstrained Optimization. *Complexity*. 2020;2020:1-18. doi:10.1155/2020/2010545

[73] Eswaran T, Kumar VS. Particle swarm optimization (PSO)-based tuning technique for PI controller for management of a distributed static synchronous compensator

(DSTATCOM) for improved dynamic response and power quality. *Journal of Applied Research and Technology*. 2017;15(2):173-189. doi:10.1016/j.jart.2017.01.011

CHAPTER-3 REFRENCES

[1] Pointon AJ, Howarth HM. Electrical resonance. In: AC and DC Network Theory. Springer Netherlands; 1991:79-89. doi:10.1007/978-94-011-3142-1_7

[2] Maamar AET, Helaimi M, Taleb R, Chabni F. Design and Control of a Single-Phase Series Resonance Inverter using an Arduino Microcontroller. *In: 2019 International Conference on Advanced Electrical Engineering (ICAEE).* IEEE; 2019. doi:10.1109/icaee47123.2019.9014782

[3] ESSADAOUI J. Commande d'un onduleur de puissance destine au chauffage par induction par la modulation de densité d'impulsions avec améliorations du facteur de puissance. *PH-D thesis*, at UNIVERSITÉ DU QUÉBEC À TROIS-RIVIÈRES, 2003

[4] Serrano J, Acero J, Alonso R, Carretero C, Lope I, Burdío J. Design and Implementation of a Test-Bench for Efficiency Measurement of Domestic Induction Heating Appliances. *Energies*. 2016;9(8):636. doi:10.3390/en9080636

[5] Meng L, Cheng KWE. Wireless power transfer technology for electric iron based on multi-coils induction heating design. *IET Power Electronics*. 2019;12(10):2566-2577. doi:10.1049/iet-pel.2018.6305

[6] Séguier G, Delarue P, Labrique F. Electronique de puissance: Structures, commandes, applications. Dunod; 2015.

[7] Toubal Maamar AE, Helaimi M, and Taleb R. Analysis, Simulation and Experimental Validation of High Frequency DC/AC Multilevel Inverter. *Prz Elektrotech*. 2020;1(8):16-19. doi:10.15199/48.2020.08.03

[8] Venkatasubramanian M, Tomsovic K. Power System Operation and Control. *In: The Electrical Engineering Handbook. Elsevier*; 2005:779-785. doi:10.1016/b978-012170960-0/50057-8.

[9] Singh AK, Pal BC. Introduction. In: Dynamic Estimation and Control of Power Systems. Elsevier; 2019:1-8. doi:10.1016/b978-0-12-814005-5.00012-1

[10] Rao.Jalakanuru N. Switching Angle Calculation by EP, HEP, HH and FF Methods For Modified 11-Level Cascade H-Bridge Multilevel Inverter. *International Journal of Engineering Science Invention (IJESI).*2017; 6(12): 69-75.

CHAPTER-4 REFRENCES

[1] Lee FC, Li Q, Nabih A. High Frequency Resonant Converters: An Overview on the Magnetic Design and Control Methods. *IEEE J Emerg Sel Topics Power Electron*. 2021; 9(1): 11-23. doi:10.1109/jestpe.2020.3011166

[2] Yan D, Yang C, Hang L, et al. Review of general modeling approaches of power converters. *Chin J Electr Eng.* 2021; 7(1):27-36. doi:10.23919/cjee.2021.000002

[3] Yang EX, Lee FC, Jovanovic MM. Small-signal modeling of series and parallel resonant converters. *In: [Proceedings] APEC '92 Seventh Annual Applied Power Electronics Conference and Exposition. IEEE.* doi:10.1109/apec.1992.228333

[4] Ayachit A, Kazimierczuk MK. Averaged Small-Signal Model of PWM DC-DC Converters in CCM Including Switching Power Loss. *IEEE Trans Circuits Syst II.* 2019; 66(2): 262-266. doi:10.1109/tcsii.2018.2848623

[5] Toubal Maamar AE, Helaimi M, Taleb R, et al. Analysis and Small Signal Modeling of Five-Level Series Resonant Inverter. *IEEE Access*. 2021; 9: 109384-109395. doi:10.1109/access.2021.3102102

[6] Tian S, Lee FC, Mattavelli P, Yan Y. Small-Signal Analysis and Optimal Design of Constant Frequency V^2 Control. *IEEE Trans Power Electron*. 2015;30(3):1724-1733. doi:10.1109/tpel.2014.2320980

[7] Riccobono A, and Turevskiy A. Estimating the Frequency Response of a Power Electronics Model. MathWorks. Published 2020. Accessed on: April. 11, 2021. [Online]. Available:https://www.mathworks.com/company/newsletters/articles/estimating-the-frequency-response-of-a-power-electronics-model.html

[8] Toubal Maamar AE, Helaimi M, Taleb R, Kermadi M, Mekhilef S. A neural network-based selective harmonic elimination scheme for five-level inverter. *Int J Circuit Theory Appl*. 2022;50(1):298-316. doi:10.1002/cta.3130

[9] Memon MA, Mekhilef S, Mubin M, Aamir M. Selective harmonic elimination in inverters using bio-inspired intelligent algorithms for renewable energy conversion applications: A review. *Renewable and Sustainable Energy Reviews.* 2018; 82:2235–2253. DOI: 10.1016/j.rser.2017.08.068.

[10] Panda KP, Lee SS, Panda G. Reduced Switch Cascaded Multilevel Inverter With New Selective Harmonic Elimination Control for Standalone Renewable Energy System. *IEEE Transactions on Industry Applications*. 2019; 55(6):7561–7574. DOI: 10.1109/tia.2019.2904923.

[11] Siddique MD, Mekhilef S, Padmanaban S, Memon MA, Kumar C. Single-Phase Step-Up Switched-Capacitor-Based Multilevel Inverter Topology With SHEPWM. *IEEE Transactions on Industry Applications*. 2021; 57(3):3107–3119. DOI: 10.1109/tia.2020.3002182.

[12] Buccella C, Cecati C, Cimoroni MG, Razi K. Analytical Method for Pattern Generation in Five-Level Cascaded H-Bridge Inverter Using Selective Harmonic Elimination. *IEEE Transactions on Industrial Electronics.* 2014; 61(11):5811-58-19. Doi: 10.1109/TIE.2014.2308163

[13] Caccamo MT, Cannuli A, Magazù S. Wavelet analysis of near-resonant series RLC circuit with time-dependent forcing frequency. *Eur J Phys*. 2018;39(4):045702. doi:10.1088/1361-6404/aaae77

[14] Toubal Maamar AE, Helaimi M, Taleb R. Analysis and Experimental Validation of Single Phase Series Resonance Inverter. *Proceedings of the 4th ICEECA 2019-Lecture Notes in Electrical Engineering, Springer, Singapore*. vol. 682. 2021:203-216. doi:10.1007/978-981-15-6403-1_14

CHAPTER-5 REFRENCES

[1] Manabe S. Coefficient Diagram Method. *IFAC Proceedings Volumes*. 1998;31(21):211-222. doi:10.1016/s1474-6670(17)41080-9

[2] Heshmati M, Noroozian R, Jalilzadeh S, Shayeghi H. Optimal design of CDM controller to frequency control of a realistic power system equipped with storage devices using grasshopper optimization algorithm. *ISA Transactions*. 2020;97:202-215. doi:10.1016/j.isatra.2019.08.028

[3] Ikeda H. PID Controller Design Methods for Multi-Mass Resonance System. *In: PID Control for Industrial Processes. InTech; Chapter 9*, 2018. pp.187-207, doi:10.5772/intechopen.74298

[4] Manabe S, Kim YC. Coefficient Diagram Method for Control System Design. *Book in*

Intelligent Systems, Control and Automation: Science and Engineering, Springer Singapore; 2021. doi:10.1007/978-981-16-0546-8

[5] Haouari F, Nourdine B, Boucherit MS, Tadjine M. A Coefficient Diagram Method Controller with Backstepping Methodology for Robotic Manipulators. *Journal of Electrical Engineering.* 2015;66(5):270-276. doi:10.2478/jee-2015-0044

[6] Fadali MS, Visioli A. Chapter 5-Analog control system design. *Digital Control Engineering (Third Edition).* 2020: 141–179. doi:10.1016/b978-0-12-814433-6.00005-3

[7] Ladjouzi S, Grouni S. PID controller parameters adjustment using a single memory neuron. *Journal of the Franklin Institute.* 2020; 357(9): 5143-5172. doi:10.1016/j.jfranklin.2020.02.027

[8] Jeffrey A. Britton, Tutorial on IEEE High Voltage Testing Techniques (Standard 4) - Presentation of STD 4 and the latest changes by subcommittee members, *Fall 2016 IEEE switchgear Committee Meeting*, October 9-13, Pittsburgh, Pennsylvanie, 2016, USA.

[9] Narendra KS, Han Z. Adaptive Control Using Collective Information Obtained from Multiple Models*. *IFAC Proceedings Volumes*. 2011;44(1):362-367. doi:10.3182/20110828-6-it-1002.02237

[10] Airikka P. Advanced control methods for industrial process control. *Computing and Control Engineering*. 2004; 15(3): 18–23. Doi: 10.1049/cce:20040303

[11] Landau ID, Lozano R, M'Saad M, Karimi A. Indirect Adaptive Control. *In: Adaptive Control. Springer London*; 2011:409-456. doi:10.1007/978-0-85729-664-1_12

[12] Lam Q, Xin M, Cloutier J. A View of SDRE Control Methods as One Branch of Indirect Adaptive Control. *In: Infotech@Aerospace 2012. American Institute of Aeronautics and Astronautics*; 2012. doi:10.2514/6.2012-2495

[13] Venanzi I. A Review on Adaptive Methods for Structural Control. *The Open Civil Engineering Journal (TOCIEJ)*. 2016;10(1):653-667. doi:10.2174/1874149501610010653

[14] Shekhar A, Sharma A. Review of Model Reference Adaptive Control. *In: 2018 International Conference on Information, Communication, Engineering and Technology (ICICET). IEEE*; 2018. doi:10.1109/icicet.2018.8533713

[15] Jain P, Nigam MJ. Design of a Model Reference Adaptive Controller Using Modified MIT Rule for a Second Order System. *Advance in Electronic and Electric Engineering*. 2013;3(4): 477-484.

[16] Zhang D, Wei B. A review on model reference adaptive control of robotic manipulators. *Annu Rev Control*. 2017;43:188-198. doi:10.1016/j.arcontrol.2017.02.002

[17] Tariba N, Bouknadel A, Haddou A, Ikken N, Omari HE, Omari HE. Comparative study of adaptive controller using MIT rules and Lyapunov method for MPPT standalone PV systems. In: AIP Conference Proceedings 1801, 040008; 2017. doi:10.1063/1.4973097

[18] Mareels IMY, Anderson BDO, Bitmead RR, Bodson M, Sastry SS. Revisiting the Mit Rule for Adaptive Control. *IFAC Proceedings Volumes*. 1987;20(2):161-166. doi:10.1016/s1474-6670(17)55954-6

[19] Machacek Z, Pies M, Ozana S. Simulation of MIT rule-based adaptive controller of a power plant superheater. In: *Frontiers in Computer Education*. Berlin, Heidelberg: Springer Berlin Heidelberg; 2012:473-479. doi:10.1007/978-3-642-27552-4_65

[20] Pankaj S, Kumar JS, Nema RK. Comparative Analysis of MIT Rule and Lyapunov Rule in Model Reference Adaptive Control Scheme. *Innovative Systems Design and Engineering*. 2011;2(4): 154–162.

[21] Diethelm K. Riemann-Liouville Differential and Integral Operators. *In: Lecture Notes in Mathematics. Springer Berlin Heidelberg*; 2010:13-47. doi:10.1007/978-3-642-14574-2_2

[22] Helaimi M. Contribution a la commande d'un onduleur a resonance destine au chauffage par induction. *PhD-Thesis-Electrical control*, USTOMB, Oran, Algeria, 2014.

[23] Djari A, Bouden T, and Boulkroune A. Design of a fractional order PID controller, (FOPID) for a class of fractional order MIMO system. *Journal of Automation and Systems Engineering*. 2014;8(1):25-39.

[24] Popovic MB, Lamkin-Kennard KA, Bowers MP. Control and Physical Intelligence. *In: Biomechatronics. Elsevier*; 2019:109-138. doi:10.1016/b978-0-12-812939-5.00005-7.

[25] Podlubny I. Fractional-order systems and $PI^{\alpha}D^{\beta}$ controllers. *IEEE Trans Automat Contr*. 1999;44(1):208-214. doi:10.1109/9.739144

[26] Tepljakov A. FOMCON: Fractional-Order Modeling and Control Toolbox. In: Fractional-order Modeling and Control of Dynamic Systems. Springer Theses (Recognizing Outstanding Ph.D. Research). Springer, Cham. 2017:107-129. doi:10.1007/978-3-319-52950-9_6

[27] Yang X-S. Genetic Algorithms. In: Nature-Inspired Optimization Algorithms. Elsevier; 2021:91-100. doi:10.1016/b978-0-12-821986-7.00013-5

[28] Swayamsiddha S. Bio-inspired algorithms: principles, implementation, and applications to wireless communication. *In: Nature-Inspired Computation and Swarm Intelligence*. Elsevier; 2020:49-63. doi:10.1016/b978-0-12-819714-1.00013-0

[29] Belgaid Y, Helaimi M, Taleb R, Benali Youcef M. Optimal tuning of PI controller using genetic algorithm for wind turbine application. IJEECS. 2020;18(1):167. doi:10.11591/ijeecs.v18.i1.pp167-178

[30] Vijini Mallawaarachchi. Introduction to Genetic Algorithms — Including Example Code. Article: e396e98d8bf3, Jul 8, 2017. [Available online] https://towardsdatascience.com/ last access:11/11/2021.

[31] Ünal M, Ak A, Topuz V, Erdal H. Genetic Algorithm. In: Optimization of PID Controllers Using Ant Colony and Genetic Algorithms. Berlin, Heidelberg: Springer Berlin Heidelberg; 2013:19-29. Doi: 10.1007/978-3-642-32900-5_3

[32] Okwu MO, Tartibu LK. Genetic Algorithm. In: *Metaheuristic Optimization: Nature-Inspired Algorithms Swarm and Computational Intelligence, Theory and Applications*. Cham: Springer International Publishing; 2021:125-132. Doi: 10.1007/978-3-030-61111-8_13

[33] Beg AH, Islam MZ. Advantages and limitations of genetic algorithms for clustering records. *In: 2016 IEEE 11th Conference on Industrial Electronics and Applications (ICIEA).* IEEE; 2016. doi:10.1109/iciea.2016.7604009

[34] Katoch S, Chauhan SS, Kumar V. A review on genetic algorithm: past, present, and future. *Multimed Tools Appl*. 2021;80: 8091–8126. doi:10.1007/s11042-020-10139-6

[35] Drachal K, Pawłowski M. A Review of the Applications of Genetic Algorithms to Forecasting Prices of Commodities. *Economies.* 2021; 9(1):6. Doi: 10.3390/economies9010006

[36] Wang D, Tan D, Liu L. Particle swarm optimization algorithm: an overview. *Soft Comput*. 2018;22(2):387-408. doi:10.1007/s00500-016-2474-6

[37] Kennedy J, Eberhart R. Particle swarm optimization. In: *Proceedings of ICNN'95 - International Conference on Neural Networks*. 2002. doi: 10.1109/ICNN.1995.488968.

[38] Hadian M, Aarabi A, Makvand AB, Mehrshadian M. A New Event-Based PI Controller Using Evolutionary Algorithms. *J Control Autom Electr Syst.* 2019;30(6):841-849. doi:10.1007/s40313-019-00519-1

[39] Mishra SK, Chandra D. Stabilization of Inverted Cart-Pendulum System Using Controller: A Frequency-Domain Approach. *Chinese Journal of Engineering.* 2013;2013:1-7. doi:10.1155/2013/962401

[40] Mohammed El-Said El-Telbany. Employing Particle Swarm Optimizer and Genetic Algorithms for Optimal Tuning of PID Controllers: A Comparative Study. *ICGST-ACSE Journal*. 2007;7(2):49-54.

[41] Rahman I, Vasant PM, Singh BSM, Abdullah-Al-Wadud M. On the performance of accelerated particle swarm optimization for charging plug-in hybrid electric vehicles. *Alexandria Engineering Journal.* 2016;55(1):419-426. doi:10.1016/j.aej.2015.11.002

[42] Lee K, Park J. Application of Particle Swarm Optimization to Economic Dispatch Problem: Advantages and Disadvantages. *2006 IEEE PES Power Systems Conference and Exposition.* 2006. doi:10.1109/psce.2006.296295

[43] Freitas D, Lopes LG, Morgado-Dias F. Particle Swarm Optimisation: A Historical Review Up to the Current Developments. Entropy. 2020; 22(3):362. https://doi.org/10.3390/e22030362

RESEARCH CONTRIBUTIONS

RESEARCH CONTRIBUTIONS

The present thesis is part of the doctoral formation, was begin after passing a national exam for getting a doctoral student position, then study a specified number of classes, publishing research papers related to the thesis subject in international indexed journals in a web of science (Clarivate) database with impact factor (class A according to the DGRSDT'21 lists), and Scopus database (class B according to the DGRSDT'21 lists); Also, the participation in several international and national conferences.

Articles published in journals

1. **Toubal Maamar AE**, Helaimi M, Taleb R, Kermadi M, Mekhilef S, Wahyudie A, and Rawa M, "Analysis and Small Signal Modeling of Five-Level Series Resonant Inverter," *IEEE Access*, vol. 9, pp. 109384-109395, 2021, doi: 10.1109/ACCESS.2021.3102102
2. **Toubal Maamar AE**, Kermadi M, Helaimi M, Taleb R and Mekhilef S, "An Improved Single-Phase Asymmetrical Multilevel Inverter Structure With Reduced Number of Switches and Higher Power Quality," *in IEEE Transactions on Circuits and Systems II: Express Briefs*, vol. 68, no. 6, pp. 2092-2096, June 2021, doi: 10.1109/TCSII.2020.3046186.
3. **Toubal Maamar AE**, Helaimi M, Taleb R, Kermadi M, and Mekhilef S, " A Neural Network-based Selective Harmonic Elimination Scheme for Five-Level Inverter," *in International Journal of Circuit Theory and Applications*, Accepted for publication, doi: 10.1002/CTA.3130
4. **Toubal Maamar AE**, Helaimi M, Taleb R. Analysis, Simulation and Experimental Validation of High Frequency DC/AC Multilevel Inverter. *Przeglad Elektrotechniczny* 2020; 1(8):16–19. doi: 10.15199/48.2020.08.03.

Articles of conferences

1. **A. E. T. Maamar**, M. Helaimi, R. Taleb and F. Chabni, "Design and Control of a Single-Phase Series Resonance Inverter using an Arduino Microcontroller," *2019 International Conference on Advanced Electrical Engineering (ICAEE)*, Algiers, Algeria, 2019, pp. 1-6, doi: 10.1109/ICAEE47123.2019.9014782
2. **Toubal Maamar A.E.**, Helaimi M., Taleb R. (2021) Analysis and Experimental Validation of Single Phase Series Resonance Inverter. In: Bououden S., Chadli M.,

Ziani S., Zelinka I. (eds) Proceedings of the 4th International Conference on Electrical Engineering and Control Applications. ICEECA 2019. Lecture Notes in Electrical Engineering, vol 682. Springer, Singapore. https://doi.org/10.1007/978-981-15-6403-1_14

3. **A.E. Toubal Maamar**, M. HELAIMI, R. Taleb, F. Chabni, "Analysis and implementation of half bridge series resonant inverter using Arduino," *ICCEE'18 International conference on communications and electrical engineering* El-Oued, 2018, Algeria.
4. **Toubal Maamar A.E.**, Helaimi M., Taleb R., HAMZA H., HENNI HOMRI H., "Conception et réalisation d'un onduleur à résonance série pour: $4 < f < 6\ kHz$," Conférence Nationale sur l'Electrotechnique et Les Energies Renouvelables (CNEER'18), Saida, 2018, Algeria.
5. **Toubal Maamar A.E.**, Helaimi M., Taleb R., "Etude et Conception d'un Onduleur Multiniveaux à Résonance", The First Doctoral Symposium on Technology: Process, Mechanical and Electrical Engineering DST'01-2019, Chlef, Algeria.

APPENDICES

APPENDIX A

The general algorithm of Newton-Raphson for selective harmonic elimination

The algebraic system of nonlinear equations:

$$\begin{cases} \cos(\theta_1) - \cos(\theta_2) + \cdots \mp \cos(\theta_P) = M\dfrac{\pi}{4} \\ \vdots \\ \cos(n\theta_1) - \cos(n\theta_2) + \cdots \mp \cos(n\theta_P) = 0 \end{cases}$$

n: The odd harmonic ranks

P: The number of switching angles in quarter waveform.

M: Modulation Index, where $M = \frac{h_1}{V}$

The switching angles:

$$\theta^j = [\theta_1^j;\ \theta_2^j; \ldots;\ \theta_P^j]$$

The nonlinear system can be written:

$$F(\theta^j) = T$$

$$F(\theta^j) = \begin{pmatrix} \cos(\theta_1^j) & -\cos(\theta_2^j) & \cdots & \mp\cos(\theta_P^j) \\ \vdots & \vdots & \ddots & \vdots \\ \cos(n\theta_1^j) & -\cos(n\theta_2^j) & \cdots & \mp\cos(n\theta_P^j) \end{pmatrix}$$

$$T = \begin{pmatrix} M\frac{\pi}{4} \\ \vdots \\ 0 \end{pmatrix}$$

Derivate of the nonlinear system matrix:

$$\left[\frac{\partial F(\theta)}{\partial \theta}\right]^j = \begin{pmatrix} -\sin(\theta_1^j) & \sin(\theta_2^j) & \cdots & \mp\sin(\theta_P^j) \\ \vdots & \vdots & \ddots & \vdots \\ -n\sin(n\theta_1^j) & n\sin(n\theta_2^j) & \cdots & \mp n\sin(n\theta_P^j) \end{pmatrix}$$

The statement of algorithm:

1. Set of initial values for θ^j with j=0:

$$\theta^j = [\theta_1^j;\ \theta_2^j; \ldots;\ \theta_P^j]$$

2. Calculate the value of:

$$F\left(\theta^j\right) = F^j$$

3. Linearize system of equation about θ^j

$$F^j + \left[\frac{\partial F}{\partial \theta}\right]^j d\theta^j = T$$

Such as:

$$d\theta^j = \left[d\theta_1^j \quad \cdots \quad d\theta_P^j\right]^T$$

4. Solve $d\theta^j$ from equation:

$$d\theta^j = \left(inv\left(\left[\frac{\partial F}{\partial \theta}\right]^j\right)\right)\left(T - F^j\right)$$

5. Update the initial values:

$$\theta^{j+1} = \theta^j + d\theta^j$$

6. Repeat the process for equations until:

$d\theta^j$ is satisfied to the desired degree of accuracy.

The solution must satisfy the condition: $0 < \theta_1 < \theta_2 < \cdots < \theta_P < \frac{\pi}{2}$

APPENDIX B

Newton-Raphson algorithm to calculate the appropriated switching angles for elimination of third harmonic and their multiples in five-level inverter.

The algebraic system of nonlinear equations:

$$\cos(\theta_1) - \cos(\theta_2) = \frac{\pi}{4}\mathrm{M}$$

$$\cos(3\theta_1) - \cos(3\theta_2) = 0$$

The initial values of switching angle: $\theta^j = [\theta_1^j;\ \theta_2^j]$

The nonlinear system can be written: $F(\theta^j) = T$

Where :

$$F(\theta^j) = \begin{bmatrix} \cos(\theta_1^j) & -\cos(\theta_2^j) \\ \cos(3\theta_1^j) & -\cos(3\theta_2^j) \end{bmatrix}$$

$$T = \begin{bmatrix} M\frac{\pi}{4} \\ 0 \end{bmatrix}$$

Derivate of the nonlinear system matrix $F(\theta^j)$:

$$\left[\frac{\partial F(\theta)}{\partial \theta}\right]^j = \begin{bmatrix} -\sin(\theta_1^j) & \sin(\theta_2^j) \\ -3\sin(3\theta_1^j) & 3\sin(3\theta_2^j) \end{bmatrix}$$

The statement of algorithm is shown as follows:

1. Set of initial values for θ^j with j=0:

$$\theta^0 = \begin{bmatrix} \theta_1^0 \\ \theta_2^0 \end{bmatrix}$$

2. Calculate the value of:

$$F(\theta^0) = F^0$$

3. Linearize system of equation about θ^0

$$F^0 + \left[\frac{\partial F}{\partial \theta}\right]^0 d\theta^0 = T$$

Such as:

$$d\theta^0 = \begin{bmatrix} d\theta_1^0 \\ d\theta_2^0 \end{bmatrix}$$

4. Solve $d\theta^0$ from equation:

$$d\theta^0 = \left(inv\left(\left[\frac{\partial F}{\partial \theta}\right]^0\right)\right)(T - F^0)$$

Where $inv\left(\left[\frac{\partial F}{\partial \theta}\right]^0\right)$ is the inverse matrix of: $\left[\frac{\partial F}{\partial \theta}\right]^0$

5. Update the initial values:

$$\theta^{j+1} = \theta^j + d\theta^j$$

6. Repeat the process for equations until:

$d\theta^j$ is satisfied to the desired degree of accuracy.

The solution must satisfy the condition: $0 < \theta_1 < \theta_2 < \frac{\pi}{2}$